Microfluidic Platform for the Fabrication and Loading of Nanoscale Liposomes by 2D Hydrodynamic Flow Focusing

Selya Amrani

Biomat'X Research Laboratories

Department of Biomedical Engineering

Program of Biological and Biomedical Engineering

McGill University, Montreal

August 2017

A Thesis Submitted to McGill University in Partial Fulfillment of the Requirements of

The Degree of Master of Engineering (M. Eng)

Table of Contents

ABSTRACT

This thesis aims to examine liposomes generation in microfluidic systems. As such, it presents the continuous flow formation by two dimensional hydrodynamic flow focusing (2D HFF) of nano-sized liposomes in microfluidic channels. Using our platform, different lipid size particles are generated by altering the flow rates and flow rate ratios of two miscible fluids; a central stream of DPPC (*1,2-dipalmitoyl-sn-glycero-3-phosphocholine*) lipids in ethanol and an aqueous buffer. The effect of varying both the lipid composition and flow parameters for the synthesis of DPPC nano-sized liposomes within our platform was assessed with regards to size, concentration, charge and polydispersity of the resulting liposomes. The addition of either positively and negatively charged lipid particles to the main DPPC bilayer constituent, by respectively incorporating DDAB (*didodecyl-dimethyl-ammonium bromide*) and DOPG (*1,2 dioleoyl-sn-glycero-3-phosphoglycerol*) was studied as to its effect of liposome charge, size and polydispersity. Experimental flow conditions were duplicated within a COMSOL Multiphysics© in order to gain insight into the fluidic behavior of the system, and study the effect of FRR on flow focusing. Finally, encapsulation of a fluorescent FITC-LC-TAT peptide was performed to validate the potential of this device as an all-in-one liposome synthesis and drug loading platform. Liposomes with sizes ranging between 60 nm to 800 nm were produced with low polydispersity and high particle throughput from alteration of the flow rate ratio and lipid concentration. Control of liposomes size was attained by adjusting the FRR or the inlet concentration with higher FRR and lower concentrations reducing the size of the liposomes generated. Stable, unilamellar and mono-disperse liposomes are generated at a maximum concentration of 1740 x E8 $particles/mL$ in less than two minutes, with higher FRR enabling the most rapid generation of liposomes with similar diameter and significant lower polydispersity index than the obtained by other batch technique. The results suggest that the use of microfluidic devices could be employed for liposome production with a possible advantage to minimize the degree of parallelization of processes. It also emphasizes on the potential technical feasibility of microfluidic processes for future industrial applications.

ABRÉGÉ

Cette thèse traite de la formation de liposomes par le biais de systèmes microfluidiques. Plus précisément, elle aborde la formation continue par concentration axiale hydrodynamique bi-dimensionnelle (2D HFF ou hydrodynamic flow focusing) de nano-liposomes dans les conduits microfludiques. Par ce processus, un flux central de phospholipides dissous dans un solvant (ethanol) est focalisé par deux flux aqueux concomitants, résultant en la diffusion du solvant dans l'eau et en la diminution de la concentration des lipides dans le solvant, formant ainsi des liposomes. Dans le cadre de cette thèse, différentes tailles de liposomes sont générés en contrôlant les paramètres du flux continu des conduits microfluidiques. De ce fait, un contrôle du débit des flux lipidiques et aqueux ainsi que du taux entre les débits (plus communément appelé FRR pour Flow Rate Ratio) garantit la production continue et controlée de liposomes isuues d'un large éventail de taille. Nos résultats démontrent que la taille des liposomes est dépendante du taux de débit entre les deux fluides, ainsi que la composition et la concentration des lipides formant les liposomes. Des liposomes stables et relativement monodisperses à base de DPPC (*1,2-dipalmitoyl-sn-glycero-3-phosphocholine*) et de taille comprise entre 60-800 nm sont générés et ce avec un haut taux de reproducibilité. Par ailleurs, l'ajout de molecules lipidiques chargées positivement ou negativement au flux de lipide contenant le DPPC, par le biais de l'incorportaion de molecules de DDAB (*didodecyl-dimethyl-ammonium bromide*) et de DOPG (*1,2 dioleoyl-sn-glycero-3-phosphoglycerol*), fut étudié quant à son influence sur la charge, la polysidpersité et la taille des lipsoomes qui en résultent. Pour finir, l'encapsulation d'un peptide fluorescent FITC-LC-TAT à l'interieur des liposomes a été démontrée et imagéee par microscopie à fluorescence. La taille des liposomes ayant un impact déterminant sur leur capacité à charger des molécules biologiques, leur biodistribution in-vivo ainsi que sur leur taux de clairance, il devient primordial de développer des méthodes de production de liposomes qui sont à la fois reproductibles et qui permettent un contrôle efficace de la taille des liposomes générés et de leur polydispersité.

ACKNOWLEDGMENTS

I would like to thank my supervisor, Professor Maryam Tabrizian, for her guidance, support and patience during the completion of my thesis and graduate studies. I would also like to thank Biomat'X Members for their mentor-ship, help and guidance. Raphael Castiello, Paresa Modarres and Khalil Heileman: thank you for the guidance through the early stages of this project. Special thanks to Kaushar Jahan, Feriel Melaine, Agnese Bregnocchi, Saadia Shoaib and Timothée Baudequin, who in addition to being my colleagues, have been my closest friends inside this lab as well as outside of it; your friendship and support cannot be appreciated highly enough. My gratitude goes also to Sarayu Rao for the training and the use of the NTA equipment. My final thanks goes to my family for always supporting me during these years and for Jeremie Piú Laplante who introduced me to LaTeX.

Support from the McGill Biomedical Engineering Department for the Recruitment Award and Natural Sciences and Engineering Research Council of Canada (NSERC) for the Canada Graduate Scholarships-Master's (CGS M) are also gratefully acknowledged.

Selya Amrani

PREFACE & CONTRIBUTION of AUTHORS

Every chapter of this thesis is an original, independent work by the author, Selya Amrani. This thesis has been submitted for publication in ACS Biomaterials and Engineering on August 10^{th} 2017, and is at the time of this thesis submission, currently under review. A submitted draft of the paper is provided for consultation in the Appendix; Section F. The paper is an original work by Selya Amrani who conducted all the experiments and generated the figures and data present both in this paper and in the thesis. The paper's co-author, Maryam Tabrizian is acknowledged for her help providing spelling corrections as well as for her help in the formatting of the paper.

Selya Amrani

List of Figures

List of Tables

List of Abbreviations

2D	Two-dimensional.
3D	Three-dimensional.
ASES	Aerosol Solvent Extraction System.
BM	Bulk Mixing.
CAD	Computer-Assisted Design.
CAS	Continuous Anti-Solvent.
DAC	Dual Asymmetric Centrifugation.
DDAB	Didodecyldimethylammonium bromide.
DELOS-SUSP	Depressurization of Expanded Liquid Organic Solution–Suspension.
DESAM	Depressurization of Expanded Solution into Aqueous Media.
DOPG	Dioleoyl-sn-glycero-3-phosphoglycerol.
DPPC	Dipalmitoylphosphatidylcholine.
EM	Electron Microscopy.
EtOH	Anhydrous ethyl alcohol.
FITC	Fluorescein Isothiocyanate.
FRR	Flow Rate Ratio.
GAS	Gas Antisolvent Precipitation.
HFF	Hydrodynamic Flow Focusing.
HPH	High-pressure Homogenization Method.
HPLC	High Performance Liquid Chromatography.
IPA	Iso-propyl Alcohol or 2-propanol.
ISCRPE	Improved Supercritical Reverse Phase Evaporation.

LUVs	Large Unilamellar Vesicles.
MeOH	Methanol.
MHF	Microfluidic Hydrodynamic Flow Focusing.
MLVs	Multilamellar Vesicles.
NTA	Nanoparticle Tracking Analysis.
PDMS	Polydimethylsiloxane.
PFOTS	Trichloroperfluorooctylsilane.
PGSS	Gas-Saturated Solutions.
RESS	Rapid Expansion of Supercritical Solutions.
SAS	Supercritical Anti-Solvent.
SCF	Supercritical Fluids Technology.
SCRPE	Supercritical Reverse Phase Evaporation.
SFEE	Supercritical Fluid Extraction of Emulsion.
SFS-CFN	Super Fluids phospholipid nanosomes.
SUVs	Small Unilamellar Vesicles.
SVR	Surface-to-Volume Ratio.

List of Symbols

D	Diffusion Coefficient
D_h	Hydraulic Diameter or Characteristic Length
J	Diffusion Flux
P	Wetted Perimeter of Cross-Section
Q	Fluid Flow Rate
Re	Reynolds Number
T_m	Transition Temperature
μ	Dynamic Viscosity of Fluid Medium
ϕ	Species Concentration
ρ	Fluid Density
k	Boltzmann's Constant
v	Mean velocity

List of Equations

Chapter 1

Introduction

1.1 Background and Motivation

A major challenge in the development of nanoparticles (NPs) for drug delivery is the control of size and size distribution [1, 2]. To avoid measurements perturbed by polydispersity in vesicle size, a solution of vesicles of uniform diameters is a prerequisite for studying size-dependent properties [2]. In addition, NPs diameters have been shown to play an important role on their circulation time within the body and their elimination [3]. Traditional bulk methods of NPs preparation are however limited by difficulty in controlling size [4], as well as by problems of scale-up [5–8], inconsistent encapsulation efficiency [9–11], along with difficulty in effective sterilization [12]. In addition, long processing times, difficulty in obtaining relatively monodisperse products, large reagent volumes [13], and the multiple and lengthy steps necessary for encapsulation [14–16], make bulk synthesis methods time-consuming and uneconomical [1, 17].

Compared to their non-organic nanoparticles counterparts, the use of liposomes as a delivery vehicle offers many advantages including longer circulation times within the body [18], protection and controlled release of the encapsulated molecules [19, 20], and the ability to overcome biological barriers to achieve targeted delivery [21, 22]. The search for new strategies to alleviate the current issues facing liposome fabrication and provide control over both lipid aggregation and particle size while enabling encapsulation of various compounds, continues to remain a challenge in the field of liposome technology [23]. In this context, drug-loaded nano-liposomes can be produced in one step only with a microfluidic continuous process with many advantages over classical methods. This includes reducing the use of organic solvents, as well as providing fast, single-stage production and producing stable, uniform liposomes [24, 25].

The production of nano/microsized liposomes is mostly based on the formation of a dried lipid film [26, 27], and include processes such as thin-film hydration [28–30], ethanol injection [31–34], and detergent dialysis methods [35, 36]. Because these processes rely

on the self-assembly of lipids in a bulk phase, which is heterogeneous and uncontrolled [18, 37, 38], the resultant liposomes are polydispersed in size and often multilamellar. Further post-processing by extrusion [28, 29], freeze–thaw [11, 39, 40], sonication [29], and/or high-pressure homogenization [25, 39] is often required, in order to obtain liposomes with specific size and conformations [41]. In this context, drug-loaded nano-liposomes can be produced in one step only with a microfluidic continuous process with many advantages over classical methods. This includes reducing the use of organic solvents, as well as providing fast, single-stage production and producing stable, uniform liposomes [24, 25].

1.2 Purpose

This thesis provides an analysis of a 2-D hydrodynamic flow focusing microfluidic technique for the continuous flow production of nanoscale lipid-based vesicular systems. The main goal of this project is to develop an integrated microfluidic platform for the formulation of liposome-based nanoparticles for the encapsulation of a fluorescent protein more specifically an FITC labeled LC-TAT cell-penetrating peptide. TAT (Trans-Activator of Transcription) is a protein encoded for by the TAT gene in HIV-1 and stimulates HIV-1 gene expression during transcription initiation and elongation [42]. In addition, by antagonizing the CXCR4 receptor, reports suggest that TAT selectively encourage the reproduction of less virulent M-tropic (macrophage-tropic) strains of HIV early in the course of infection, allowing the more rapidly pathogenic T-cell-tropic strains (which use the CXCR4 receptor) to emerge later after mutating from M-tropic strains [43]. We hypothesize that microfluidics will enable a lower polydispersity and more homogeneous size distribution of the synthesized nano-liposomes, by providing an acute control over the flow conditions inside the microfluidic channels. Controlling the lipid and water stream flow conditions and composition will thus guarantee loading of the encapsulated molecules by enhancing the controllability and reproducibility of the size of the synthesized liposomes. This work is divided into three distinct parts: (1) Simulation and optimization of fluid flow and design geometry using COMSOL Multiphysics© and a Computer-Assisted Design (CAD) Solidworks© softwares, (2) Fabrication of the microfluidic platform using microfabrication techniques and (3) Visualization and characterization of the device and the synthesized fluorescent peptide encapsulating liposomes.

1.3 Overview of the Thesis

The thesis is divided into eight different chapters that follows this Introduction chapter. In the second chapter, the advantages of liposome formation using the microfluidic approach over traditional bulk-mixing techniques are discussed. For that purpose, a description of several state-of-the art microfluidic methods used to produce nano-sized liposomes (mainly SUVs and LUVs) with narrower size distribution will be included, focusing on the use of continuous-flow microfluidics. For that purpose, the theory and other fundamental principles of microfluidics and hydrodynamic flow focusing will be exposed. The third chapter describes the microfabrication methods and methodology associated with the design and manufacturing of our proposed microfluidic device. In the fifth and sixth chapters respectively, the 2D/3D numerical simulations, flow visualization as well as the HFF device characterization experiments will be presented. As such, the synthesis and characterization of DPPC based liposomes is described in the sixth chapter where we will discuss the role of flow parameters such as the flow rate ratio (FRR) as well as lipid composition (lipid concentration and lipid bilayer constituents) in determining liposome characteristics such as size, charge and particle concentration. The seventh chapter will discuss the loading and encapsulation of FITC-LC TAT peptide into the liposomes. Finally, we will conclude with a summary and suggested improvements for future iterations of this device with a view to potential industrial translation of this technology. The Appendix section follows the conclusion section and is divided into four different parts: (A) The CFD simulation results, (B) Flow Visualisation (C) Micro-fabrication visuals and protocols (D) Liposomes Preparation protocols and (E) The Nanoparticle Tracking Analysis (NTA) reports and raw data and (F) A draft of the submitted manuscript resulting from this thesis.

Chapter 2

Literature Review

2.1 What are Liposomes?

Liposomes are vesicular structures consisting of one or more lipid bilayer membranes that encapsulate an aqueous volume as illustrated in Figure 2.1. Whether the drug is encapsulated in the core or in the bilayer of the liposome is dependent on the characteristics of the drug and the encapsulation process [44]. Hydrophilic drugs can be loaded into the interior aqueous core of liposomes, whereas lipophilic and amphiphilic drugs can be incorporated into the lipid bilayers.

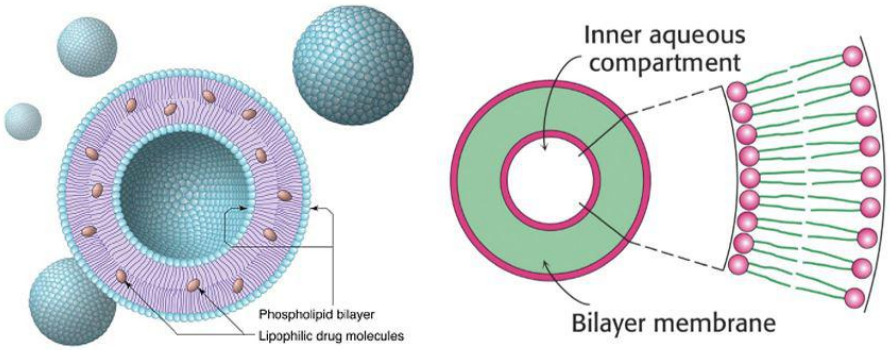

Figure 2.1: Unilamellar vesicular liposomes with incorporated lipophilic drug.

Liposomes application had important impact in several industries. The industrial applications contain liposomes as drug delivery vehicles in medicine, adjuvants in vaccination, signal enhancers/carriers in medical diagnostics and analytical biochemistry, solubilizers for various ingredients as well as support matrix for various ingredients and penetration enhancer in cosmetics [21]. As such liposomes are widely used as drug and gene delivery vehicles [44]. The main advantages and disadvantages associated with liposomes and their use is illustrated in Table 1. As drug delivery vehicles, liposomes can provide metabolic protection, prolong circulation time, reduce toxicity, control drug release, and enhance cell/tissue specificity of delivery. Several liposomal drugs, for example Doxil (PEGylated

liposomal doxorubicin), have reached clinical use [1]. In addition to conventional drugs, liposomes hold great promises as delivery vehicles for oligonucleotide-based therapeutics, including siRNA [25].

Table 2.1: Advantages and disadvantages of liposomes [21].

Advantages	**Disadvantages**
Liposomes increased efficacy and therapeutic index of drugs (for example: actinomycin-D)	Low solubility
Liposome increased stability by encapsulation	Short half-life
Liposomes are non-toxic, flexible, biocompatible, completely biodegradable, and non-immunogenic for both systemic and non-systemic administrations.	Possible oxidation and hydrolysis-like reaction of phospholipids.
They reduce the toxicity of the encapsulated agent (amphotericin B, Taxol)	Leakage and fusion of the drugs or molecules encapsulated
They help reduce the exposure of sensitive tissues to toxic drugs	High production costs (using conventional batch techniques)
Site avoidance effect	Polynomial order in each direction of each element
Flexibility to couple with site-specific ligands for active targeting purposes.	Fewer stables

Due to their structure, chemical composition and colloidal size, all of which can be well controlled by preparation methods, liposomes exhibit several properties which may be useful in various applications. The most important liposomal properties are their colloidal size, and special membrane and surface characteristics. They include bilayer phase behavior, its mechanical properties and permeability, charge density, presence of surface bound, or attachment of special ligands, correspondingly [2]. The characteristics of liposomes are determined by the choice of lipid, their composition, method of preparation, size and surface charge. Liposomes have been applied as drug carriers due to their ability to prevent degradation of drugs, reduce side effects and target drugs to site of action. However, limitations of liposomes include low encapsulation efficiency, rapid leakage of water-soluble drug in the presence of blood components and poor storage stability [44].

2.1.1 Classification of Liposomes

Classifications of liposomes are based on their size and lamellarity. Different size and lamellarity (number of lamellae or bilayers) depends on their composition and their method of preparation. Even though the lipid bilayer itself is only about 4 nm thick, the diameters of liposomes and vesicles are an order of magnitude larger. The diameters

of liposomes and vesicles range between 20 nm to 50 um [3]. These classifications, which are important as different classes of liposomes have very different suitability for drug delivery purposes, are shown in Figure 2.2:

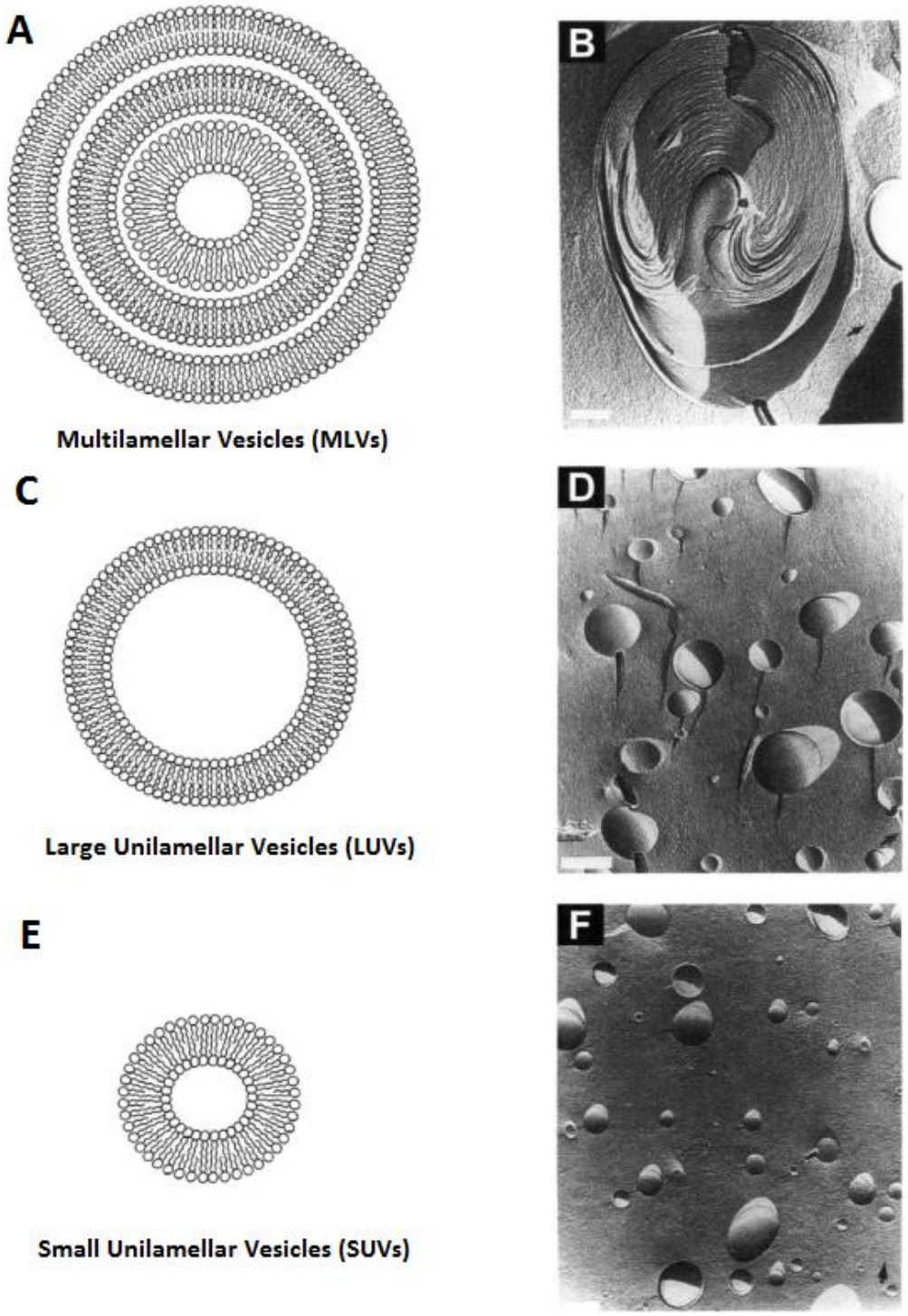

Figure 2.2: Schematic illustrations of (A) MLVs, (C) LUVs and (E) SUVs, as well as their respective freeze-fracture electron micrographs in (B), (D) and (F).

Multilamellar Vesicles (MLVs): Multilamellar vesicles contain two or more concentric lamellae and range in size from 0.2-10 μm. The advantages of MLV systems are that they are extremely easy to prepare. The preparation simply involves the addition of an aqueous solution to a dry lipid film followed by mechanical agitation [3]. MLVs have also been shown to encapsulate a variety of molecules [15, 16, 45]. One disadvantage of MLVs, however, is that due to their large size they are very rapidly eliminated from the circulation following intravenous administration [46].

Small Unilamellar Vesicles (SUVs): In contrast to MLVs, SUVs have a single bilayer and their size is typically below 100 nm [16]. These vesicles are most commonly formed by sonication of a solution containing MLVs, which re-forms the MLV systems into single bilayer vesicles [47]. Otherwise, SUVs can be formed by detergent dialysis [3]. SUVs have low encapsulation efficiency due to their size and are eliminated from the circulation more rapidly than LUVs [19]. Due to the high radius of curvature in these vesicles, there is an asymmetric distribution of lipids in the outer and inner monolayer that can result in rapid destabilization of the vesicle. Therefore, SUVs below 100 nm have not been commonly used as drug delivery systems. Examples of the use of SUVs include acting as contrast agents for MRI imaging by encapsulating gold nanoparticles [48] or as a membrane model system for studying the interaction of molecules [49, 50].

Large Unilamellar Vesicles (LUVs): LUVs also consist of a single bilayer and typically range in size from 100-400 nm . These systems can be prepared from MLV preparations by a well-established extrusion procedure which involves forcing the MLVs through polycarbonate filters of a defined pore size under nitrogen gas pressure [21]. In vivo studies have suggested that vesicles in the size range of 100-200 nm have prolonged half-lives in circulation compared with larger vesicles and have exhibited optimal tumor localization and retention [19]. A large majority of liposomal formulations intended for in vivo drug delivery applications utilize LUVs because they are more stable and are eliminated more slowly from the circulation than SUVs and MLVs. However, it has been proven that their elimination is highly dependent on liposomal lipid composition [51, 52].

2.1.2 The Role of Liposome Properties

Consideration of shape and size in nanoparticle design is crucial for application like drug delivery and targeting. Whereas the geometry of a particle it what drives initial internalization, its size is what ultimately determines the successful completion of uptake [19]. Therefore, control of liposomes properties such as uniform particle size and good colloidal stability are essential for liposomes to be developed as in vivo drug carriers.

Particle Size: The size of a nanoparticle is an important design parameter that can be tailored for purposes of directing particle distribution in vivo. Size drives several biological phenomena with discrete cut-off size ranges that include circulation half-lives, extravasation through leaky vasculature and macrophage uptake [19]. As such, the rate of opsonisation and clearance by the reticuloendothelial system (RES) of the injected liposomes from the blood circulation is dependent on the composition and size. RES is part of the immune system and their main function is to eliminate foreign materials from the body. It consists of cells such as blood monocytes and macrophages found mainly in the Kuepfer cells in liver, the lung and the spleen. Shortly after intravenous injection, the liposomes become coated by serum proteins called opsonins. Once they are opsonized, they will rapidly be phagocyted by the RES cells, and the major part of the injected liposomes will be accumulated in the liver and spleen [19]. As shown in Figure 2.3, depending on their size, shape and surface charge, nanoparticles display disparate in-vivo fates.

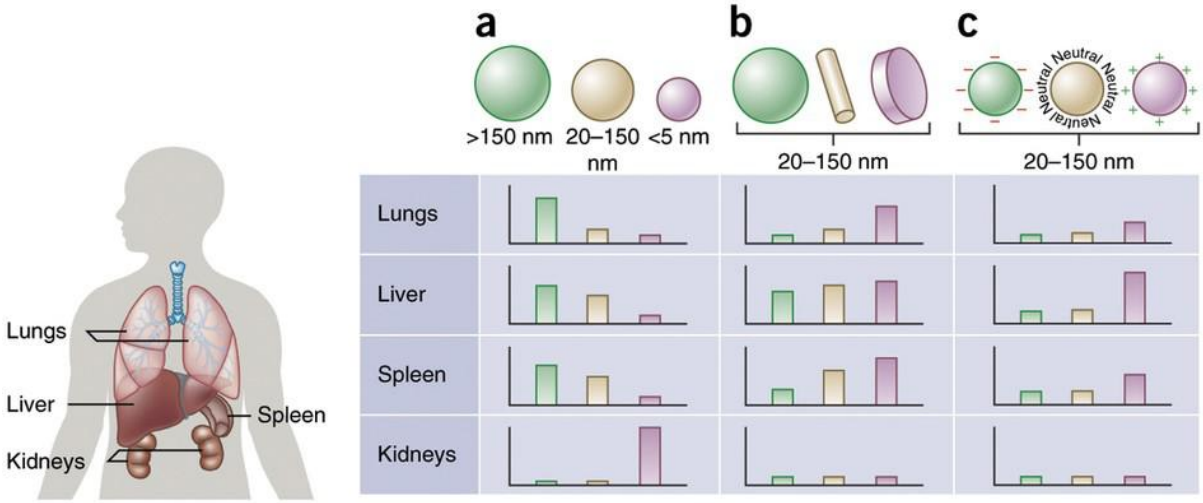

Figure 2.3: Accumulation of nanoparticles in the lungs, liver, spleen and kidneys depending on their (a) size, (b) shape and (c) surface charge [19].

From Figure 2.3, small-sized nanoparticles (including liposomes) with diameters <5 nm rapidly undergo renal clearance upon intravenous administration and are filtered out by the kidneys. In addition, due to the presence of vascular fenestrations measuring 50–100 nm in the liver, nonspecific accumulation of larger particles occur. Consequently, small liposomes (< 70 nm in diameter) show shorter circulation time as they extravasate through the fenestrated capillary walls in the liver. Because opsonisation decreases with a decreasing in liposome size, liposomes with a size of 70 to 200 nm will have a greater chance to escape from RES and remain in the circulation longer to eventually reach their target. Small liposomes have a relatively larger surface area, and will have a lower density of opsonins on the membrane surface which results in lower uptake by the macrophages.

Moreover, particles >200 nm are rapidly filtered by the spleen, due to the 200–500 nm size range of inter-endothelial cell slits. Therefore, large liposomes (>200 nm in diameter) are rapidly opsonized and taken up by the (RES) disappear from the blood circulation within short time and primarily end up in the spleen.
Finally, larger, more rigid particles in the micrometer range (2–5 μm), have been shown to accumulate readily within capillaries of the lungs, providing possibly a distinct advantage when targeting one of the predominant sites of metastatic disease. In this case, resident macrophages of the liver, spleen and lungs contribute to substantial particle uptake. Taken together, nanoparticles averaging ≈100 nm generally prove long-lasting in the circulation.

Particle Shape: The circulation half-life of a particle is also heavily affected by shape. Novel 'top-down' and 'bottom up' fabrication techniques have enabled the exploration of different geometries of nanoparticles, including cylindrical and discoidal shapes, which have been shown to exhibit pronounced effects on pharmacokinetics and biodistribution [19]. Different nanoparticle shapes exhibit unique flow characteristics that substantially alter circulating lifetimes, cell membrane interactions and macrophage uptake, which in turn affect biodistribution among the different organs. The principle of form follows function has heavily influenced nanoparticle architecture, with distinct geometries affecting hemorheological dynamics, cellular uptake and in vivo fate (Figure 2.3). As an example, discoidal particles exhibit unique tumbling and margination dynamics that favor vessel wall interaction substantially more than spherical particles, with implications for particle binding and adhesion to endothelium [19].

Particle Charge: Nanoparticle surface charge represents another design feature that can be tailored to prolong circulation lifetimes and selectively enhance accumulation at specific sites of interest (Fig.2.3). NPs with neutral and negative surface charges have been shown to reduce the adsorption of serum proteins, resulting in longer circulation half-lives. Neutral-charged liposomes with tightly packed membranes tend to remain longer in the circulation and exhibit increased drug retention, compared to charged systems. In addition, certain plasma proteins have an affinity for liposomes, and the affinity is enhanced if the liposomes are charged. In particular, cationic systems are expected quickly interaction with various components in systemic circulation and thus having shorter half-life in vivo [19]. It is also known that anionic liposomes containing negatively charged lipids such as phosphatidyl-serine (PS), phosphatidic-acid (PA) and phosphatidyl-glycerol (PG) are quickly taken up by macrophages and thus disappear from the circulation in short time. In Figure 2.3, taking into account singular design parameters of size, shape and surface charge independent of one another. We can conclude that the in-vivo biodistribution of the particles relies on the interplay of several of the above parameters.

2.2 Liposomes Synthesis Techniques

Since their discovery by Bangham et. al [53], numerous lab-scale and a few large scale techniques for liposome preparation have been developed, each with its own advantages and possible limitations. The present section aims at providing a concise review of liposomes conventional preparation techniques, focusing on the processes tailored towards nano/micro scale liposome fabrication of MLVs, LUVs and SUVs as opposed to large micro-scale liposomes like giant unilamellar vesicles (GUVs).

2.2.1 Conventional Fabrication Methods

The key factor which governs the manufacture of liposomes is the realization that lipid/ phospholipid membranes form as a result of unfavourable interactions between lipids or phospholipids and water molecules. Thus, the emphasis in making liposomes is not towards assembling the membranes, but towards getting the membranes to form vesicles of the right size and structure, and to entrap materials with high efficiency and in such a way that these materials do not leak out of the liposomes randomly [54]. As a result, liposome synthesis generally involve four basic stages which include: drying down lipids from organic solvents; dispersing the liquid in aqueous media, purifying the resultant liposome and analyzing the final product [21]. In the following sections, some of the most applied conventional methods of liposome production are described.

Bangham Method: The Bangham method is one of the first methods for liposome formation and is still widely used [3, 21]. The process involves the dissolution of lipids in an organic phase, the removal of the organic solvent, usually via evaporation, and finally the formation a lipid film [55]. The final step is the dispersion or hydration of the lipid film with an aqueous media, carried out in conjunction with agitation to separate the swelling lamellae from the vessel surface and form sealed spherical structure. The main drawback of the Bangham method lies in the solvent removal stage which is time-consuming. Furthermore, this technique often produces liposomes who are several microns in size (usually MLVs) which limit their consumption due to low entrapment efficiency specially for water soluble active agents. In addition to the difficulty in removing organic solvent, this technique is associated with small scale production rates which limits its use for large-scale, industrial applications [55].

Detergent Depletion Method: The detergent depletion is a mild process for the production of a wide variety of vesicle types and highly homogeneous liposomes [55]. The method is based on the formation of detergent-lipid micelles, followed by the removal of the detergent to form liposomes. The disadvantages of this method are that the final concentration of liposomes in the solution as well as the entrapment efficiency of any

hydrophobic compound are very low. The detergent also remains in the formulation. Also, because the size and homogeneity of liposomes produced are based on the rate at which the detergent is removed and the initial ratio of detergent to phospholipid, this method is very time consuming. Furthermore, the process of removing the detergent may also remove any other small hydrophilic compound [55].

Cross-Flow Filtration (CFF) Detergent Depletion Method: In 1998, Peschka et al. [56] developed a combined conventional detergent depletion method with a cross-flow technique as shown in Figure 2.4, a combination which can meet the demand for the fast removal of detergents.

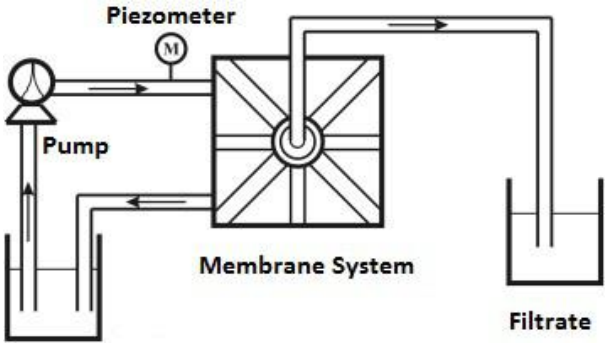

Figure 2.4: Schematic representation of the experimental setup of a CFF unit [41].

The cross-flow filtration unit consists of a starting reservoir (which contains the mixed micelle solution which is subjected to tangential filtration), a pump, a filtration device (membrane system with a cutoff of a selected molecular weight) and tubing with an integrated rotary slide valve and a manometer to monitor pressure. As the pressure on the membrane increases, fast removal of detergent occurs. By using the cross-flow filtration process, liposomes of defined size, homogeneity and high stability can be obtained. Large quantities of liposomes can be produced in a significantly shorter time compared with other methods used for detergent removal. In addition, sterile products can be obtained by these methods when starting with sterile filtered mixed micelles and autoclaved devices. The waste filtrate can also be recycled to minimize the production costs [41]. Regardless of the advantages of this method compared with other liposome formation techniques, there is still the issue of residual ethanol in the final product [17].

Emulsion: Emulsion methods for the production of liposomes generally involve the formation of a water-in-oil emulsion through the addition of a small amount of aqueous media to a larger volume of immiscible organic solution containing the phospholipid [17]. The mixture is agitated to disperse the aqueous media as tiny droplets throughout the organic solvent and the lipid aligns itself into a monolayer at the boundary between the organic and aqueous phases [57]. The size of the droplets is controlled by the agitation

applied and the amount of lipid present, since there must be sufficient lipid to surround the droplet or it may fuse with other droplets [58]. The water-in-oil emulsion is transformed into a liposomal suspension through the formation of a double emulsion. The organic solution containing the water droplets is added to a large volume of aqueous media and agitated, producing a water-in-oil-in-water emulsion. A lipid monolayer also forms around the organic droplets producing aqueous cores surrounded by two lipid monolayers that are separated by an organic layer [17]. Unilamellar liposomes with high entrapment of the initial aqueous media can then be formed by the removal of the organic solvent, for example, by passing a stream of nitrogen through the double emulsion [58].

Injection Method: The ethanol injection method was first described in 1973 by Batzri and Korn [13]. It involve the dissolution of the lipid into an organic phase, followed by the injection of the lipid solution into aqueous media, forming liposomes [55]. The particle size of liposomes produced by this method is a function of lipid nature and concentration, the drug to lipid ratio and the organic solvent and aqueous phase composition [32]. Overall, the ethanol injection method is a simple method, but some lipids are poorly soluble in ethanol and heterogeneous liposomes are formed if adequate mixing is not achieved [55]. Notably, the inkjet method, a modern variation of the ethanol injection method, was developed by Hauschild et al. [59] for liposome formation with excellent control on particle size and high potential for scaling up.

Membrane Contractor: Developed by Charcosset el al. [31], this technique for lipid vesicles preparation was developed for large-scale industrial production of liposomes for both its scaling-up properties as well as its large range of possible operating conditions. This new process for solid lipid nanoparticle formation consisted of a membrane contractor, which can be used for large scale production of liposomes [17]. Figure 2.5a shows a device using a syringe for injection (V = 60 mL); Figure 2.5b a pilot plant (V = 3 L) using two pumps for the injection of both organic and aqueous phases through a membrane.

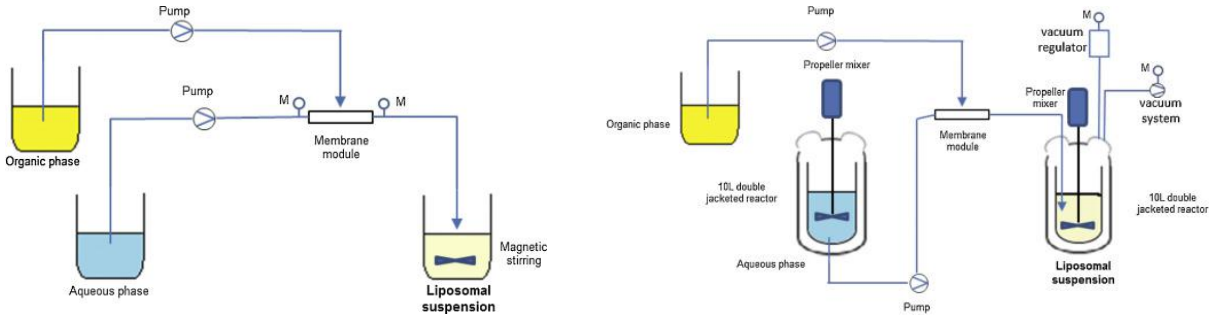

(a) Small Volumes Set-up (V= 60 mL) (b) Large Volumes Set-up (V= 3L)

Figure 2.5: Schematic drawing of the experimental set-up for preparation of liposomes at intermediate volume of preparation using membrane injection [31].

In this method shown in Figure 2.5, a lipid phase was pressed at temperatures above the melting point of the lipid through a membrane with a specified pore size. Nitrogen gas at pressures below 6 bar was sufficient for passing the molten phase through the membrane. Solid lipid nanoparticles with particle size between 70 and 215 nm were formed and collected by recirculation of a cold stream of aqueous phase inside the membrane module. The advantages of this new technique it that it is advantageous for the preparation of small vesicles having narrow size distributions, with good reproducibility, yield and stability [31].

Reverse Phase Evaporation Method: The reverse-phase evaporation process was first described by Szoka and Papahadjopoulos [35]. The technique is carried out by dissolving the lipids in an organic solvent, adding a small volume of aqueous phase, then sonicating the solution to produce inverted micelles [55]. The organic solvent is removed using a rotary evaporator and a viscous gel forms [60]. A disadvantage of the reverse-phase evaporation method is that the compound to be encapsulated within the vesicles is in contact with an organic solvent, therefore the process is not suitable for fragile molecules such as peptides [61].

Heating Method: The heating method developed by Mozafari [54] to produce liposomes involves hydration of the phospholipid components in an aqueous solution containing 3% (vol) glycerol and increasing the temperature to 60 °C or 120 °C, depending on the absence or presence of cholesterol, respectively. Glycerol is utilized since it is a water soluble and physiologically acceptable chemical with the ability to act as an isotonising agent and increase the stability of lipid vesicles due to preventing coagulation and sedimentation. No degradation of the lipid ingredients was reported for liposomes fabricated by the heating method [62]. Also there is no need for sterilization once high temperature (i.e. 120°C) is used in this technique. A further improved version of the heating method, called the Mozafari method [62], has recently been employed for the encapsulation and targeted delivery of the food-grade antimicrobial nisin. The Mozafari method allows large-scale manufacture of the carrier systems in one step without the need for the prehydration of the ingredient material, and without employing toxic solvents or detergents [55].

Supercritical Fluid Methods: Supercritical fluids technology (SCF) has been utilized in liposomal preparation because of its friendliness, non-toxicity to the environment and its possibility to achieve solvent-free liposomes and industrial- scale of liposome production [63]. It can provide sterile operating conditions and one-step production that can alleviate the current liposome sterilization issues [55].
Several SCF processes have been used to generate drug carrier systems (Figure 2.6).

This includes: Supercritical Anti-Solvent (SAS) process [64, 65], the Rapid Expansion of Supercritical Solutions (RESS) process [64, 66], the Aerosol Solvent Extraction System (ASES) process [7], the Gas Antisolvent Precipitation (GAS) [5], and the Particles from Gas-Saturated Solutions (PGSS) [30]. Various DG processes have been developed to produce drug carrier systems. The processes include the Supercritical Liposome Method [67], the Supercritical Reverse Phase Evaporation (scRPE) method [68], Depressurization of an Expanded Solution into Aqueous Media (DESAM) technique [17], SuperFluids phospholipid nanosomes (SFS-CFN) process [69], the Supercritical Fluid Extraction of Emulsion (SFEE) [4], the Depressurization of an Expanded Liquid Organic Solution–Suspension (DELOS-SUSP) [8], and the Continuous Anti-Solvent (CAS) [70].

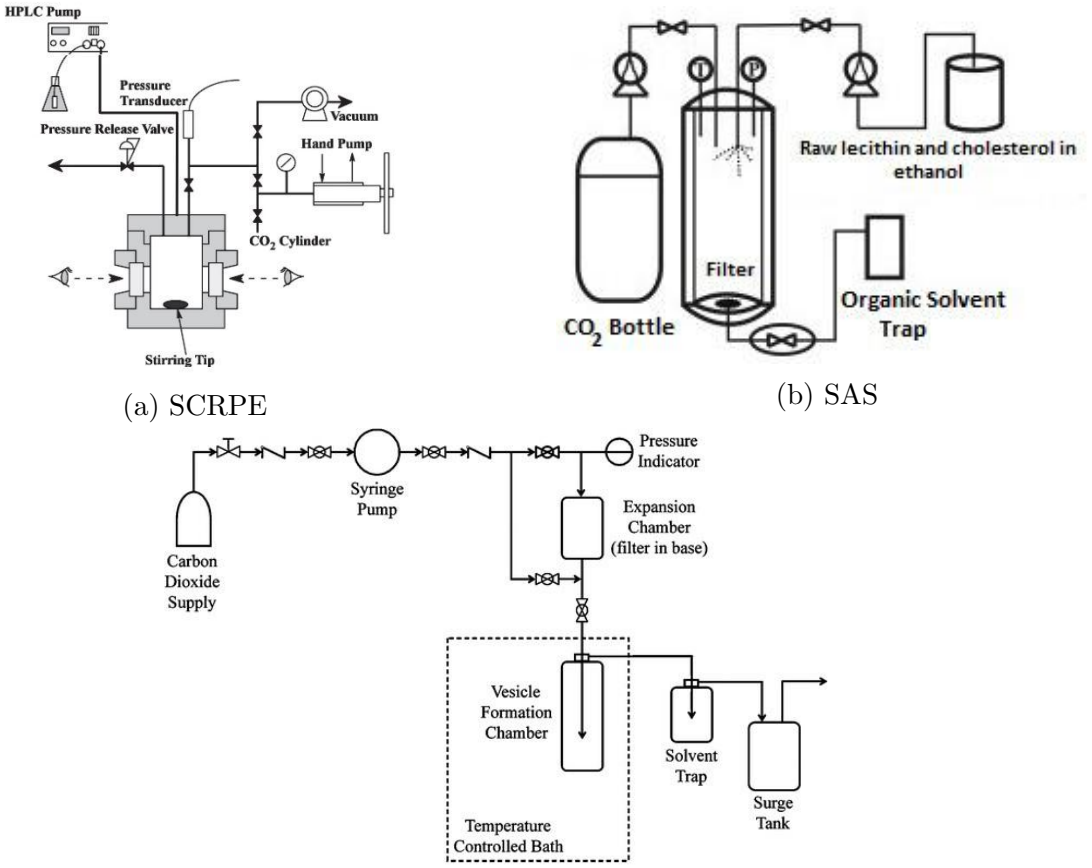

(a) SCRPE

(b) SAS

(c) DESAM

Figure 2.6: Super Critical Fluid Processes for Liposome Production.

On the downside, the encapsulation efficiency using SCFs methods is usually lower than that achieved using other conventional liposome formation techniques [55] and the stability of the liposomes is short [71]. Otake et al. [68] recently developed a new method known as the improved supercritical reverse phase evaporation (ISCRPE) technique to avoid the use of organic solvents in liposome formation and enhance the stability and the drug loading efficiency of the vesicles.

High-pressure Homogenization Method (HPH): High–pressure homogenizers are used for the preparation of liposomes and lipid dispersions because of their vesicle disruption capability. The sample is injected at high and constant pressure in a specially designed part of the homogenizer where rearrangement of liposome structure takes place due to turbulence, cavitations and shear [55, 61].

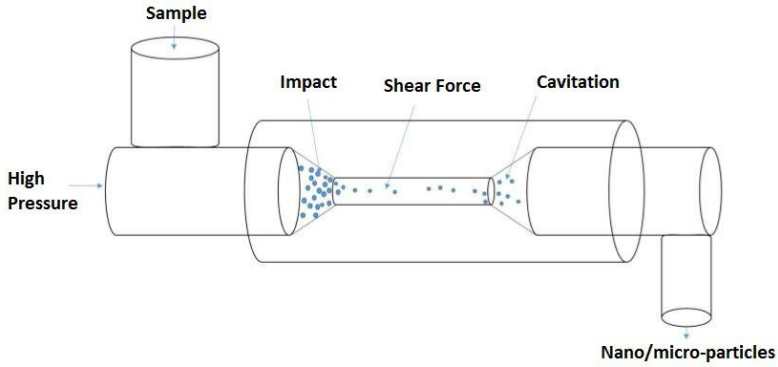

Figure 2.7: Schematic of high-pressure homogenization showing the process of impact, shear and cavitation. [61].

Properties of liposomes prepared by high pressure homogenization depend on the interplay of different experimental parameters: Mean liposome diameter decreases with increasing inlet pressure, number of cycles and ethanol concentration, and increases raising ionic strength [72]. HPH is especially useful for the production of very small liposomes as they are especially suitable for intravenous applications [55].

Dual Asymmetric Centrifugation (DAC): First reported by Massing et al. [73] for the preparation of liposomes, DAC differs from conventional centrifugation by an additional rotation of the sample around its own vertical axis. While the conventional centrifugation constantly pushes the sample material outwards, this additional rotation constantly forces the sample material towards the center of the centrifuge as shown in Figure 2.8. This unique combination of two contra-rotating movements results in shear forces, mechanical turbulence and cavitations thus resulting in efficient homogenization.

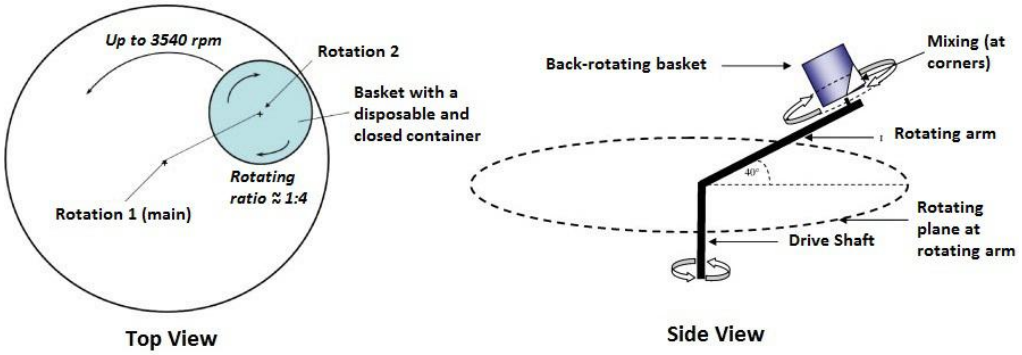

Figure 2.8: Schematics of the principle of Dual Asymmetric Centrifugation (DAC) [73].

It was shown that the DAC speed, the lipid concentration, the homogenization time and the addition of a mixing aid (glass beads) are all critical for the size of the liposomes. Optimized conditions resulted in liposomes of 60 ± 5 nm and a trapping efficacy of 56 ± 3.3 % for the model compound calcein [73]. On the downside, although DAC has high trapping efficiency, this method is especially useful for producing batch sizes of about a gram or even less [40].

Freeze-drying: Freeze-drying is a relatively new method for the preparation of submicron liposomes of narrow size distribution which was developed by Li et al in 2005 [74]. The method is based on the formation of a homogeneous dispersion of lipids in water-soluble carrier materials. To obtain the lipid-containing solid dispersion, liposome-forming lipids and water-soluble carrier materials are dissolved in tert-butyl alcohol/water co-solvent systems to form an isotropic monophase solution, and then the resulting solution is lyophilized after sterilization by filtration through 0.2 μm pores. On addition of water, the lyophilized product spontaneously forms homogeneous liposome preparation which are also sterile and pyrogen-free [74]. In this method, the lipid/carrier ratio is the key factor affecting the size and the polydispersity of liposome preparation.

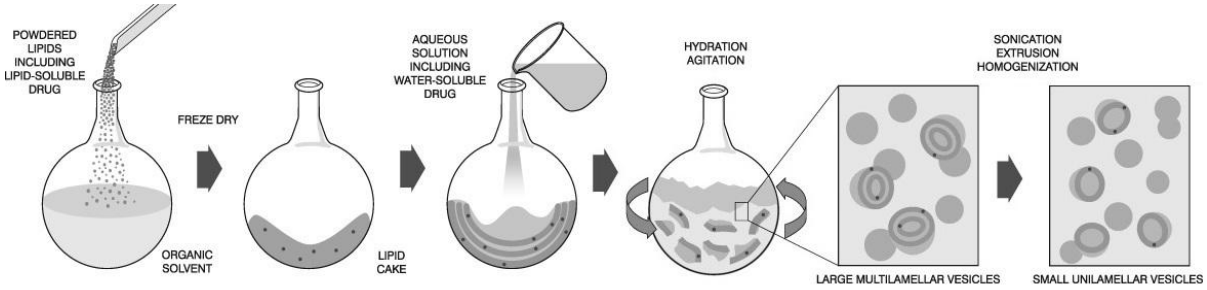

Figure 2.9: Schematic diagram explaining the process of freeze-drying [40].

Freeze-drying processes still suffer from some difficulties in terms of residual water content and drug leakage due to ice crystals as well as phase transition of bilayers during rehydration. Besides, this process naturally consumes a larger amount of energy with considerably high cost due to the lyophilizing step [40]. Finally, the process is very time consuming as it requires first, freezing the sample at -40 °C for 8 h, followed by drying for 48 hours and finally drying the product at 25 °C for 10 h [17].

A summary of the advantages and disadvantages of the conventional methods of liposomal production is reported in Table 2.3.

Table 2.3: Advantages and disadvantages of conventional methods of liposomal production. (Adapted from [17, 55])

Methods	**Advantages**	**Disadvantages**
Bangham	Simple Process	Contains the organic solvent, requires vigorous agitation, large vesicles without control on particle size, time consuming, sterilization issue.
Ethanol Injection	Simple Process	Organic solvent residue, time consuming, sterilization issue.
Reverse Phase Evaporation	Simple design, suitable encapsulation efficiency	Large quantity of organic solvent use, time consuming, sterilization issue.
Detergent Depletion	Simple design, homogenous product, control of particle size	Organic solvent and detergent residue, time consuming, poor entrapment efficiency, low yield, need sterilization.
Cross-Flow Detergent Depletion	Homogeneous product, control of particle size. Sterile products. Waste filtration to minimize production costs.	Cross-flow membranes are prone to failure. Some detergent residue remain.
Emulsion	Simple, potential to fabricate multivesicular liposome for delivery of multiple compounds that are not stable in combination	Large amount of organic solvent, requires vigorous agitation, sterilization issue.
Dense Gas Techniques	Possible in situ sterilization, producing stabilize and homogenous liposome, low organic solvent consumption.	Need to multiple stages to achieve the final size of liposome. High pressure(200-300 bar) readily block nozzles. High capital cost, low yield and encapsulation efficiency.
Dual asymmetric centrifugation	Simple method, homogenous liposome production with 60 nm size, high trapping efficiency.	Not suitable for bulk production, high pressure, with agitation.
High-pressure Homogenization	Produce liposome with diameter up 100 nm, simple design, suitable for bulk production.	High pressure, sterilization issue, non homogenous liposome production, organic solvent residue.
Heating method	Simple design, organic solvent free, no sterilization need, scale-up.	Use of high temperature that may not be cost effective for large scale.
Freeze-drying method	Produce highly homogenous liposome solution which are also sterile and pyrogene-free	Residual water content and drug leakage. High energy consumption. Time consuming.
Membrane Contractor	Simple process for controlled particle size, no use of organic solvent	High temperature, membrane blockage and sterilization issues.

In summary, limitations of conventional preparation methods include complexity and length of procedures, low drug encapsulation efficiency and polydisperse size distributions. Furthermore, most of these techniques are not suitable for the encapsulation of sensitive substances because of their exposure to mechanical stresses (e. sonication, high-shear homogenisation, a high pressures), potentially harmful chemicals (eg. volatile organic solvents and detergents) or low/high values of pH during the preparation. Recently, new procedures have been reported for producing liposomes to address the issues in conventional production technologies. They include microfluidic methods which are going to be addressed in the next section.

2.2.2 Microfluidic Techniques

Microfluidics is a technology that enables precise control and manipulation of fluids and fluid interfaces at the micrometer scale. In microfluidic chips, the fluid streams can merge and form well-defined interface by laminar flow, as opposed to the typically chaotic flows in bulk mixing (BM) [25]. According to the difference in manipulation modes of flow, microfluidics is categorized into two classes: continuous-flow microfluidics and digital (droplet-based) microfluidics [1]. In continuous-flow microfluidics, liquid flow is continuously manipulated through micro-fabricated channels, whereas discrete and controllable droplets are manipulated in droplet-based microfluidics [37].
In this sub-section, the fundamental theory of fluid and mass transfer, and the implication of using microfluidic devices for mixing are firstly discussed. This is followed by a review of the use of different microfluidics techniques for the production of liposomes, emphasizing on continuous-flow microfluidics based liposomal production. Finally, the advantages of liposome formation using microfluidics compared to traditional bulk mixing are also discussed.

Fluid Dynamics Principles at the Microscale

A microfluidic mixer is not simply a miniaturized version of a macroscale mixing device. It has to be designed in such a way as to leverage the physical characteristics of mass and fluid transfer in a micro-confined domain [24]. This is because many physical characteristics, including the surface-to-volume ratio (SVR) and diffusion-based mass transfer, do not scale linearly from macro- to micro-domains [25]. Another peculiarity of microfluidic systems is represented by the omnipresence of laminar flow, due to the predominant role exerted by viscous forces [75]. These factors thus become significant at the microscale, and their effects should be considered while designing and developing microfluidic devices [24].

The behavior and motion of fluids can be described by the Navier-Stokes equations (Eq.2.1), which are based on a couple of partial equations. The first equation is the

conservation of mass, which states for a fluid in steady-state, that the rate of mass entering a system is equal to the rate of mass leaving the system. The second equation is the conservation of momentum, which states that in a closed system (no exchange of any matter with the outside and no outside forces acting) is the total momentum constant. The third equation conservation of angular momentum, which states that when no outer torque acts on an object or closed system, no change of angular momentum can occur. The fourth and last equation is the conservation of energy, which states that the total energy of an isolated system (a system where no matter or energy can pass) cannot change.

The final form of the equations, for incompressible Newtonian fluids, is presented below:

$$\rho \left[\frac{\delta v}{\delta t} + (v \cdot \nabla) v \right] = -\nabla p + \mu \nabla^2 + F \tag{2.1}$$

Where: v is the flow velocity, ρ is the fluid density, p is the pressure, μ is the dynamic viscosity and F represents outer forces.

From Eq. (2.1), one can determine which forces that are governing for a specific system. At high flow rates and long characteristic length scales the inertial and mass movement dominates and the flow will be turbulent, while at low flow rates viscous forces dominate and the flow will be laminar. As shown in 2.10, fluid flow is generally categorized into two regimes: laminar (a) and turbulent (b). In laminar regime the fluid flows in parallel layers with no cross currents perpendicular to the main flow direction, whereas turbulent flow is generally characterized by the formation of vortices and flow fluctuations in space and time [75].

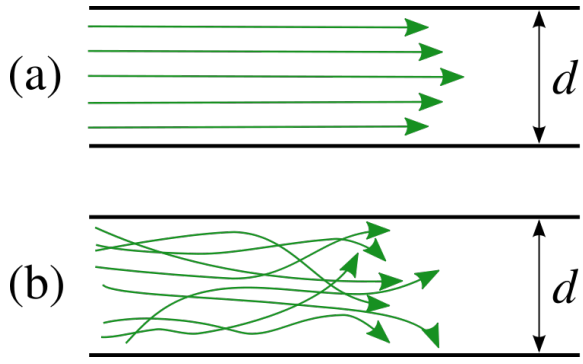

Figure 2.10: Fluid flow lines represented in the case of (a) laminar and (b) turbulent flow regimes [75].

The Reynolds number (Re) and gives the ratio of inertial forces to viscous forces. A fluid flow is then said to flow laminar if Reynolds number is low (Re < 1500) but to be turbulent if the number is high (Re > 1500). The Reynolds number can be derived from

the Navier-Stokes equations, (Eq.2.2), by neglecting the non-linear term $\rho(\mathrm{v}\cdot\nabla\ \mathrm{v})$ (which can be done at low flow velocities) and making the equation dimensionless (replace all physical variables in units of the characteristic length scale).

The Reynolds number is defined as:

$$Re = \frac{\rho D_h v}{\mu} \tag{2.2}$$

Where: ρ is the density, D_h is the hydraulic diameter or characteristic length, v is the mean velocity of the fluid and μ is the dynamic viscosity. At low Reynolds number the viscous forces tend to dominate over the inertial forces, resulting in linear flows (laminar flow). The hydraulic diameter is a term used when handling flows in non-circular channels. In other terms, the hydraulic diameter is used so one can calculate different entities, such as Reynolds number, as if the channel of interest were circular. It is defined as:

$$D_h = \frac{4A}{P} \tag{2.3}$$

Where: A is the cross-sectional area and P the wetted perimeter of the cross-section. Often, micro-system deals with very small Reynolds number $10^{(-6)}$, and the flow can be said to be laminar in most microfluidic devices.

Notably, in a fluidic domain where the flow is laminar, mass transfer is dominated by passive molecular diffusion and advection. Diffusion is defined as the mechanism of molecule transport from a domain of higher concentration to a domain of lower concentration by Brownian motion, resulting in a gradual mixing of material. Diffusion-based mass transfer is described mathematically using Fick's laws [76].

$$J = -D\frac{d\phi}{dx} \tag{2.4}$$

Where: J is the "diffusion flux," and measures the amount of substance that will flow through a unit area during a unit time interval, ϕ is the species concentration, x is a spatial coordinate, and D is the diffusion coefficient. For spherical particles, D can be derived from the Stokes–Einstein equation [77]:

$$D = \frac{kT}{6\pi\mu r} \tag{2.5}$$

Where: k is Boltzmann's constant; T is the absolute temperature; r is the radius of the particles (or molecules) and μ is the dynamic viscosity of the fluid medium. The diffusion coefficient for a small molecule in water at room temperature has a typical value of $10^{-9}m^2s^{-1}$ [76].
Diffusion is a non-linear process in which the time required for a species to diffuse scales quadratically with the distance covered. On a microscale, the diffusion distance can be extremely small, especially if fluid streams are hydrodynamically focused. A decrease in diffusion distance has the effect of dramatically reducing the time required for complete mixing to be achieved. Therefore, diffusion becomes a viable method to transport particles and mix chemical species in microfluidic systems [24].

Microfluidic Liposomes Fabrication Processes:

Based on the flow types in microfluidic devices, nanoparticles synthesis can be primarily divided into two categories: The single phase continuous flow synthesis and emulsion (2-phase) micro droplets/segmented flow synthesis [78]. The easiest and most basic design for a micro-mixer is represented by either T- or Y shaped channel micro-mixers [79]. The mixing process in this type of micro mixer is obtained by guiding the two liquids to be mixed in contact through a flow-through channel. Continuous flow synthesis mix and react reagents in microchannels under diffusion-based laminar flow reaction conditions. Reaction times, temperatures, mixing efficiency, and reagent concentrations are parameters to control particle quality. The microfluidic generation of micro droplets for nanoparticle synthesis is taking place in micro droplet reactors to improve the mixing efficiency in microfluidic channels, and further reduces the particle size distributions.

Droplet Generators: Within the microfluidic context, droplet-based microfluidics make use of small volumes (droplets) of fluids to carry out different chemical reactions and assays [6]. The devices that are used to create these droplets are called Microfluidic Droplet Generators (MFDG). MFDGs produce monodisperse emulsions of two immiscible fluids when shearing forces of a continuous phase (CP) overcome the surface tension of the disperse phase (DP), thus forming droplets. These oil-in-water O/W or water-in-oil W/O droplets, are then used as confined reaction containers in which reagents and conditions can be manipulated to our benefit [6]. Since these droplets are in the order of Pico-liter to Nanoliter volumes the reagent consumption is minimal thus allowing high-throughput screening of chemical libraries and conditions at low cost, and offering a unique environment for chemical synthesis.
In droplet microfluidic devices, T-shaped junction and "flow-focusing" are the most commonly used channel geometries for generating droplets [79]. Droplet formation in a T-junction was first proposed by Thorsen et al. [80] to form water droplets in a set of oil phases. In the T-junction device, the disperse phase and continuous phase flowed out

from two perpendicular channels and formed an interface at the junction. Due to the shear force exerted by the continuous phase, the disperse phase thinned gradually and eventually broke into droplets.Droplet size in this type of microfluidic devices depends on several parameters such as: the dynamic behavior related to the flow rates, intrinsic properties of the fluids (viscosities, densities and interfacial tension) and parameters correspondent to the geometry of the device [6].

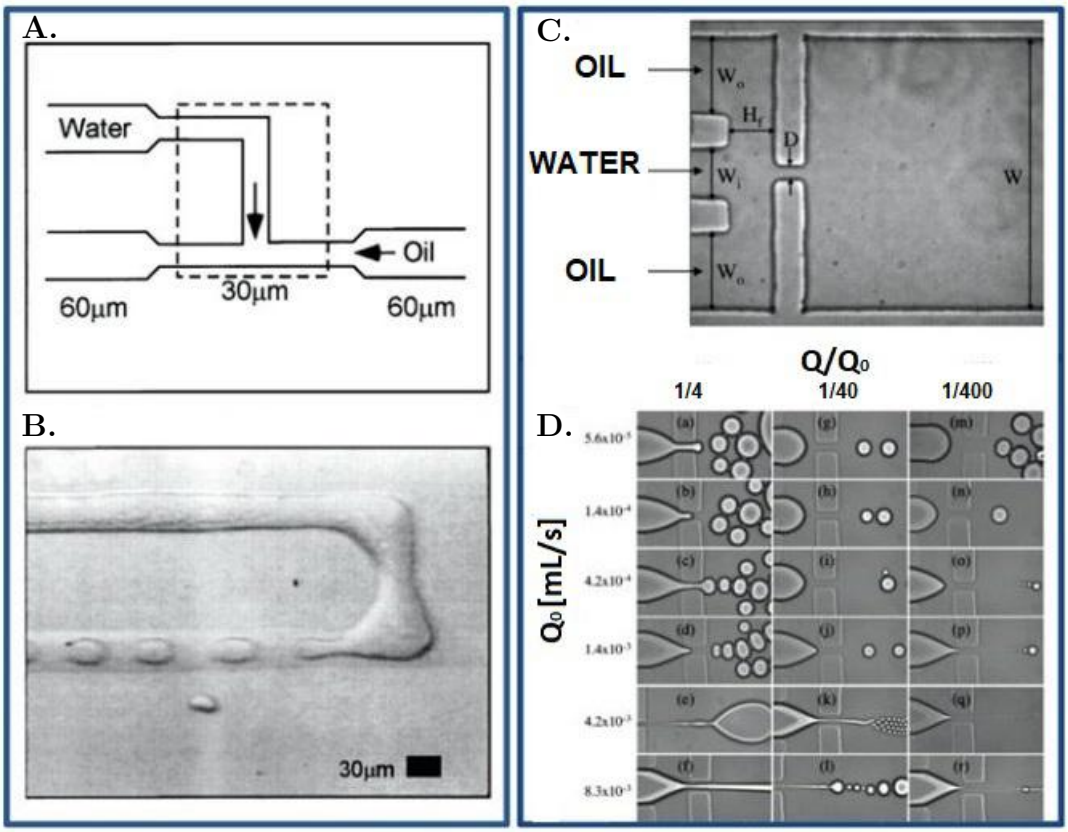

Figure 2.11: Droplets generation in microfluidic devices: (A) Channel layout of T-junction device. (B) Formation of droplets in a T-junction device. (C) A "flow-focusing" droplet device. (d) Droplets generation at different flow conditions in "flow-focusing" device.

Conventional methods for making droplets involve manual or mechanical agitation of multiphase fluids. Since there is no way to control the uniformity of the shear or impact stresses involved in droplet breakup, droplets formed in these ways are highly polydisperse in size. In contrast, using microfluidic devices with prescribed channel dimensions and geometries, and by controlling the flow rates of two immiscible liquids, the flow conditions in droplet breakup can be highly repeatable and thus it is feasible to generate microdroplets of uniform size distributions (1–3% dispersity) [79]. Applications of this technology are found in high added value industries such as those in pharmaceuticals, photonics, aggressive chemical industry, small molecule synthesis, molecular biology, and cosmetics [6].

Continuous Flow 2D HFF: Typically, the process of HFF involves forcing a stream of lipid in alcohol solution to flow in the central (or inner) channel of a microfluidic device. The lipid stream is then intersected and sheathed by two lateral (or coaxial) stream(s) of a water phase (typically distilled water or aqueous buffers) [24]. This process is shown in Figure 2.12, where we see a stream of lipid solution dissolved in ethanol being hydrodynamically focused into a narrow sheet having a rectangular cross-section in the case of microchips with cross flow geometry, or a circular cross-section in the case of 3D annular coaxial chips. Microfluidic flow focusing techniques have been shown to produce uniformly dispersed liposomes and allow for direct control of liposome size via fine adjustments to either FRR or TFR [51]. Jahn et al. [37] postulated that: "decreasing the sample stream width to micrometer length scales allows for controlled and reproducible mechanical and chemical conditions across the stream width, especially compared to more traditional bulk-phase preparation techniques (i.e., test tubes and beakers)". Figure 2.12B illustrates one of such bulk method which is the process of ethanol injection.

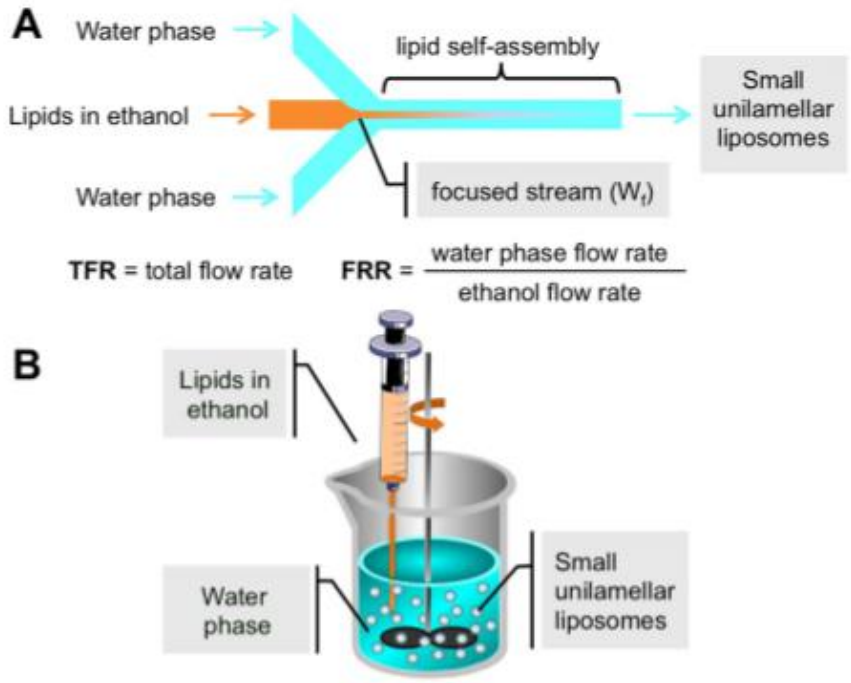

Figure 2.12: Schematic representation of the process of liposome formation using (A) a microfluidic device by the process of liposome (SUV) self-assembly and (B) via the ethanol injection procedure [51].

Compared to other bulk methods, this method is a relatively simply technique which results in the formation of small unilamellar vesicles (SUVs); therefore it does not require post-processing homogenisation steps. Like many microfluidic protocols, phospholipids are firstly dissolved in ethanol; a small amount of the lipid solution is then injected into water, above the transition temperature (T_m), triggering SUV formation. Analogously to MHF, the formation of liposomes is ascribed to the miscibility of ethanol and water that

causes the diffusion of alcohol molecules into water and the consequent "self assembly" of lipids to form liposomes. The size and homogeneity of the SUVs is dependent upon the experimental parameters, specifically: lipid concentration, rate of injection of the alcoholic lipid solution and stirring rate [51]. Conventional bulk production of liposomes mainly relies on self-assembly of lipids in a bulk phase, which is heterogeneous and uncontrolled. The resultant liposomes are polydispersed in size and are multilamellar. Further post-processing by extrusion, freeze–thaw, sonication, and/or high-pressure homogenization is often required to produce mono-disperse solutions [51].

Confinement and well-defined mixing in microfluidics makes it attractive for production of liposomes ranging from tens of nanometers to tens of micrometers in diameter [25]. The self-assembly in microfluidics can be controlled by varying liquid flow rates, ratios of cross-flows and the composition and concentration of lipids, resulting in tunable sizes, and narrower size distributions [38]. Several studies on liposome production by planar (2D) flow focusing in microfluidics have been reported (Figure 2.13).

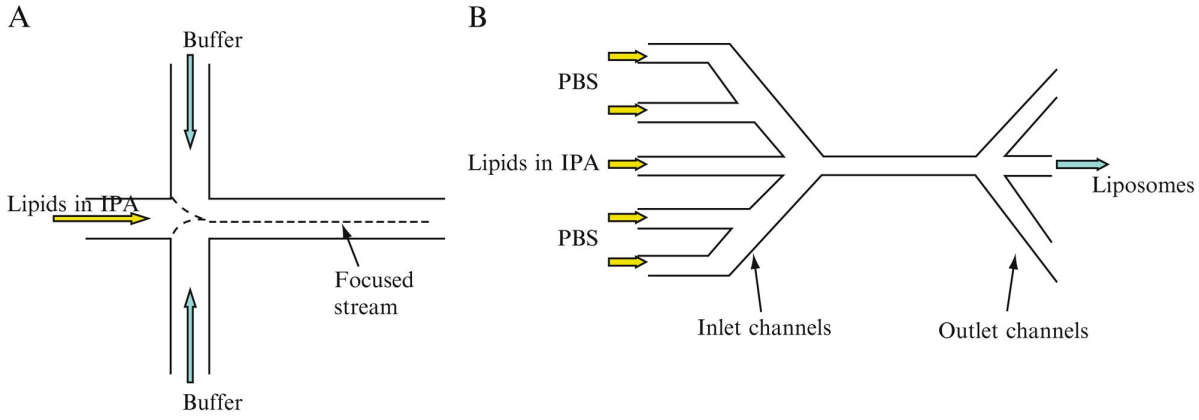

Figure 2.13: Schematic diagram of microfluidic channels for liposome formation: (A) three-inlet design [37] and (B) five-inlet design [38].

Jahn et al. (2004) [37] first reported on the controlled synthesis of submicrometer-sized liposomes through MHF, where an isopropyl alcohol (IPA) containing the dissolved lipids flows through a center inlet channel, and an aqueous solution flows through the two side inlet channels (Fig. 2.13A). The stream of lipids in IPA is hydrodynamically focused by two aqueous streams at the cross junction of the microfluidic chip [37]. Jahn et al. (2007) then made significant modifications in their microfluidic system to greatly improve the control over size and size distribution. As shown in Fig. Figure 2.13B, their new microfluidics device has five-inlet channels and three-outlet channels, which are fabricated in a silicon wafer. The lipid IPA solution is injected into the center channel of the microfluidics network, while phosphate-buffered saline (PBS) is injected into two side channels intersecting with the center channel. Owing to this three-outlet design, relatively high

liposome concentration were produced at the center point in the channel once the focused IPA stream is diluted to the critical concentration for formation of the more stable liposomes along the interfacial region [25].

Carugo et al. [51] evaluated the production of liposomes employing different microfluidic chips (see Fig. 2.14) and lipid formulations in terms of the size and homogeneity of the end product. Moreover, a detailed analysis of the effects of the operating parameters (especially FRR) on liposomes dimensions, taking into consideration the effect of residual alcohol on the viscosity of the liposomal samples and thus on the determination of liposome size by light scattering measurements was provided.

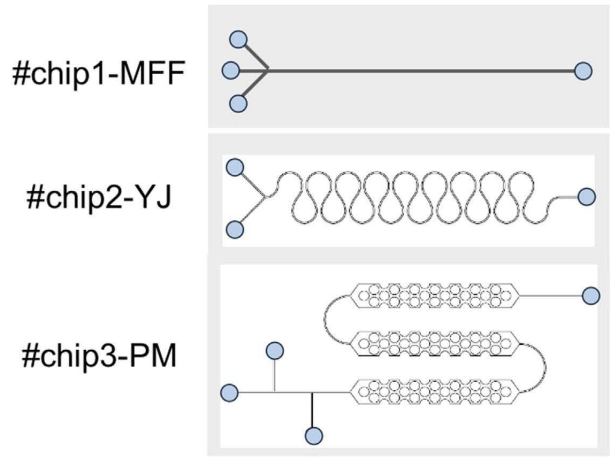

Figure 2.14: Schematic diagram of microfluidic channels for liposome formation with a table explaining the geometrical characteristics of the chips employed for the microfluidic experiments[51].

Liposomes produced using MHF were compared with those obtained by the bulk ethanol injection method [51]. Different device architectures have been considered for liposome production. Devices include microscale chips (cross-sectional dimensional range of 100–320 μm) with mixing channel displaying distinct architectural features (i.e., straight, serpentine-like, and containing micropillar structures) and scaled-up versions of microscale flow focusing architectures, with cross-sectional channel dimension in the millimetre range. In addition, the effective encapsulation of drugs by liposomes produced using MHF was investigated. Ivermectin was employed as a model drug since it has recently been shown to be a highly potent inhibitor of yellow fever virus replication and, although less efficiently, of several other flaviviruses. Results shows that this drug did not cause large modification of the liposome size produced by MHF microfluidics, as the liposome containing ivermectin were only marginally larger than the empty ones [51].

More recently, in May 2017, Michelon et al. [81] presented a simple T-junction plan focusing design for nanoscale liposome formation. Their work aimed to perform a sys-

tematic study of the liposome formation using planar (2D HFF) microfluidic devices with different channel aspect-ratios, as an alternative to enhance the throughput of liposome synthesis as shown in Figure 2.15.

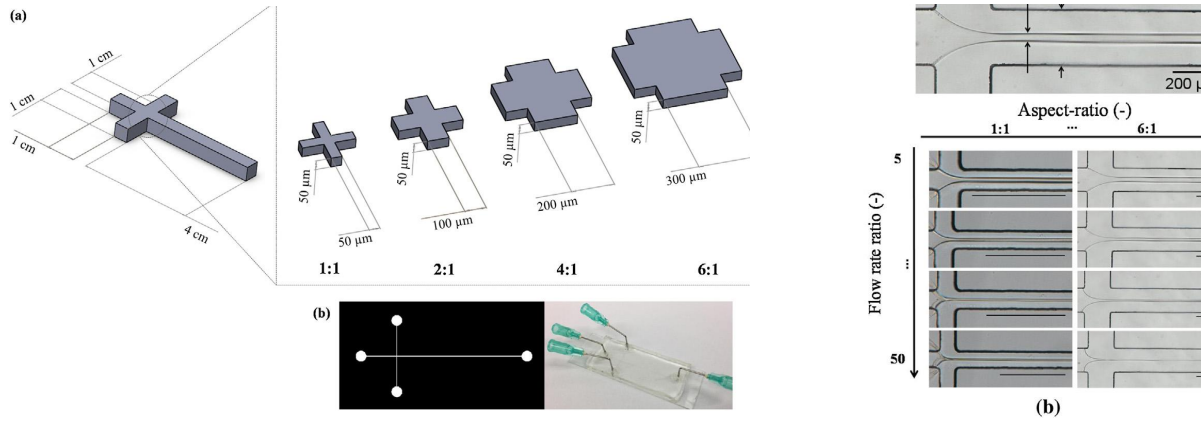

Figure 2.15: Schematic diagram of microfluidic device aspect-ratio and associated photo-mask for micro-fabrication [81].

Liposomes with a low polydispersity and a precise control of the size were successfully produced from alteration of the flow rate ratio and channel aspect-ratio. Higher aspect-ratio ensured rapid generation of liposomes with similar diameter and significant lower polydispersity index than the obtained by other batch technique. Besides, β-carotene was successfully incorporated into liposomes with efficiency of approximately 60% and was independent of the microfluidic device aspect-ratio [81].

Lately, efforts in hydrodynamic focusing shifted towards using cascaded streams to focus the sample stream first vertically, then horizontally, leading to the development of 3-D hydrodynamic flow focusing devices for the production of polymeric NPs.

3D HFF: Different authors have proposed micro-fabricated devices capable of focusing the sample horizontally and vertically [79, 82–89]. Such devices add an additional dimension of focusing and are often referred to as 3D hydrodynamic focusing devices to distinguish them from traditional 2D focusing devices. Building these devices requires complex methods such as multi-step photo-lithography, leading to an increase in fabrication cost. The process of 3D focusing in this device can be divided into two steps. First, the sample stream is focused in the vertical direction using microfluidic drifting. The lateral drift of the sample flow is caused by the effect of the Dean vortices induced by the centrifugal effect of the curve, which transports the fluid in the opposite side of the channel. Second, classic horizontal focusing is obtained using two horizontal sheath streams. The result of these two steps is a stream focused in both the vertical and horizontal directions.

3-D HFF microfluidic platforms have only been recently adopted for the synthesis of NPs, thus offering increased particle controllability and reproducibility. Recently Lim et al. [89], reported parallel synthesis of NPs using a multilayer microfluidic system to enhance the production yield without losing the advantages of reproducibility, controllability, and robustness of 3D HFF shown in Figure 2.16.

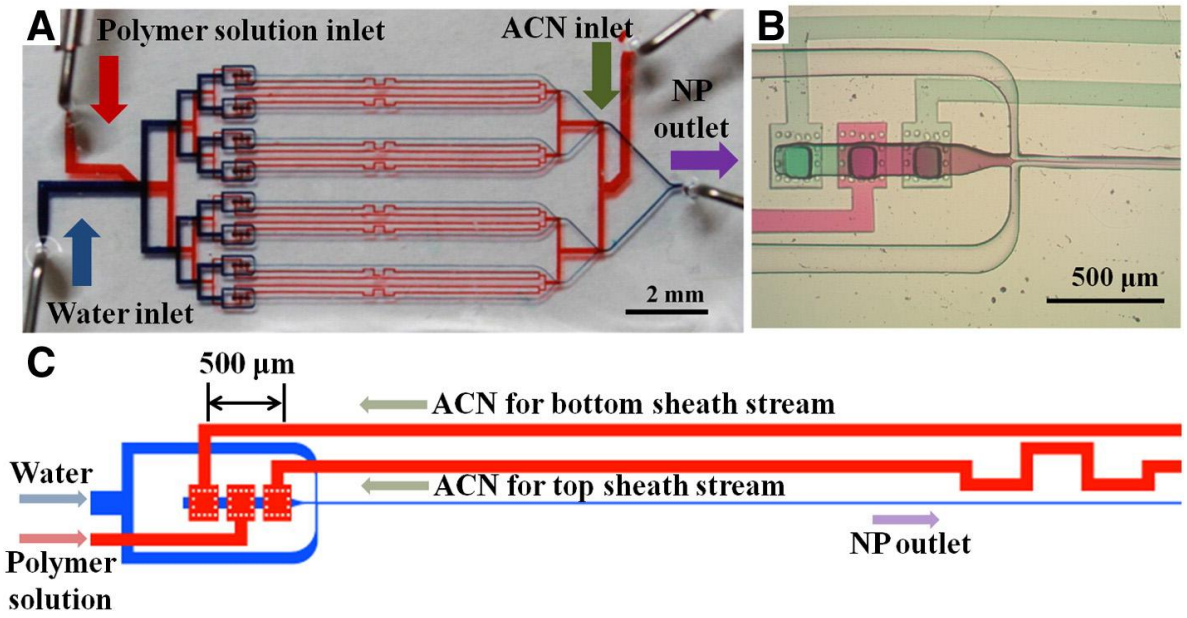

Figure 2.16: 3D HFF microfluidic device for parallel NP synthesis. (A) Top view of the Device. (B) Optical microscope image of the 3D HFF region. (C) Schematic illustration of one of the 8 parallel 3D HFF units in the device [89].

The device channels in Fig.2.16A were visualized using red and blue food coloring dyes in the upper and lower microchannels, respectively. In Fig.2.16B. the red and green food coloring dyes represent the PLGA-PEG polymer in ACN solution and pure ACN, respectively. The relevance of this novel microfluidic design for the development of polymeric PLGA-PEG NPs was assessed by synthesizing NPs in the range of 13–150 nm with high production rates. Microfluidic platforms also allowed systematic tuning of the biophysicochemical properties of NPs, facilitating their screening and optimization. They have demonstrated the controlled synthesis of PLGA-PEG NPs by rapid and tunable mixing in microfluidic platforms known as 2D hydrodynamic flow focusing (HFF) and 3D HFF. 3D HFF isolates the precipitating polymers from microchannel walls and eliminates microchannel clogging, which has enabled reproducible synthesis of monodisperse NPs with tunable sizes from 30–230 nm.

Conclusion

Several microfluidic devices have been developed to synthesize particles with diameters ranging from a few nanometers to several micrometers. Recent iterations have achieved sub-micron accuracy through the use of computational fluid dynamics to refine and improve chip design [83]. In this section, we reviewed nanoparticle synthesis in microfluidic systems which was either carried out either by continuous laminar flow or in multi-phase droplet reactors. In addition, we compared the process of 2-D and 3-D hydrodynamic flow focusing, where the prior is used for particle synthesis and the second is preferred in applications where accuracy of positioning the focused flow is paramount. In the case of 2-D HFF, reported nanoparticles demonstrated less particle size distributions compared to those produced by conventional methods. Because synthesized nanoparticles have unique properties based on their sizes, shapes, and morphology, controlled synthesis processing methods and devices are highly desirable to yield homogeneous nanoparticle populations.

Chapter 3

Thesis Objectives

3.1 Goals

The purpose of this study is three-fold; the primary task being the design and conception of a simple, low-cost, rapid, passive microfluidic device for the synthesis of liposomal nanoparticles and on-chip molecule encapsulation; secondly, the characterization of particles obtained under varying microfluidic synthesis parameters should be performed, notably varying phospholipid concentrations and flow rate ratios; and finally, the encapsulation of a water-soluble compound to validate this platform.
This device endeavors to reduce the synthesis times associated with current cumbersome production methods and eliminate the requirement for post processing (such as filter extrusion). Ideally, the device is to produce small unilamellar vesicles (SUVs), ranging between 50-300 nm, which are ideally suited for use as drug delivery systems [19]. Once a suitable concept is devised, correlations with respect to synthesized particle diameters between phospholipid: solvent concentration and fluid flow rates are determined. Finally, the encapsulation of a fluorescent molecule (namely an FITC labeled TAT peptide) is performed to demonstrate the feasibility of this proof-of-concept platform as a one-step solution for bioactive molecule-encapsulated liposomes.

3.2 Hypothesis

The formation of liposomes in microfluidic chips is governed by the diffusion of different molecular species (mainly alcohol, water, and the lipids) at the liquid interface between the solvent (alcohol) and non-solvent (water) phases which triggers the formation of liposomes by a mechanism described as "self-assembly" [51]. We hypothesize that by adjusting flow parameters such as the flow rate ratio (FRR) between the water and the solvent stream as well as the composition and concentration of the lipids composing the liposomes' bilayer, we will be able to generate liposomes with a narrow size distribution

and with low polydispersity. The size range shall be comprised within the suitable size range that guarantee optimal circulation time and clearance rate from the body but also above in order to demonstrate the versatility of this platform and its potential to prepare on-demand liposomes at any size and composition.

3.2.1 Effect of the Flow Rate Ratio (FRR)

Different microfluidic techniques have been shown to produce uniformly dispersed liposomes and allow for direct control of liposome size via fine adjustments to the flow rate ratio (FRR). Jahn et al. postulated that: "decreasing the sample stream width to micrometer length scales allows for controlled and reproducible mechanical and chemical conditions across the stream width, especially compared to more traditional bulk-phase preparation techniques (i.e., test tubes and beakers)" [37] From the literature, we expect: (a) the mean diameter of the liposomes produced to be directly related to lipid concentration and inversely related to FRR [37, 38].

3.2.2 Effect of Concentration

Both lipid and ethanol concentration have a significant effect on liposome properties (in both bulk and microfluidic methods) [51]. The mean diameter of the liposomes produced is directly related to lipid concentration [25]. In addition, previous reports on bulk injection methods have suggested a higher liposome polydispersity as the solvent concentration increases [90].

3.2.3 Effect of Charge

The coating material studied is often limited to neutral or anionic lipid mixtures such as DMPC or DPPC. Limited data is provided on the comparison between different lipid mixtures or on the use of cationic lipids, which may be more suitable for medical or biotechnological applications (e.g. as delivery systems for anticancer drugs or as transfection reagents), and which are routinely used in the industry [51]. Using DPPC as the main bilayer constituent, the effect of varying the dissolved lipid concentration as well as the flow rate ratio on the resulting liposome diameters is investigated. As a proof-of concept, the encapsulation of fluorescent labeled FITC-LC-TAT peptide (FITC-LC-Tyr-Gly-Arg-Lys-Lys-Arg-Arg-Gln-Arg-Arg-Arg-NH_2) is performed to validate the use of this microfluidic device as an all-in one synthesis and loading platform for liposomes. In addition, by adding either positively and negatively charged lipid particles to the main bilayer DPPC constituent, by incorporating DDAB and DOPG compounds respectively, the effect of liposome charge and stability in addition to its size is investigated with respect to its impact of the encapsulation of the FITC-LC-TAT peptide.

Chapter 4

Methodology

4.1 Materials

Negative photoresist, SU-8 2050, was purchased from Microchem Corp. (Boston, MA, USA). Sylgard 184 elastomer kits, consisting of a prepolymer and a curing agent of PDMS, were purchased from Dow Corning Corp. (Saint-Laurent, QC, Canada). Tygon 0.020" ID microbore tubing was purchased from Cole-Parmer Canada Inc. (Montreal, QC, Canada). A quick setting epoxy adhesive was purchased from LePage-Henkel (Mississauga, ON, Canada). 2-propanol (IPA), acetone, methanol (MeOH), all analytical grade, and glass microscope slides were purchased from Fisher Scientific (Waltham, MA, USA). Anhydrous ethyl alcohol (EtOH) was purchased from GreenField Specialty Alcohols Inc. (Brampton, ON, Canada). Trichloro(1H,1H,2H,2H-perfluorooctyl) silane, DOPG (1,2-Dioleoyl-sn-glycero-3-phosphoglycerol) and DDAB (Didodecyldimethylammonium bromide) were purchased from Sigma Aldrich (Oakville, ON, Canada). FITC-LC-TAT fluorescent peptide was purchased from AnaSpec Inc. (Fremont, CA, USA). DPPC (1,2-Dipalmitoyl-sn-glycero-3-phosphocholine) was purchased from Avanti Polar Lipids Inc. (Alabaster, AL, USA). Glass vials were purchased from VWR International (Radnor, PA, USA), 1 mL and 10 mL Hamilton glass syringes were obtained from Fisher Scientific (Ottawa, ON, Canada). Ultra-pure water (MilliQ) from a Millipore filtration system (resistivity above 18.2 MΩ-cm) was used for all experiments.

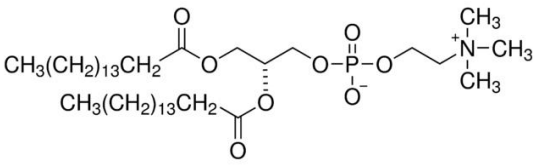

(a) DPPC

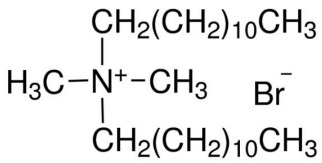

(b) DDAB

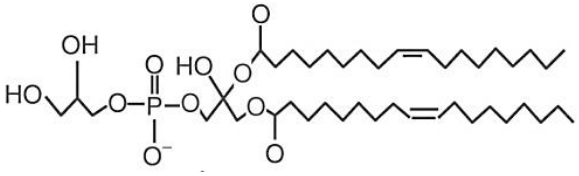

(c) DOPG

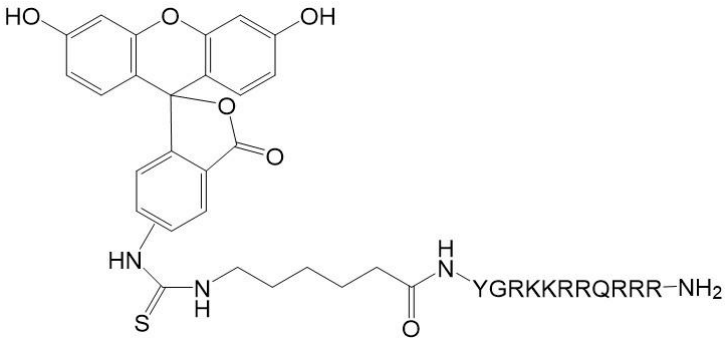

(d) FITC-LC TAT

Figure 4.1: Chemical structures of the compounds used: (a) DPPC (*1,2-Dipalmitoyl-sn-glycero-3-phosphocholine*), (b) DDAB (*Didodecyldimethylammonium bromide*), (c) DOPG (*1,2-Dioleoyl-sn-glycero-3-phosphoglycerol*) and (d) FITC labeled LC-TAT peptide.

Liposomes of DPPC have been determined to have a transition temperature of 41.3 °C [91]. This means that DPPC is in the gel phase at room temperature. For the preparation of different negatively/positively charged liposomes, DOPG and DDAB molecules, were added respectively to the DPPC lipids at a certain weight ratio. Composition of samples used for the DDAB: DPPC and DOPG: DPPC liposomes synthesis experiments are presented in Appendix D.

4.2 Methods

4.2.1 Computer-Assisted Design (CAD)

The design was primarily based on previous work done by Tien Sing Young et al. with liposomes, utilizing flow focusing as an effective means of mixture by diffusion. Once a suitable prototype was achieved, the channels were modeled using a computer aided design (CAD) software (SolidWorks 2016 - Dassault S.A., Vélizy, France) and the 3D/2D geometry was exported to be used in computational fluid dynamics (CFD) studies using the "CAD Import Module" in COMSOL. The same design was then converted to a **.dxf*

file to order the photo-mask for subsequent micro-fabrication in the cleanroom.

4.2.2 Numerical Flow Simulations

Numerical simulations were conducted using COMSOL Multiphysics 5.2a (COMSOL Inc., Burlington, MA, USA). The "COMSOL Multiphysics", "CAD Import" as well as the "Microfluidics" Modules were selected. Laminar Flow Models include both 2D and 3D "Time-Dependent" and "Steady-State" Analyses. Stationary Steady state studies are governed by "Incompressible Navier-Stokes" (4.2.2) and "Continuity" (4.2.2) equations where the final forms assuming incompressible Newtonian fluids, are presented below:

$$\rho\left[\frac{\delta u}{\delta t} + (u \cdot \nabla)\, u\right] = -\nabla p + \mu\nabla^2 + F \tag{4.1}$$

$$\rho\left[\nabla \cdot (u)\right] = 0 \tag{4.2}$$

Where: u is the flow velocity, ρ is the fluid density, p is the pressure, μ is the dynamic viscosity and F represents outer forces.

Whenever we consider mass transport of a dissolved species (solute species) concentration gradients will cause diffusion. If there is bulk fluid motion, convection will also contribute to the flux of chemical species. Therefore, we are interested in solving for the combined effect of both convection and diffusion. For a dilute species:

$$N_i = -D_i \nabla C_i + c_i u \tag{4.3}$$

$$\frac{\delta c_i}{\delta t} + (\nabla \cdot N_i) = R_i \tag{4.4}$$

Where: c_i is the species concentration (in $mol.m^{-3}$), N_i is the molar flux (in $m^{-2}s^{-1}$, R is a net volumetric source for c: $R > 0$ means that a chemical reaction is creating more of the species, and $R < 0$ means that a chemical reaction is destroying the species. D_i is the diffusion coefficient of the species (in m^2/s).

The simulation assumes water as the working fluid, with the sub-domain settings summarized in Table 4.1 as follows:

Table 4.1: Computational Parameters used for CFD Modeling and their Values.

Parameters	**Description**	**Value(s)**
Flow Rate at Inlet 1	Laminar Inflow Lipid in Ethanol Flow Rate	Q_1inlet = 10 [μL/min] = cst
Flow Rate at Inlet 2	Laminar Inflow Water Flow Rate	Q_2inlet = 40-480 [μL/min]
Material (Fluid)	Inlet 1 and 2	ρ_0= 1,000 [kg/m^3] μ_1= 0.00195 [$Pa.s$]
Mesh	Number of domain elements	2D: $N = 146,302$ 3D: $N = 711,375$

The main variable in these simulations are the inlet fluid flow rates. Flow focusing devices are typically characterized by their Flow Rate Ratio (FRR), which is defined as follows:

$$FRR = \frac{Q_1 + Q_2}{Q_1} \tag{4.5}$$

Where: Q_1 and Q_2 represent flow rate of the lipid stream dissolved in ethanol and the water flow rates respectively (in μL/min).

A no-slip boundary condition for the walls was applied. This boundary condition ensures that the fluid comes to rest at the channel walls. The inlets and outlets were defined as the openings at the extremities of the solid model, contrary to the configuration of the actual device, whereby the inlets and outlets are through the upper surface of the channels. The normal inflow sample and buffer inlet flow rates were set to the values demonstrated in Table 4.1. The outlet boundary was set to a pressure, p , of 0 Pa.

The next step is the implementation of a mesh. In the 2-D space, the mesh (shown in Figure 4.2), was user-defined to be adequate with the area of interest located at the Y junction, with a high number of elements and nodes. Meshing was optimized so that the calculated and theoretical values of the flow focusing width (Df) converge towards the same value (five significant numbers after zero which corresponds to um +/- 0.00001 um)

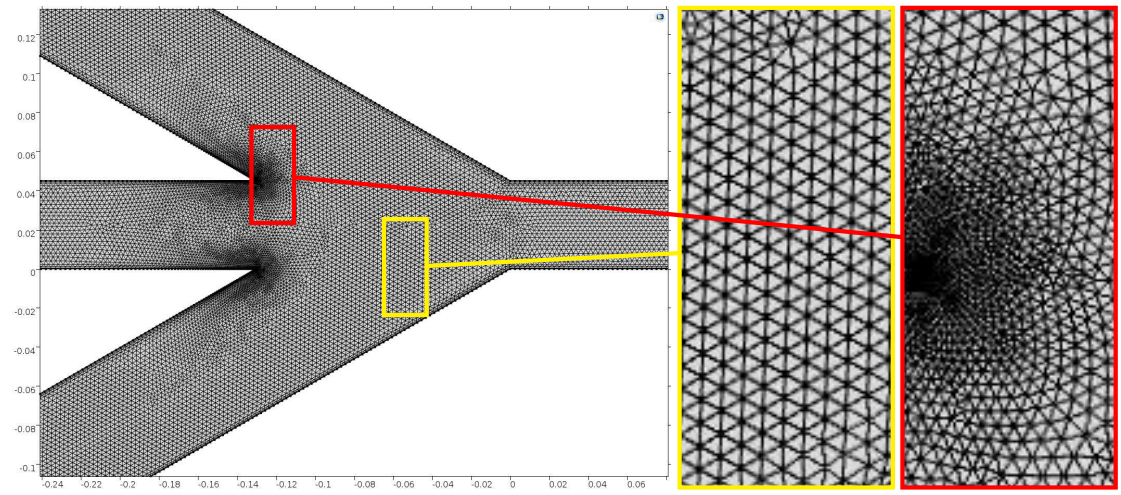

Figure 4.2: 2D Mesh of the microfluidic flow focusing junction displaying magnified views of the meshing elements at two different areas of the microfluidic structure. The red region close to the boundaries of the Y-junction has a higher number of and smaller size elements compared to the rest of the structure (yellow).

The complete 2D mesh (Figure 4.2) consists of 146,302 domain elements and 4,918 boundary elements. The parameters used to define the mesh at the model boundaries can be found under Appendix A. The 3D model, the finalized imported geometry has 1 domain, 14 boundaries, 36 edges, and 24 vertices. The complete mesh consists of 711,375 domain elements, 59,592 boundary elements, and 2881 edge elements. It is shown in Figure 4.3 :

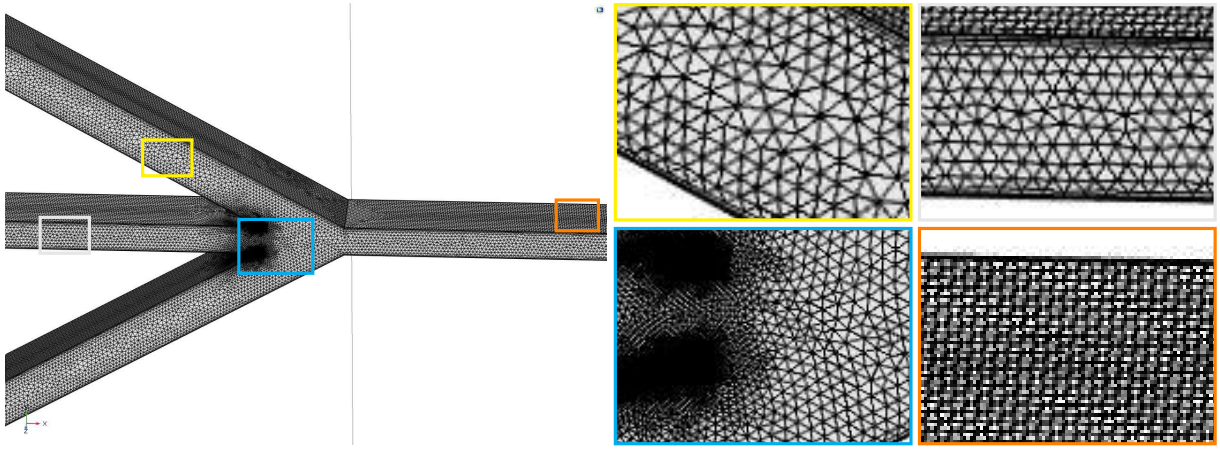

Figure 4.3: 3D Mesh of the MHF junction showing the meshing elements size and distribution at various areas of the microfluidic structure.

As shown in Figure 4.3, tetrahedral elements were used to mesh the 3D flow-focusing geometry with COMSOL Multiphysics. Tetrahedra are also known as a simplex, given that any 3D volume, regardless of their shape or topology, can be meshed with tetrahedra. They were also chosen as they represent the only kind of elements that can be used with adaptive mesh refinement. Mesh refinement was manually adjusted around the central flow focusing region (as shown in the blue box of Figure 4.3) and around the edges to get more accurate velocity/concentration profiles.

Application Builder: The optimization phase in the design of the microfluidic flow focusing device relied on the use of the Application Builder; a component of the COMSOL Microfluidics software that allows the creation easy-to-use applications based on pre-established numerical simulations [92]. To that effect, after the numerical simulations were developed and computed on Comsol, applications were created using Application Builder which exploited the different variations in the CAD designs and iterations of the microfluidic chips. These were used in order to optimize the designs 2D/3D dimensions and geometries based on the resulting velocity, concentration and pressure profiles obtained at different flow rate ratios (FRRs). Notably, as shown in Figure 4.4, control of the the inlet velocities and flow rates as well as the inlet concentrations to name a few, can be modeled. It is also possible based on the inlet flow rates to get the value of the FRR. In addition, because the volume of the syringe and thereby its cross section can change the FRR, the effect of using different syringe models was incorporated to get the best estimate of the FRR. Finally, it is possible to change the mesh size (coarse, normal, fine, finer and extra fine). As we refine the mesh, the solution will become more accurate however computation time increases correspondingly. The application therefore gives an estimate of the computation time which can range from a couple of seconds in the 2D domain to several hours for some complex 3D models.

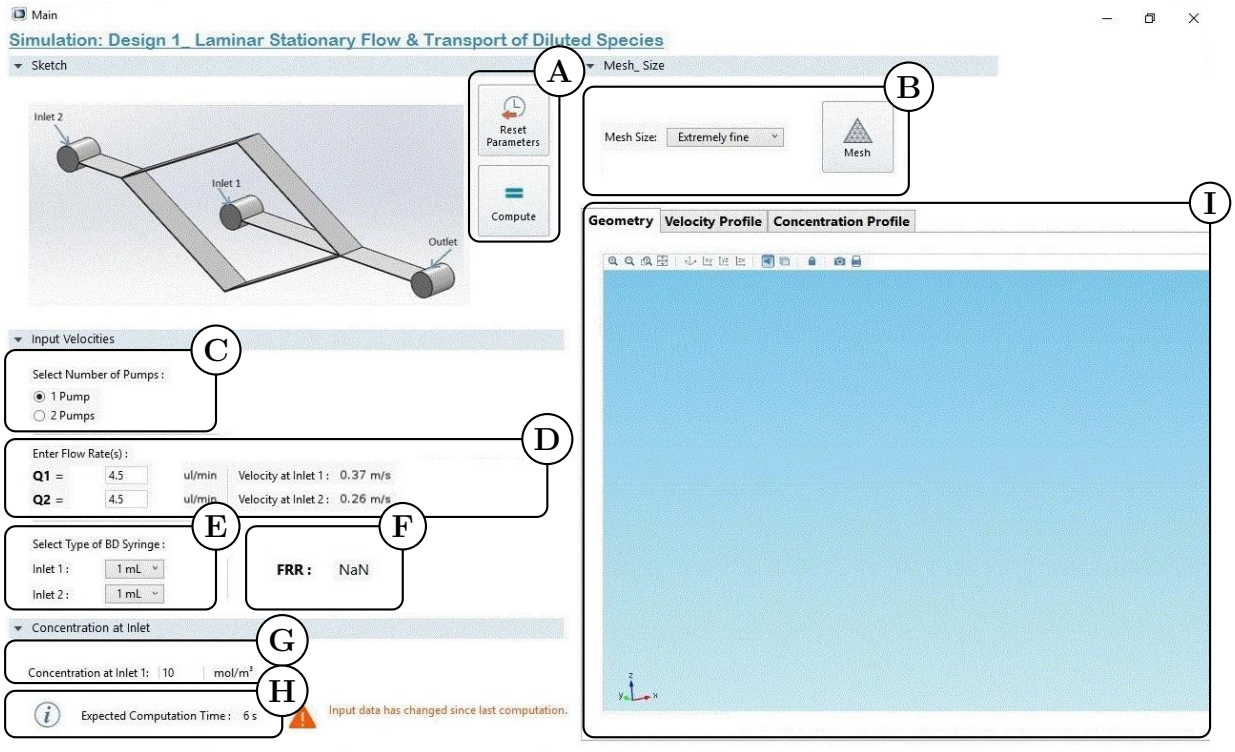

Figure 4.4: User Interface of the Application generated using Application Builder via COMSOL Multiphysics.

The Application interface shown in Figure 4.4, make it possible for any user to customize

the numerical simulation parameters based on the microfluidic CAD design without having to change the input simulation parameters or disturb the source code. This had the added bonus of reducing significantly the computation time (H). Buttons are available to compute or reset input parameters to their initial/standard values (A). The graphic/visual interface (I) with the geometry, velocity and concentration profiles of structure is also displayed. Furthermore, interactive meshing parameters let the user select the meshing size (from coarse to extremely fine) (B), without having to change manually the computational parameters displayed in the Appendix Table A.1. In addition, to ease the transition from the theoretical to the experimental field, it is possible for the user to select the number of pumps available (C) and the appropriate syringe (E), which can prove to be useful to recreate the experimental setup conditions. Similarly, the input flow rates can be inserted in (D) and corresponding calculated velocities (in m/s) at the inlets as well as the FRR (Fig.4.4 F) are calculated accordingly. Also, the input concentration at inlet (in mol/m^3) in (G) can be changed to reflect the experimental values.

Overall, this application allows the customization of the interface and a control over the inputs and outputs that the user of the application is allowed to manipulate by including only the parameters relevant to the design of a specific device or process. The code used to build the Application in Figure 4.4 as well as other versions of the App which cover other microfluidic chip designs can be found under Appendix A.

4.2.3 Device Manufacturing and Assembly

With the design of the chip validated using numerical analytical tools, the fabrication process follows. By exploiting the McGill Nanotools Microfab (MNM) facilities, the complete fabrication of the microfluidic chip was performed using photo- and soft lithography techniques.

Photo-lithography: The microfluidic channels were manufactured via negative photolithography onto a silicon wafer, followed by soft lithography in PDMS. The initial step consists of utilizing the previously constructed CAD geometry to create a chrome photomask comprised of a top view of the channels. For this negative lithographic process, a dark field photomask was created. The pattern or channels to be created were transparent, and everything else was covered in chrome. The photomasks were obtained from the Center of Microfluidic Systems (CMC, Toronto Ontario, Canada) and are shown in Appendix C. In the McGill Nanofab-Microtools facility (Montreal, QC, Canada), the photomask was used to create a positive mold onto a silicon wafer. Firstly, the process consists of spinning a negative photoresist, SU-8 2050, at 1700 rpm for 30s to achieve a thickness of 100 μm. Conventional ultraviolet photolithography was performed using the

aforementioned photomask, whereby the exposed negative photoresist was cross-linked and thus became insoluble to the developer.

Soft-lithography: Prior to the soft lithography process, the mould was treated with PFOTS (trichloro(1H, 1H, 2H, 2H perfluorooctyl)silane) via chemical vapor deposition to aid with the demolding process. Vacuum was applied for about 1-1.30 h, resulting in the vaporization of the silane. After silanizing the PDMS master, pouring of an elastomer, PDMS, onto the previously silanized mould. The elastomer kit was composed of a pre-polymer and a curing agent, which was mixed in a 10:1 w/w ratio, as per the manufacturer's protocol. The prepared mixture was poured onto the wafer, which was then degassed in the vacuum desiccator to remove any bubbles within the elastomer and cured at 70 °C for 3 hours. Once cured, the channels were carefully cut and removed from the cured polymer with a surgical scalpel or razor blade. The bottom face, containing the channels, was temporarily covered with transparent packing tape so as to avoid any contamination or dust deposits. A 1.2 mm biopsy punch was then used to puncture the inlet and outlet ports.

4.2.4 Liposome Fabrication and Loading

The phospholipid-solvent mixtures (DPPC:EtOH) were prepared using DPPC dissolved directly into EtOH at various concentrations. They were prepared in glass vials (VWR International Radnor, PA, USA) and stored at 4°C until use. For the encapsulation studies, a 0.5 mg/ml stock solution of fluorescent FITC-LC-TAT peptide was prepared as per the manufacturer's protocol by adding 2 ml of MeOH to a 1 mg of FITC-LC-TAT and stored at 20°C.

For the bare liposomes fabrication, inlet 1 was blocked, MilliQ water flowed through inlet 2, and DPPC:EtOH flowed through inlet 3. For the runs correlating diameter with lipid concentration, DPPC:EtOH solutions at concentrations of 1, 2, 3, 5, and 10 mg/ml were prepared. The flow rate ratios (FRRs), defined as the total volumetric flow rate divided by the focused sheath flow rate, investigated were ranging between 5-50. For the peptide encapsulation investigation, the FRR was set to 50 and the DPPC:EtOH concentration was 3 mg/ml. The control batch was prepared by flowing MilliQ water, 3 mg/ml DPPC:EtOH, and MeOH through inlets 1, 2, and 3, respectively. The same setup was used for encapsulation, with the exception of the incorporation of 0.5 mg/ml FITC-LC-TAT:MeOH flowing through inlet 3, i.e., loaded. Detailed batch descriptions can be found in Appendix D.

4.2.5 Characterization of Liposome Properties

Zeta Potential

Surface properties of liposome formulations can vary depending on the composition of the lipid. There are cationic, anionic and neutral lipids, which can be used for preparation of liposomes. Zeta potential can be used to identify any correlation between the liposome incorporation and retention of and surface charge properties of the liposomes. The zeta potential is charge at the slip plane of the particle surface, and although it is not a direct measurement of the surface charge, it is a good estimation. Zeta potential is one of the important factors affecting liposomes stability, incorporation efficiency and interactions with biological system in vivo. The zeta potential of liposomes was measured using a zetasizer Nano ZS (Malvern, UK). The samples were analyzed using the Zetasizer for ten cycles with a voltage of 4 mV.

Size/ Concentration

In order to evaluate the size of the loaded and unloaded liposomes (both prior and following FITC-LC-TAT peptide encapsulation), dynamic light scattering (DLS) measurements were coupled with nanoparticle tracking analysis (NTA) measurements in order to characterize the particles size, size distribution, polydispersity and concentration.

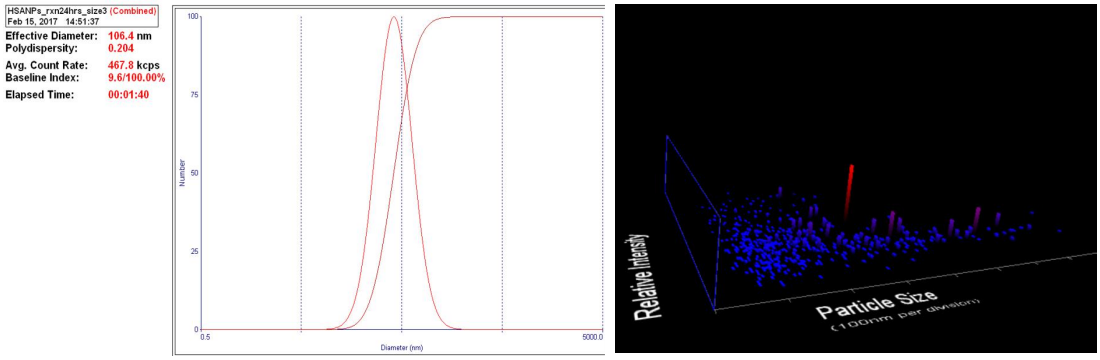

(a) DLS (b) NTA

Figure 4.5: Size Measurement using (A) Dynamic Light Scattering (DLS) and Nanoparticles Tracking Analysis (NTA) methods.

Dynamic Light Scattering (DLS): The particle diameters were determined by use of dynamic light scattering (DLS) via a ZetaPALS Zeta Potential Analyzer (Brookhaven Instruments Corp. - Holtsville, NY, USA). DLS relies on the Brownian motion of particles suspended in a solution to obtain a diffusion coefficient, from which the particle size is determined. Typically, a red laser (675 nm) is emitted at a 90° angle. The recording chamber temperature was set to 6 °C, and each run consisted of ten 10 second readings.

Nanoparticle Tracking Analysis (NTA): Nanoparticle Tracking Analysis (NTA) technique was also used for detecting simultaneously sub-micron particle size distributions and particle concentrations of multiples samples. NTA measurements were performed with a NanoSight LM14 (NanoSight, Amesbury, United Kingdom), equipped with a sample chamber with a 640-nm laser and a Viton fluoro-elastomer O-ring. The samples were injected in the sample chamber with sterile syringes (BD Discardit II, New Jersey, USA) until the liquid reached the tip of the nozzle. All measurements were performed at room temperature (T= 25 °C). The software used for capturing and analyzing the data was the NTA 3.2 Build 127. The samples were measured for 40 s with manual shutter and gain adjustments. The mean size and SD values obtained by the NTA software correspond to the arithmetic values calculated with the sizes of all the particles analyzed by the software (NANOSIGHT 3.2).

4.2.6 Imaging and Visualization

Negative Staining: Samples for negative staining were prepared using the Single-droplet method [93]. After preparing a 2% aqueous solution of an uranyl acetate stain (and adjusting the pH to 7.0 with 1M KOH, if required), formvar-carbon coated grids were glow discharged prior to use in order to increase their hydrophilicity prior to their use. A volume of 5 μL of the sample was then pipetted on the grid so as to cover the entirety of the grid surface. After approximately 10 seconds, 5 μL of the uranyl acetate stain was slowly pipetted on to sample, and the stain absorbed from the opposite side using a wedge of filter paper. The grid was then allowed to dry and then examined by TEM (transmission electron microscopy). Samples were imaged at a magnification of 50,000x at room temperature using a Philips Tecnai T12 electron microscope equipped with an LaB6 filament and operated at an acceleration voltage of 120 kV.

Device Flow Visualization: For this part of the study, the fluid flow rates were controlled with a Nexus 3000 syringe pump (Chemyx Inc. – Stafford, TX, USA) in conjunction with syringes of various volumes (BD Medical – Mississauga, ON, Canada). The image acquisition setup consisted of an inverted microscope (Eclipse TE 2000-U, Nikon Corp.—Mississauga, ON, Canada), with fluorescence capabilities, which was used to visualize the liposomes as well as the fluorescence emission from the FITC-LC-TAT peptide. All images were captured using a CCD camera (Retiga-2000R, Qimaging—Surrey, BC, Canada) and Nikon NIS-Elements D software. MilliQ water, coloured with readily available food dyes, was used as the working fluid. The pumps were set to flow at various flow rates and images of the flow focusing junctions were obtained at low (x20) and high (x40) magnifications.

Particle Count: The open-source software CellProfiler was used to quantitatively measure the fluorescent particles. A new pipeline was developed for detection of drug encapsulating liposomes. This pipeline has four major steps: 1) Background correction, 2) Colony detection & Filtering, 3) Measuring Colony parameters, 4) Overlaying and saving images. Background correction is done through its own inherent modules- Color to Gray, Correct Illumination calculation, and Correct Illumination Apply. Modules for object detection (Identify Primary Objects) based on thresholding are available in Cell Profiler.

4.2.7 Statistical Analysis

Data are expressed as mean ± standard deviation (SD) of at least 5 replicates per group. Statistical analyses were performed for multiple comparisons via one-way ANOVA and Student's t-test was used for direct result comparison. Differences were considered significant at $p < 0.05$.

Chapter 5

Numerical Simulations and Flow Visualization

The design stage involved optimizing the geometry and dimensions of the microfluidic platform. To model the microfluidic device, a layout of the architecture was performed using a CAD software program (SolidWorks 2016). Design features such as channels heights, widths and geometry were optimized by modeling and simulation of the fluid flow based on the design geometry and fluid conditions using a commercially available software; COMSOL, a general-purpose software platform based on advanced numerical methods. Finally, using an optical microscope, images of the flow focusing phenomena at the device junction will be visualized and compared with their numerical models analogs obtained using the COMSOL software. Finally, an application was created using Application Builder to access the modeled simulations in a time-efficient manner prior to and during the microfluidic experiments to validate the flow conditions inside the microfluidic device.

5.1 CAD Modeling

The following section describes the general principles that have been considered for designing and constructing the microfluidic devices employed for liposomal production.

5.1.1 Design Requirements and Constraints:

Chip dimensions: As a practical rule, the total width and length of the chip should be defined to comply with the dimensional constraints imposed by the typical size of microscope stages that are routinely used to assess the correct functioning of the chips. As a general design principle, the microfluidic device should fit within the maximum width and length of conventional glass slides for microscopy (width=25-50 mm and length = 75 mm). At the same time, as suggested by Carugo et al. [51], the thickness of the device should comply with the working distance of microscope objectives. While in

situ microscope observation may not be required in an industrial setting, it is a useful requirement at a research and development stage.

Channel dimensions: The inlet channels should be long enough to allow the fluid flows to fully develop before they intersect with each other, allowing for a stable and predictable flow focusing regime. Channels should also be designed so as to guarantee sufficient spacing between the inlet ports, allowing for robust and practical connection with tubing and pumping units. A typical inlet channel length for microfluidic HFF chips is in the range of 5-10 mm. Longer channels result in higher back-pressure, which could potentially compromise device usability. Finally, the mixing channel should be designed to allow for complete mixing of the solvents (ethanol or isopropanol, and water) at the selected operating flow rates, and to comply with the dimensional requirements imposed by microscope interfacing.

Relative orientation of the inlet channels: In MHF chips, the angle between the side and central inlet channels should be defined so as to minimize fluid dynamic perturbations at the intersection between flows, particularly if devices are designed to operate at high throughput regimes. In the literature, this angle is in the range of 30°- 90°.

Fabrication Method: The constitutive materials should satisfy different requirements, including resistance to solvents, optical transparency, compatibility with microfabrication and bonding techniques, low surface roughness, and commercial availability. Due to its versatility, PDMS is a commonly used material in soft-lithography, given its compatibility with pharmaceutical-grade solvents (i.e., ethanol), ease of surface treatment by exposure to oxygen plasma, ability to conform to a surface, and potential for bonding with commercially available glass slides [51]

Operating Regime: 2D hydrodynamic flow focusing was selected as a microfluidic-based regime for nanoscale liposome production, and its performance compared with other micromixing geometries. Laminar as opposed to turbulent flow conditions has been previously demonstrated to allow for precise control over the interfacial boundaries between solvent and co-solvent streams, resulting in diffusion dominated mass transfer and leading to liposomes of relatively uniform physical properties. Furthermore, liposome size and dispersity in MHF chips has the advantage of being potentially controlled on-demand by finely adjusting the hydraulic boundary conditions.

5.1.2 CAD Modeling

Once the final design was drafted, the 2D sketches (shown in Fig. 5.1 (top)) were converted into 3D models which can easily be done by extruding the 2D geometry. The

primary use of these models was for the CFD simulations, creation of the photomask, and ultimately, the physical master for device fabrication. Figure 5.1 (bottom) shows an isometric views for the final render of the assembled device.

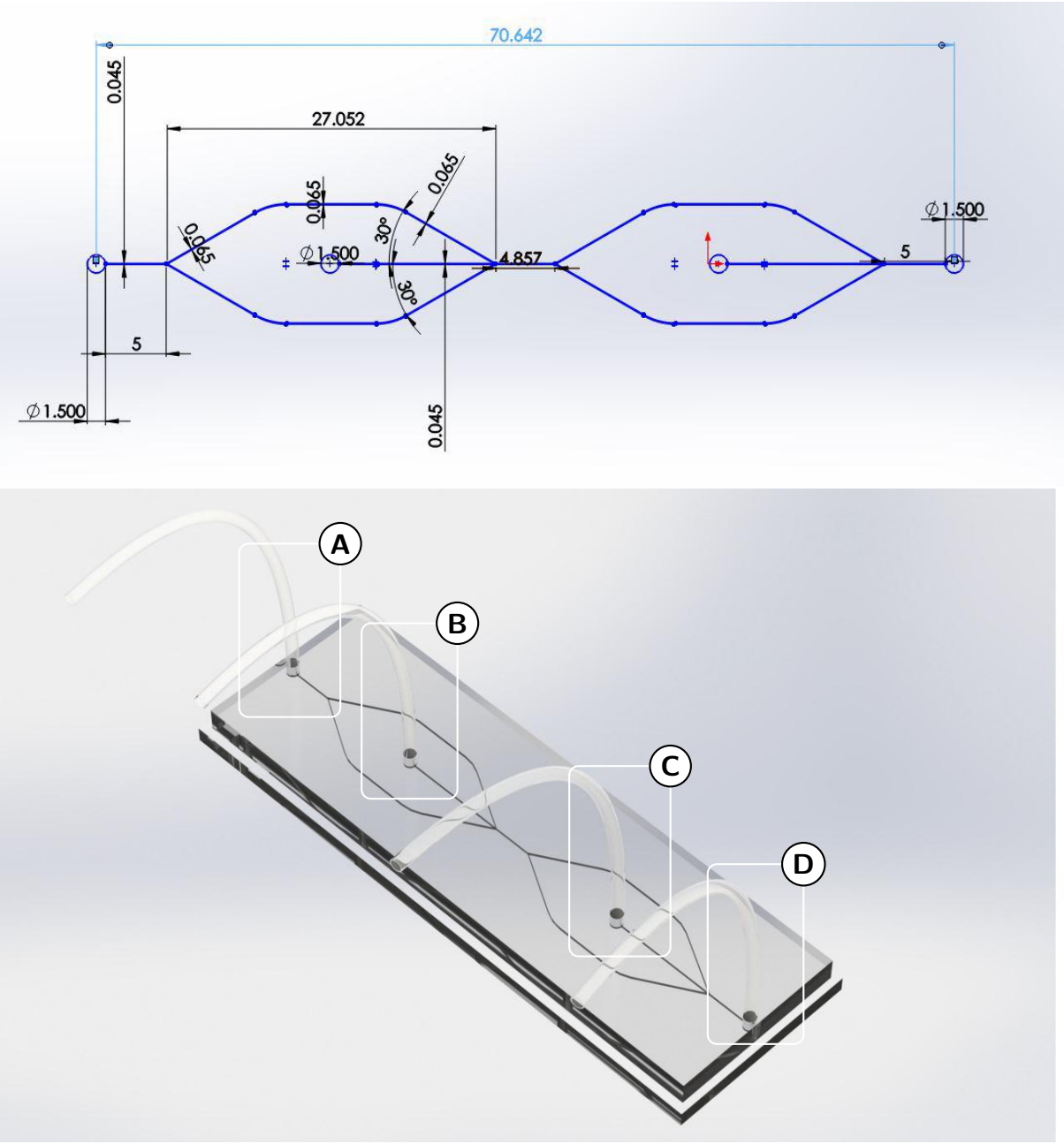

Figure 5.1: Schematic representation of the different components of the planar flow focusing microfluidic device: (A) Water inlet, (B) Lipid/alcohol inlet (DPPC +/- DOPG/DDAB in ethanol) (C) Loaded molecule for encapsulation (including FITC-LC TAT peptide) and (D) Outlet. The upper left insert represents a 2-D technical diagram of the pattern of the device geometry (all dimensions in mm).

As shown in Figure 5.1, the base of the device was a standard glass microscopy slide (25 mm x 75 mm). The patterned PDMS and glass slide are then treated with oxygen plasma, which renders the surfaces hydrophilic, and pressed together to create a fairly strong bond.

Finally, the Tygon microbore tubing was inserted into the inlets and outlet and sealed using quick-setting epoxy adhesive. Guidelines followed for designing and constructing this microfluidic devices for liposomal production have been presented under subsection 5.1.1.

5.2 CFD Simulations

Following CAD design and modeling, the CFD capabilities of COMSOL Multiphysics were exploited in order to simulate in both the 2D and 3D space the flow profiles of the one phase/ two fluid flows inside the microfluidic device. Under laminar fluid flow, the mixing of miscible liquids is governed by molecular diffusion which facilitates numerical simulation of the alcohol-water interface [90]. Relevant simulations include velocity and concentration profiles of the alcohol-water mixtures for different HFF conditions (FRR). In the current work we have reported mainly steady state and time dependent simulations. Stationary studies allows solving equations which do not vary with time. It was used to solve for the velocity profile at the flow focusing junction. On the other hand, time-dependent study, used to solve the concentration profile of the diluted lipid species over time, shows how concentration vary with time. Time-dependent study generally takes much longer to simulate and also requires a huge amount of processing memory.

5.2.1 2D Models

Our 2D model approximates flow at the vertical midplane with two-dimensional flow simulations which is an idealization of the three-dimensional channel flow in the microchannel. The analysis and prediction of the focused stream width employs a simple model based on mass-conservation principles. The 2D focused stream width is computed under these simplified assumptions:

1. Flow in the microchannel is steady, laminar and incompressible;
2. Fluids are Newtonian ;
3. The effect of gravity is neglected ;
4. No slip boundary condition at channels walls ;
5. Fluids have the same density (in both the inlet channels and the outlet channel) ;
6. Fluids flow in a rectangular microchannel ;
7. The four channels have the same height.

According to the mass conservation principle, the volume of sample liquid that passes through the inlet channel (Q_2) must match the volume of the focused stream:

$$Q_2 = v_2 w_2 h = v_f w_f h = Q_f \tag{5.1}$$

This leads to:

$$w_f = \frac{Q_2}{v_f h} \tag{5.2}$$

Where: w_f and w_2 represent the width of the focused stream and central inlet channel, respectively. Q_2 and Q_f are the volumetric flow rates of the central inlet channel and focused stream, respectively. h is the height of the channels, and v_2 and v_f are the average velocity of the flow in the central inlet channel and of the focused stream, respectively. The amount of fluid passing through the outlet channel (channel 0) must be equal to the total amount of the fluid supplied from the three inlets (central Q_2 and two lateral Q_1):

$$Q_0 = v_0 w_0 h = Q_1 + Q_2 \tag{5.3}$$

$$w_0 = \frac{Q_1 + Q_2}{v_0 h} \tag{5.4}$$

where: Q_1 and Q_2 are the volumetric flow rates for the two lateral channels, and v_0 and w_0 are the average velocities of the flow and width of the mixing channel, respectively. Combining Eq.5.1 and Eq.5.4, and assuming v_o and v_f have the same values, it is possible to obtain the relationship between the width of the focused stream and volumetric flow rate of the inlets:

$$\frac{w_f}{w_0} = \frac{Q_2}{Q_1 + Q_2} \tag{5.5}$$

For an outlet width of 45 μm, we get the following values of w_f for the given flow rates (Q_1 and Q_2) and FRRs as shown in Fig.5.2 (a):

FRR	$Q_2[\mu L/mn]$	$Q_1[\mu L/mn]$	$w_f[\mu m]$
5	10	40	9.00
10	10	90	4.50
15	10	140	3.00
20	10	190	2.25
25	10	240	1.80
30	10	290	1.50
35	10	340	1.29
40	10	390	1.13
50	10	490	1.00

(a)

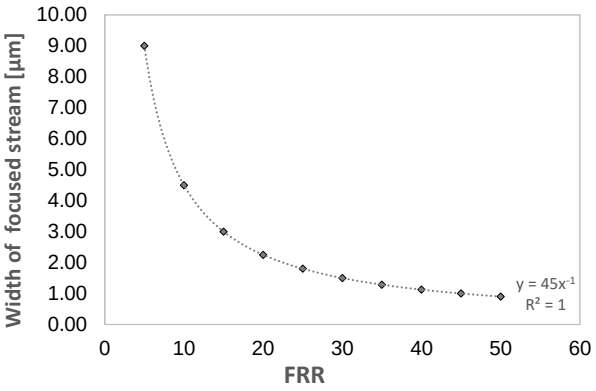

(b)

Figure 5.2: (a) Table showing the experimental Values for the width of the focused stream at channel junction (in μm) and corresponding FRRs and flow Rate values (in μm). (b) Width of the focused stream at the microfluidic device junction (in μm) as a function of the flow rate ratio (FRR).

From the graph displayed in Figure 5.2 (b), we observe a tendency of a decreasing width of the focused stream as the FRR increases. The curve was fitted with a power trendline (correlation coefficient: $R^2 = 1$) with a plateau at $w_f = 1.00\ \mu m$. Both Equation 5.5 and Figure 5.2 provides a simple guideline for predicting the focused stream width. However, it does not reflect the effect of other factors such as device structure, channel surface, and fluidic property (such as differences in fluid densities or viscosities), which could affect the focusing process.

In order to gain insight into the fluidic behavior of the system, experimental conditions and results were duplicated within the 2D/3D space using a COMSOL Multiphysics © model to elucidate the structure, direction, proportion, and fate of fluid lamina throughout the flow focusing region. It is important to visualize the flow profiles in both 2D and 3D. Ideally, a 3D representation will enable us to ensure that a laminar flow distribution is achieved inside the channels for all FRRs conditions. With turbulence, the diffusion of the lipid species and the rate of mass transfer at the alcohol/water interface is harder to predict and reproduce which would lead to chaotic mixing and correlate in heterogeneous liposome particles sizes due to their different mixing times. By varying the flow-rates at the inlets (Fig. 5.3), different flow-focusing widths were achieved. In planar (2D) focusing, the fluid is characterized by a low Reynolds number and exhibits laminar flow. Thus, the fluid stream will have maximum velocity in its center and zero velocity at the wall, if approximated with the parabolic flow profile characteristic of a low Reynolds number [83]. From figure 5.3, the flow velocity increases from zero value at the inlet to 0.45 - 4.5 m/s at the outlet depending on the FRR.

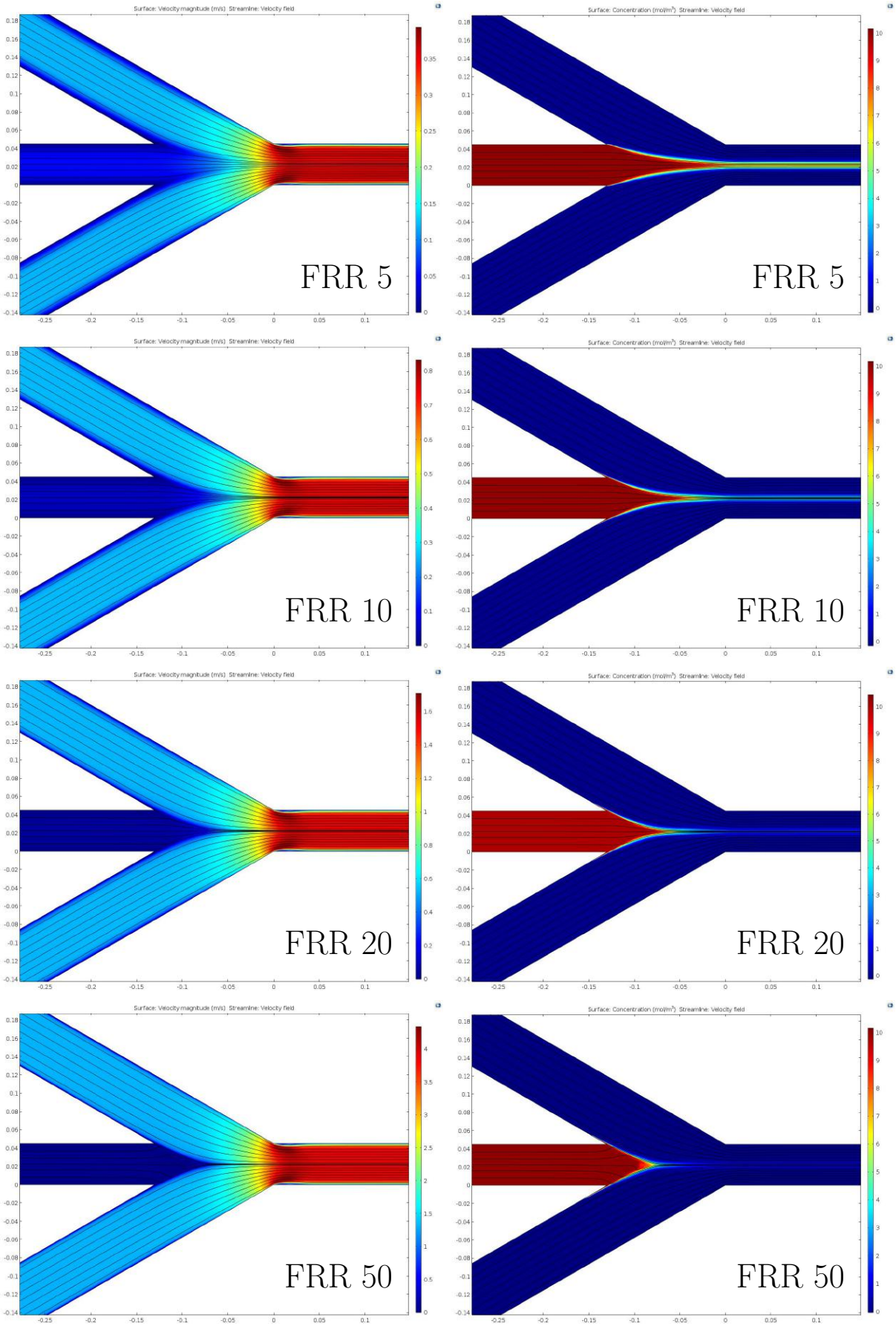

Figure 5.3: 2D CFD Simulations showing the Velocity (left) and the Concentration profiles (right) at the flow focusing junction of the microfluidic device at the given FRRs.

Whereas there is no theoretical upper limit to the FRRs that could be simulated, there is however, a practical lower limit as the back flow occurs from the side channels into main channel. As we reach high flow rates inside the device, high inlet pressures are attained which can compromise both the flow focusing capability of the device and its structural integrity as high back pressures can result in the burst of the tygon inlets and/or the PDMS interface. Consequently, the 2D pressure profiles at the flow focusing junction were also simulated and are reported in the next section.

2D Pressure Profiles

The pressure profile at the flow focusing region inside our microfluidic devices are illustrated in Figure 5.4. Pressure profiles help both evaluate and isolate the range of the maximum backpressure and therefore the maximum FRR that the device can sustain before failure (burst of the PDMS chips). As such with both the 2D pressure profiles and by experimentally increasing the FRR it was discovered that due to the device geometries (width, height an length of the channels) and the pressure associated with the tubing and syringe cross section injection the maximum FRR attainable had to be lower or equal than FRR=100. A higher FRR resulted in a backflow of the fluid and a burst and destruction of the PDMS chips. The shear modulus of PDMS being 100kPa and the internal pressure inside the device at FRR=100 being close to 80 kPa [84]

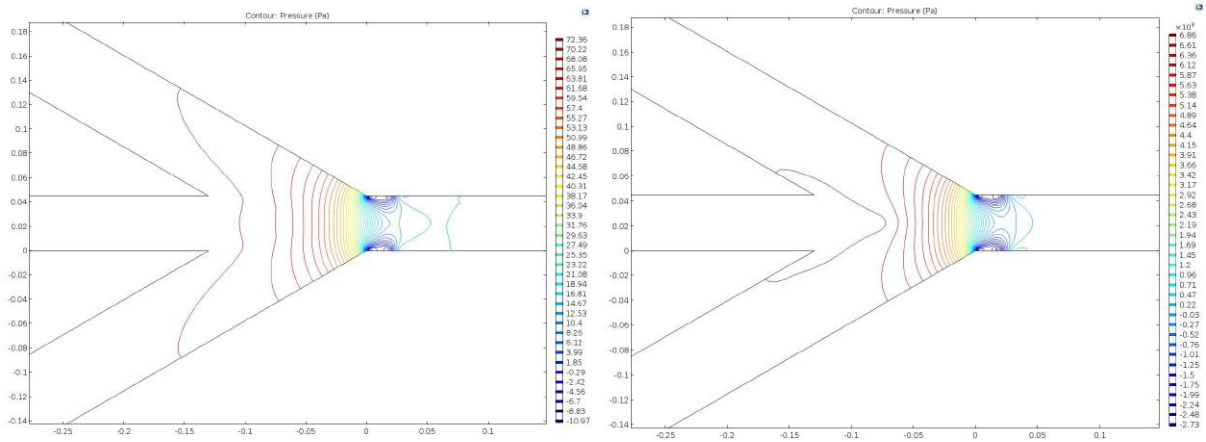

(a) FRR=5 (b) FRR=50

Figure 5.4: 2D Pressure Profiles at Flow Focusing Junction

It can be seen that pressure decreases from inlet to the outlet and varies also depending on the FRRs. From Figure 5.4a, at FRR=5 (low flow rate ratio), the maximum pressure located at the inlet is of 72.36 Pa and the minimum at the outlet around 10.4 Pa. At a higher FRR=50 (Figure 5.4b), the maximum pressure is more than a hundred time higher at the inlet (6.86×10^3 Pa) and also a hundred times lower at the outlet (around 0.96 Pa). A C-shaped pressure profile is observed at the junction of three channels. The

pressure is at maximum at the inlets and then gradually decreases as we travel along the channel.

5.2.2 3D Simulations

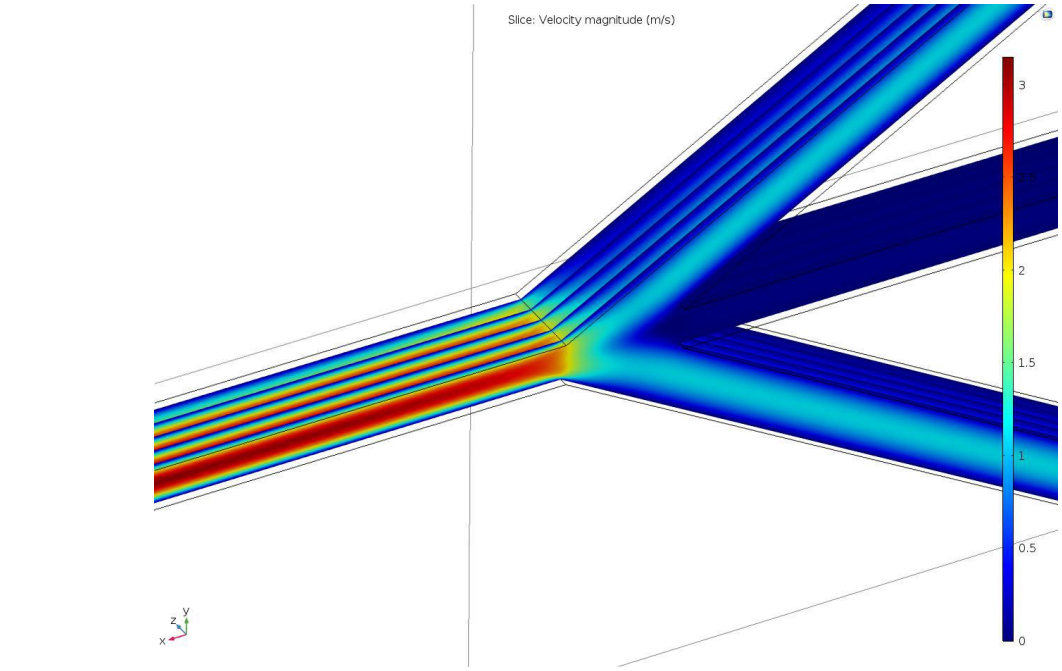

(a) Isometric View

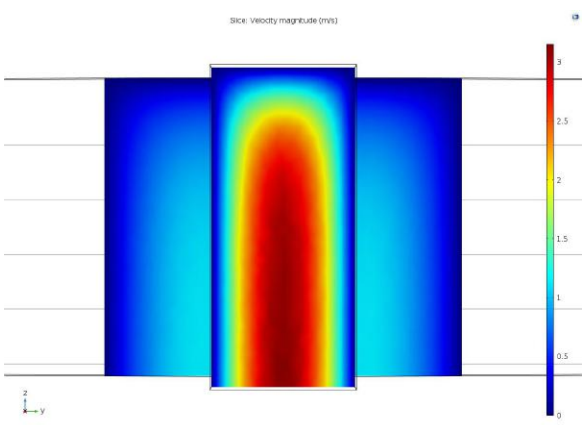

(b) *yz* Plane

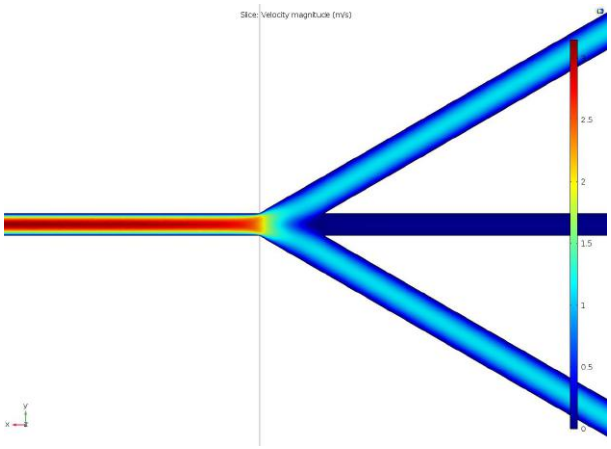

(c) *xy* Plane

Figure 5.5: 3D Velocity Profiles at Flow Focusing Junction at FRR = 50.

Velocity Profile: The 3D numerical simulation performed for the different focusing ratios (FRR: 5-50) indicates that thickness of the focused plane decreases with an increase of the focusing ratio as expected from the 2D simulations. Also, along the xy axis of symmetry, from Figure 5.5b, which shows a cross-section of the velocity profile at the yz plane, it appears that the velocity is maximum at the center of flow focusing junction. Its maximum value reaches approximately 3.5 m/s for a FRR of 50 which is in accordance with findings from the 2D simulations.

Concentration Profile: The concentration distribution of lipid in ethanol sheathed by two adjacent water streams is simulated with a 3-dimensional model in Comsol Multiphysics. Assuming an inlet concentration of 10 mol/m^3 and a time-dependent, laminar flow, we obtain the following 3D concentration profile:

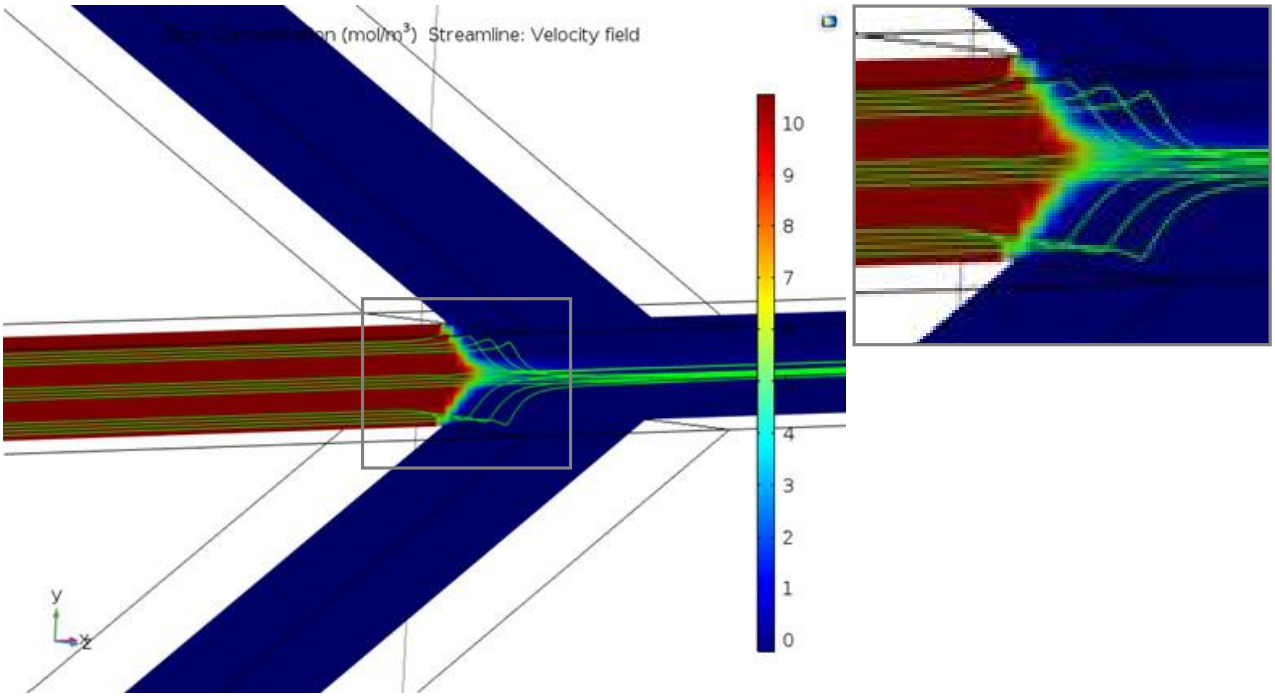

Figure 5.6: 3D Concentration Profiles at Flow Focusing Junction at FRR=50. The small insert on the right shows the 3-D flow focusing velocity profile lines at the microfluidic junction.

The simulation couples the convective and diffusive mass transfer of ethanol with the full Navier-Stokes equation (Eq. 2.1) for incompressible flow, considering spatially varying viscosity that depends on the local alcohol/water volume fraction. The mass diffusivity of alcohol and water results from the mass flux due to diffusion and the concentration gradient at the diffusive EtOH/water interface. The directionality of the mass flux occurs from high concentration towards low concentrations of the respective solute [38]. This means ethanol diffuses from high concentration of alcohol towards the aqueous phase whereas the water diffuses towards the focused alcohol stream, resulting in the concentration profile shown in Figure 5.6.

In the 3D models, the diffusion of color particles across the boundary results in a color intensity profile across the flow that is not perfectly sharp. The 2D simulations are therefore preferred for better visualization of the diffusion of the diluted species as well as the velocity profile along the boundary of the flow. They also mobilize less extensive processing and computing resources and require less time to compute.

Chapter 6

Device Characterization

In order to fully characterize our HFF device and its liposomes synthesis and loading capabilities, flow visualization of the flow focusing junction was first conducted to qualitatively visualize the effect of varying the FRR on the width and behavior of the focused stream at the focusing junction. A comparison between the simulated flows, computed using Comsol Microfluidics and the experimental flows inside the platform is then provided. Next, visualization of the synthesized liposomes was conducted by negative stating TEM microscopy thus offering both a quantitative and qualitative representation of both the shape and morphology as well as the size of synthesized liposomes in aqueous conditions. Finally, in the third section, the effect of varying both the lipid composition and flow parameters for the synthesis of DPPC nano-sized liposomes within our platform was assessed with regards to size, concentration, charge and polydispersity of the resulting liposomes.

6.1 Flow Visualization

Hydrodynamic flow focusing was first examined from the plan view using an inverted light microscope to visualize the flow focusing at the microfluidic junction. Focusing stream at magnifications of (x20) and (x40) are shown for different flow rate ratios (FRRs) in the following chapters. The remaining pictures are displayed in Appendix B.

6.1.1 Qualitative Flow Visualization Results:

Liposomes formation in HFF occurs by a diffusively driven process, when a stream of lipids dissolved in an organic solvent such as ethanol is hydrodynamically sheathed between two oblique aqueous streams in a microfluidic channel [37]. The main concept of hydrodynamic focusing is to reduce the stream width and consequently the mixing path length of the focused stream. A stream of lipids resolubilized in ethanol is hydrodynamically focused into a very narrow sheet with a thickness varying from a few micrometers

down to sub-micrometers depending on the respective water-to-ethanol volumetric flow rate ratios (FRR).

Light microscopy images are shown in Figure 6.1 that depicts the focusing of a central lipid stream (dark stream) by two aqueous water streams (not visible) in a microfluidic device.

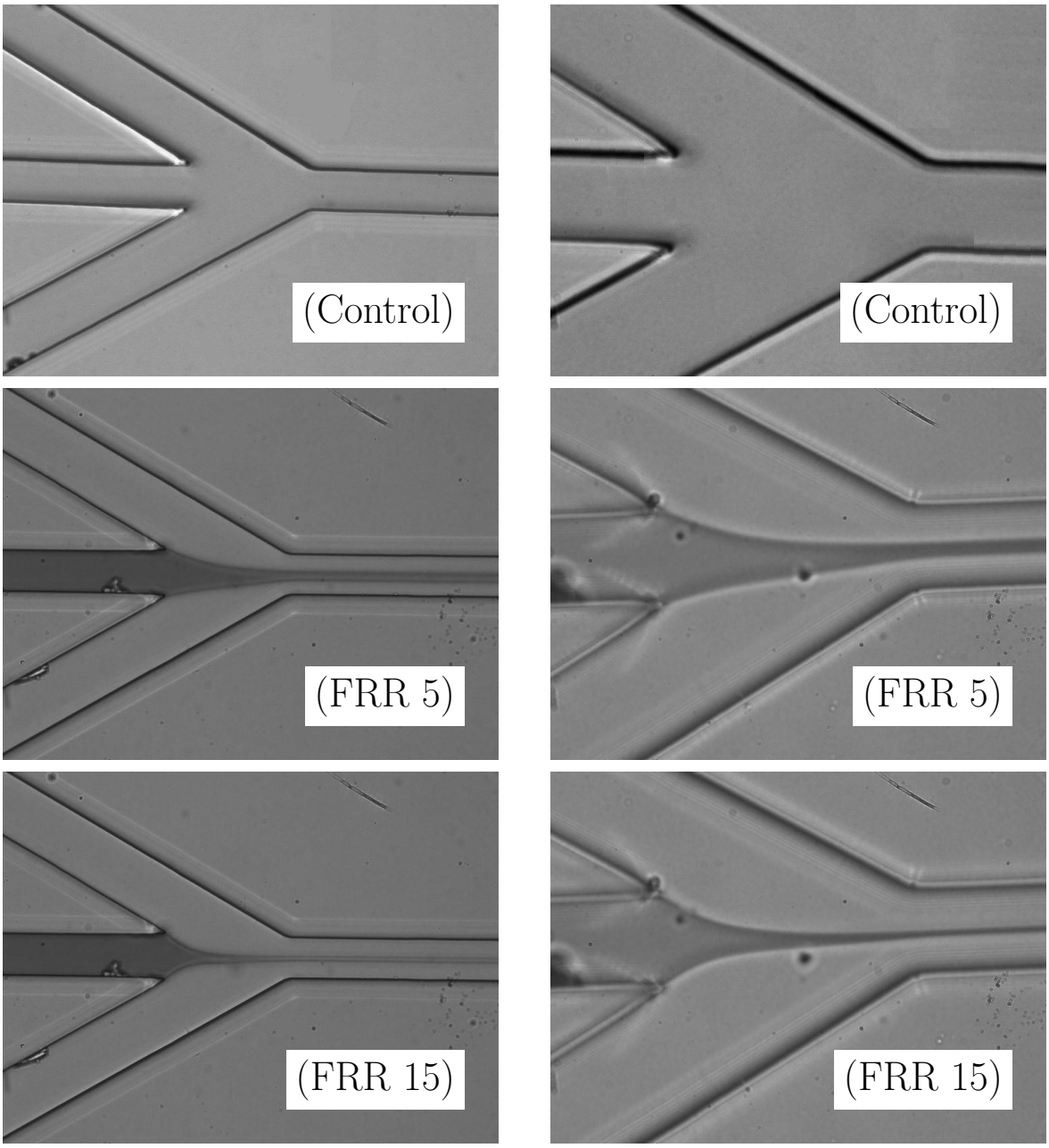

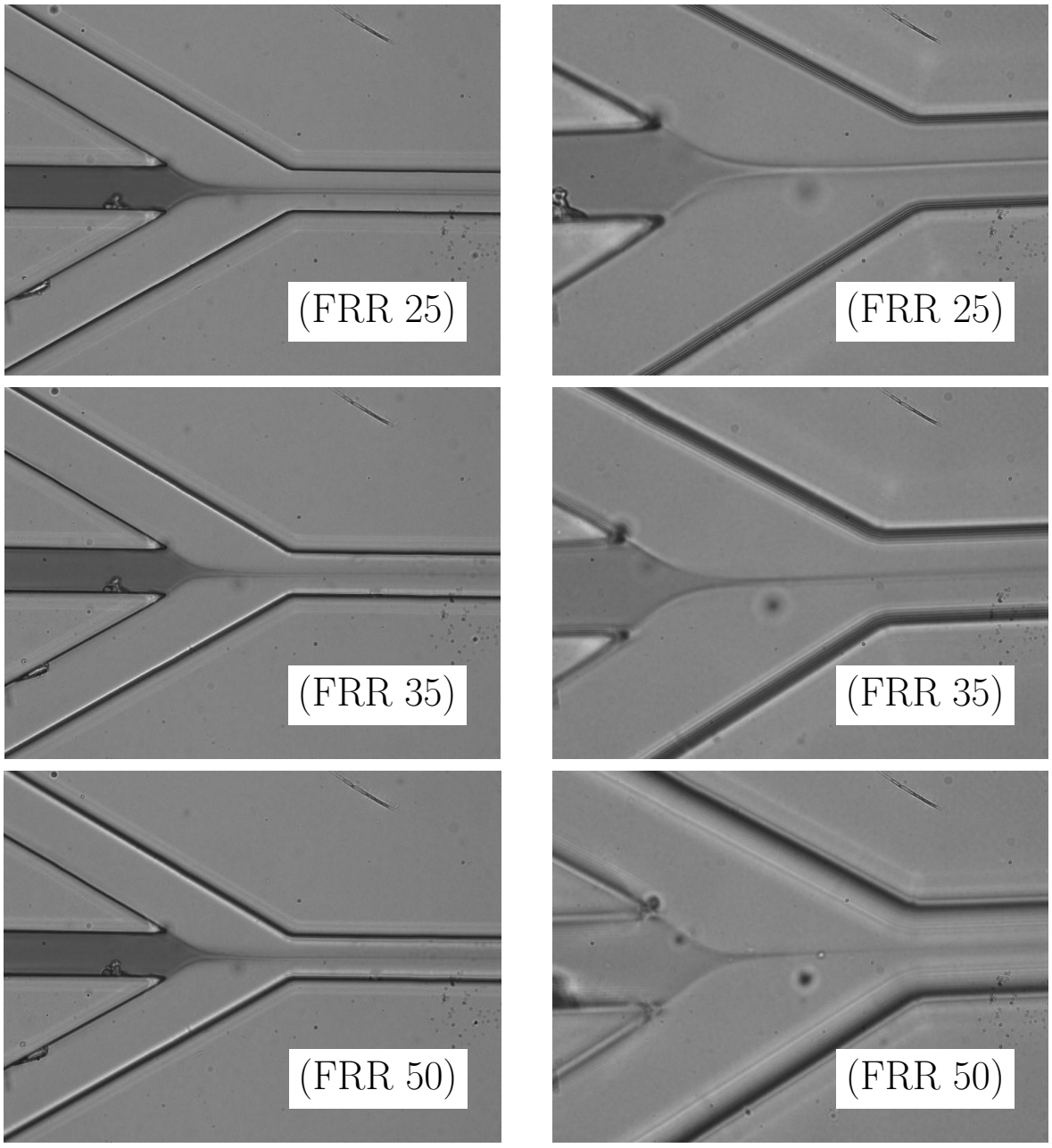

Figure 6.1: (Continued from Previous Page) Light microscopy images of the flow focusing junction at (x20) and (x40).

As shown in Figure 6.1, the focused stream at the center of the flow focusing junction is not always centered along the mid-line of the channel and symmetrical. In practical hydrodynamic focusing applications, the centerline of the hydrodynamically focused stream may not coincide with the centerline of the channel [94]. This has led to studies focusing towards developing theoretical models for asymmetric hydrodynamic focusing (for unequal flow rates at device inlets) in rectangular microchannels with either high or low aspect ratios, as an attempt to predict both the location and the width of the focused stream [94].

Overall, it has been proven that the width of the focused stream is independent of the stream location but is dependent on the aspect ratio (height/width) for the rectangular channels [94]. Other studies demonstrate that for low Reynolds numbers ($Re < 5$), a slightly convex shape of the focused streams is generated [95] and is to be expected in microfluidic channels due to viscous forces dominating inertial ones at low Re numbers. This can cause flow disturbances in a way reminiscent of that of a turbulent flow at high Re numbers. This phenomenon can be observed in our flow focusing device at low flow rate ratios (FRRs) (*Figure 6.1; FRR 5*), where one can see that the flow is not symmetrical but in fact leans slightly towards the upper side of the central channel wall. In this case, the flow rate being so low, our pump was not able to minimize flow perturbations and provide a continuous pulsatile-free flow and a fixed, constant focused stream width. Retrospectively, this can give us to expect a higher polydispersity and standard-deviation of the particles diameters at low FRRs compared to high FRRs, where a better control of the flow focusing enables a constant more laminar flow.

6.1.2 Comparison between Experimental and Simulated Flows:

Initial attempts at hydrodynamic focusing were aimed at confining sample flow to a narrow column, which is generally referred to as 2D flow focusing [96]. In 1998, Knight et al. demonstrated the possibility of significant microfluidic focusing in 2D by confining the sample flow from a 10 μm nozzle to a width of only 50 nm [82, 83].

The following image sequence in Figure 6.2 shows a comparison of the focused alcohol stream in a the 65 μm wide central micro-channel and the two 45 μm wide side micro-channels, imaged with an optical microscope and the 2-D model simulation for the respective FRRs of 5, 10, 20 and 50 for flow rates corresponding to 40, 90, 190 and 490 $\mu L/min$.

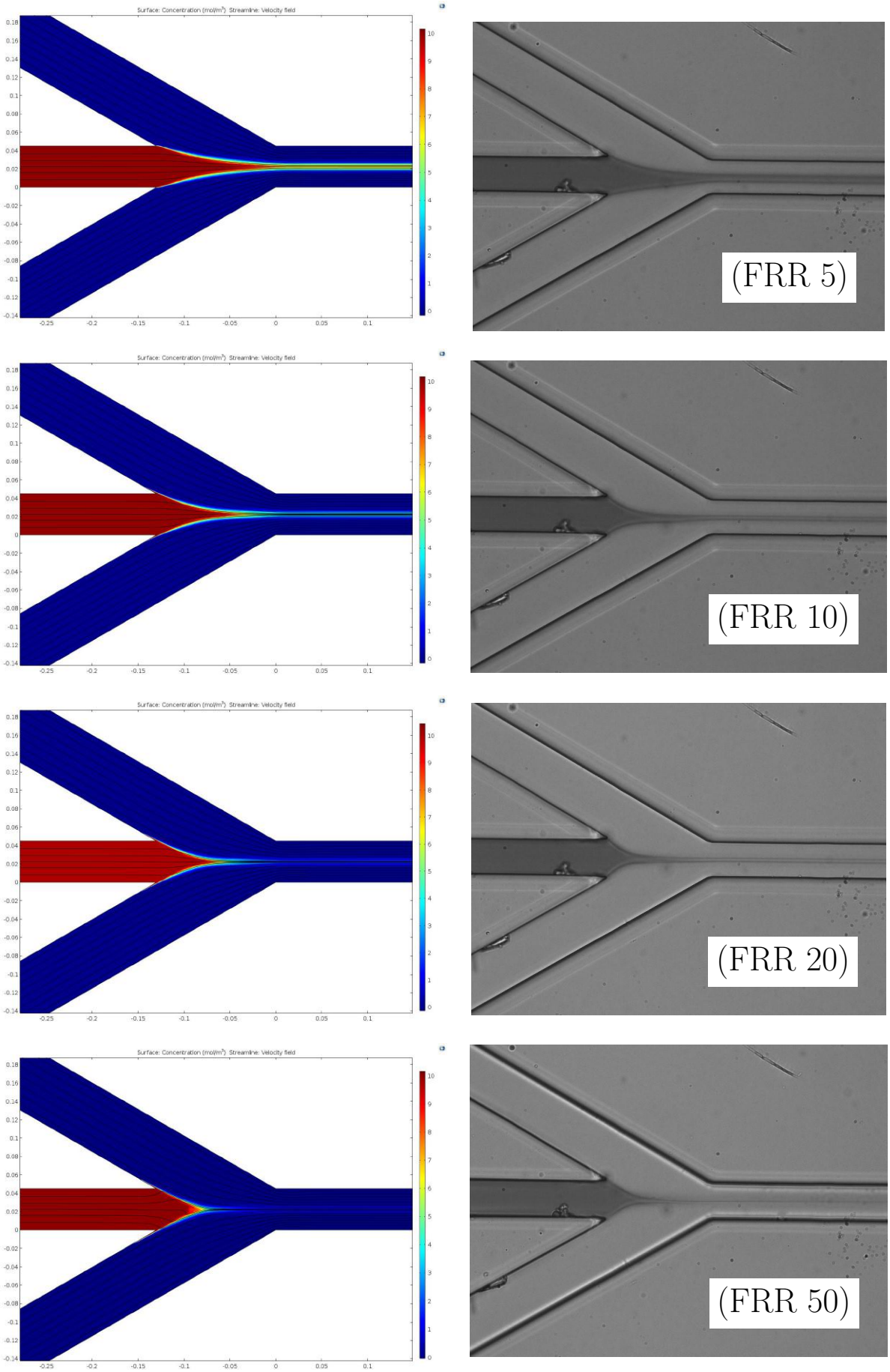

Figure 6.2: Comparison of the focused stream imaged with an optical microscope and the 2-D model simulations for the respective FRRs of 5, 10, 20 and 50.

Overall, the 2D simulation results are well substantiated with the experimental findings. The shape and width of the focused ethanol stream is represented correctly in the simulation with a tendency to decrease its thickness with an increase in the FRR. Experimentally however, obtaining precise measurements of the width of the focused stream in the micrometer scale is not possible as ethanol and water continuously inter-diffuse along the interface.

Conclusion:

In conclusion, changes in FRR resulted in variable stream widths of the focused solvent/lipid stream. Experimental investigations indicated that in the case of symmetric side streams focused flow sheet was not necessarily uniform with undesirable thickening close to the walls of a micro-channel observed in the case of low FRRs (Figure 6.1). By manipulating flow rates of the focusing flows, location of the focused sheet can be deformed and moved out of the symmetry plane and most importantly, a precise control of the width of the focused stream, on which the size and polydispersity of the generated liposomes depend on, is achieved. Maintaining a precise control of the focused stream width is crucial in various applications of the flow focusing systems [83].

6.2 Visualization of Liposomes by EM

In order to characterize the synthesized liposomes, their morphology, shape and structure has visualized by negative staining cryogenic transmission electron microscopy (Cryo-TEM). Negative-staining, a rapid, simple and conventional technique of electron microscopy (EM), has been commonly used to initially study the morphology and structure of proteins and lipids for half a century [97]. In addition to providing a visual of the liposomes formed, it can also give us an approximation of the size distribution of the liposomes in solution.

Figure 6.3 shows the nano-lipsoomes formed at FRR= 30 and C_{DPPC}= 10 mg/mL.

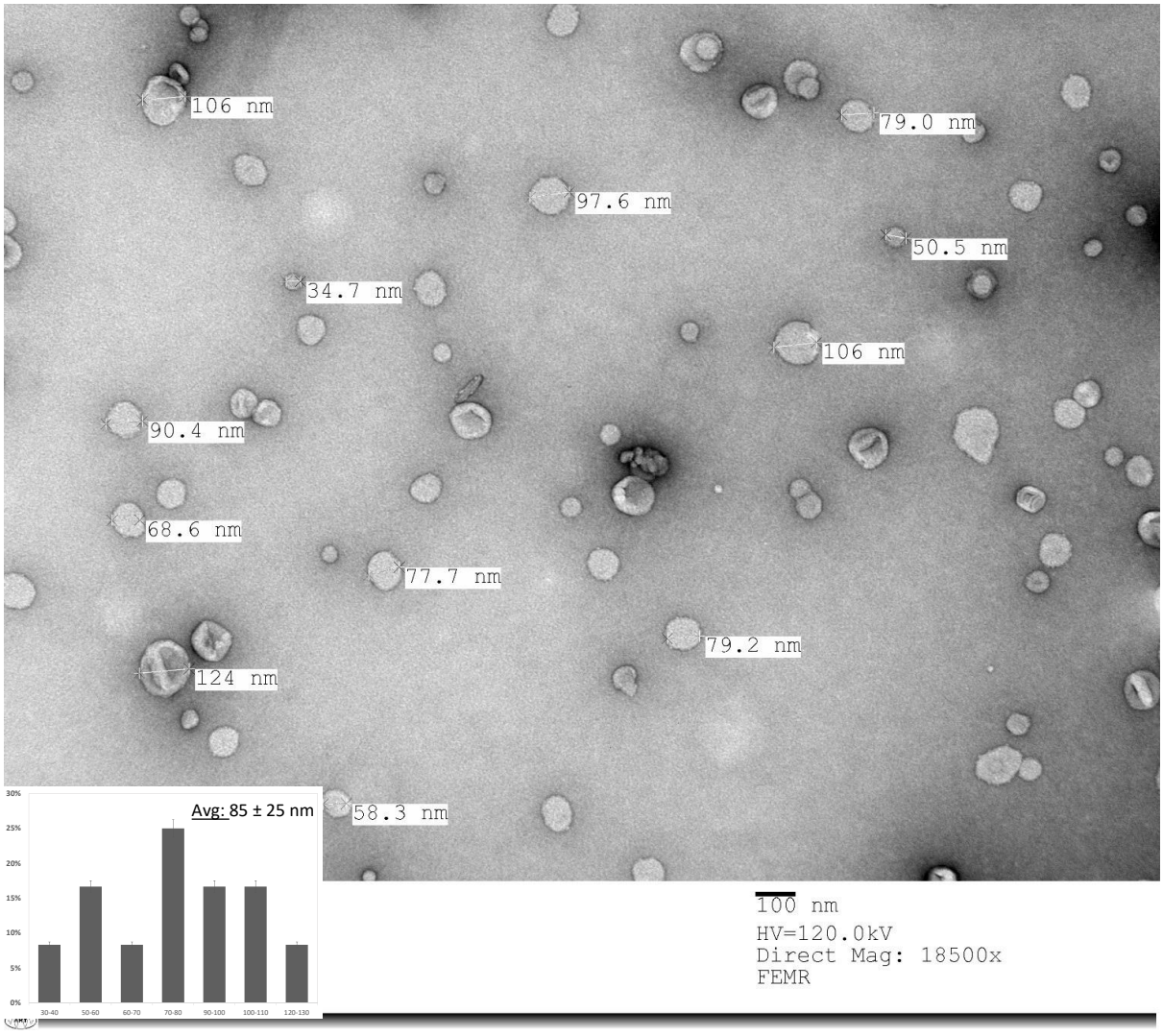

Figure 6.3: TEM image of the nanoliposomes after negative staining (FRR= 30, C_{DPPC}= 10 mg/mL). The small insert show the size distribution of the particles as measured by Cell Profiler with the average value (in nm ± SD).

The measuring tool of the TEM gave an approximate estimation of the particle size dis-

tribution within the sample which in turn gives an global overview of the polydispersity of the liposome product. A quantitative analysis of the size distribution of the liposomal particles has then been drafted as displayed in the small insert (Fig. 6.3). On average, particle sizes approximate 85 nm ± 25 nm.

Furthermore, at this condition (FRR=30, C_{DPPC}= 10 mg/mL), the liposomes particles have a good size distribution but are not completely monodisperse. In term of their morphology, the particles are spherical and mostly unilamellar or bilamellar (multilamellar). Aggregates has been detected but are not significant. In comparison, for a lower flow rate ratio and for the same concentration, the aggregate formation is significant which in turn, causes significant artifact and noise, making it difficult to get an estimate of particle size distribution. This is shown in Figure 6.4:

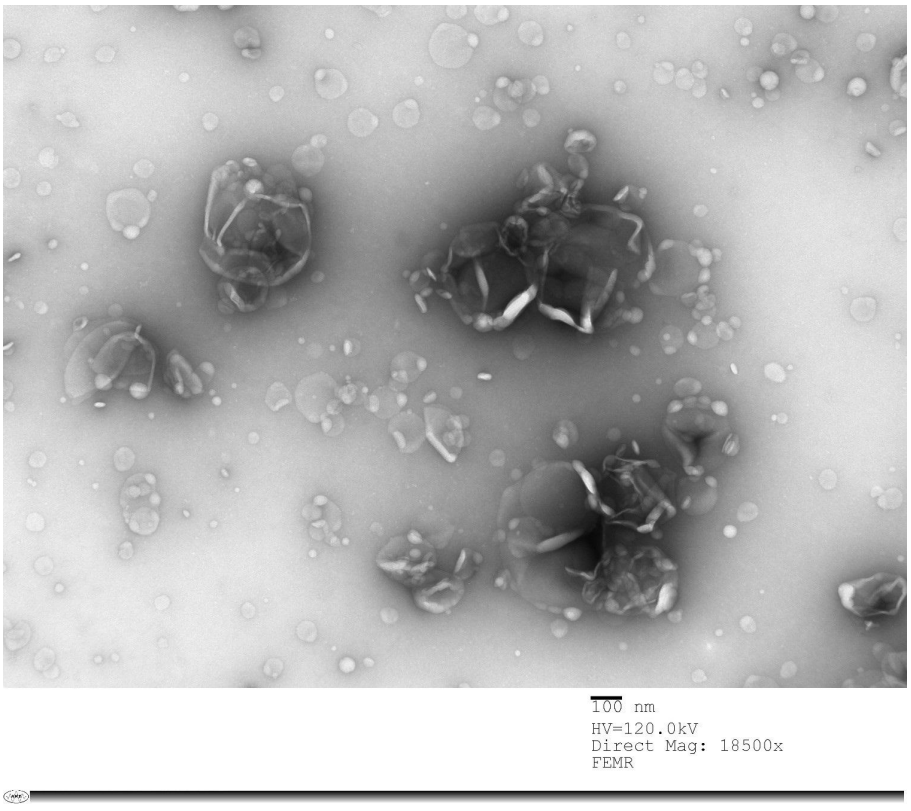

Figure 6.4: TEM image of the nanoliposomes after negative staining (FRR= 10, C_{DPPC}= 10 mg/mL).

Overall, we conclude that at low FRRs and high DPPC concentrations, aggregation of liposomes is significant which results in high particle polydispersity.

Another condition was tested for an intermediate flow rate ratio (FRR =30) and a lower concentration (C=5 mg/mL). This is shown in Figure 6.5:

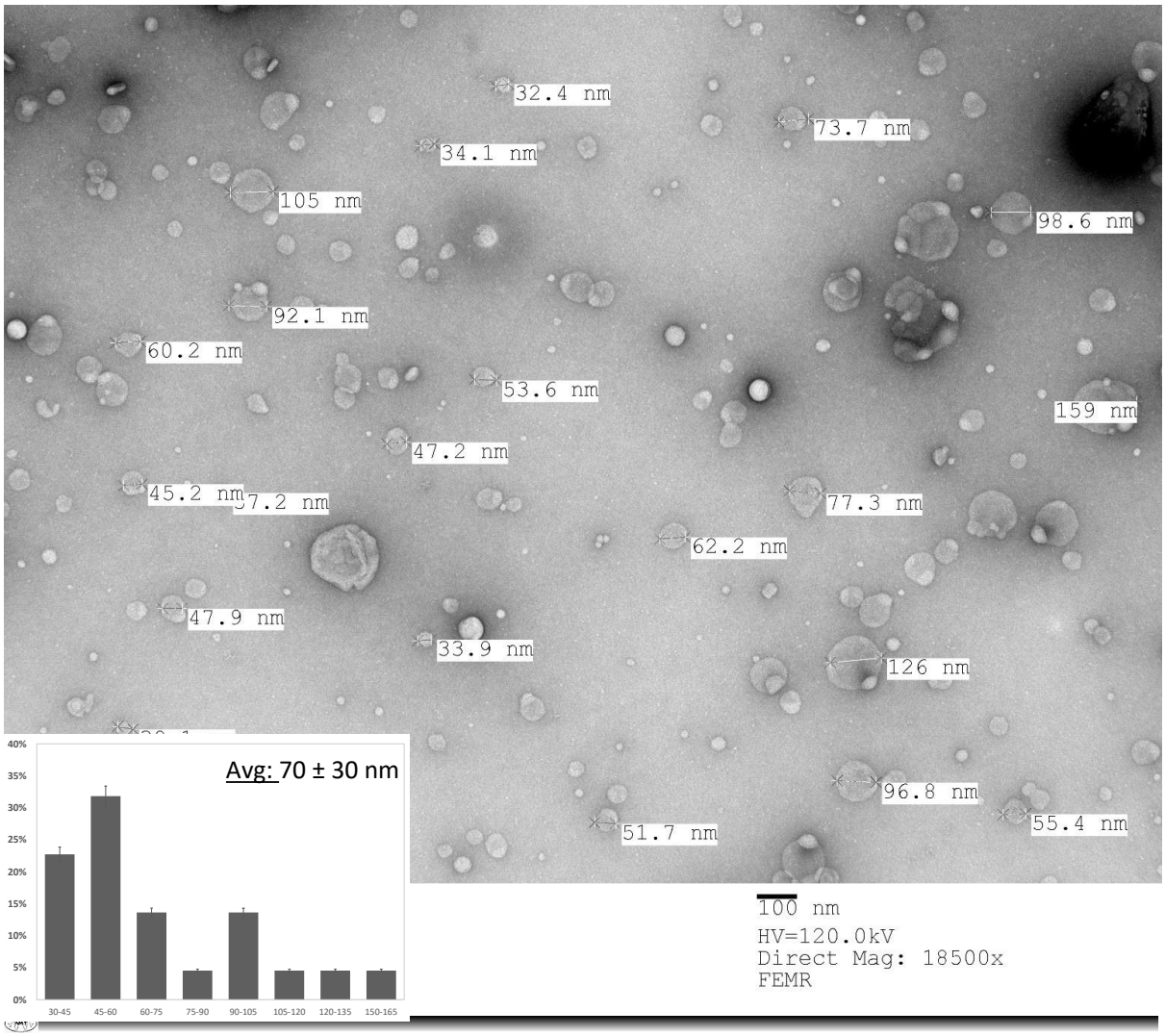

Figure 6.5: TEM image of the nano-liposomes after negative staining (FRR= 30, C_{DPPC}= 5 mg/mL). The small insert show the size distribution of the particles as measured by Cell Profiler with the average value (in nm± SD).

Particles have a good size distribution but polydispersity is more significant. As shown in the small insert of Fig.6.5 here a plot of particle size distribution ranging from 30-160 nm is displayed, particle size average 70 nm ± 30 nm but the liposomal population is highly heterogeneous. In this condition however, aggregate formation was however insignificant. In term of their morphology, the particles are spherical and mostly unilamellar (no multilamellarily). This can be seen in Figure 6.6 where a close-up of the liposomes is given.

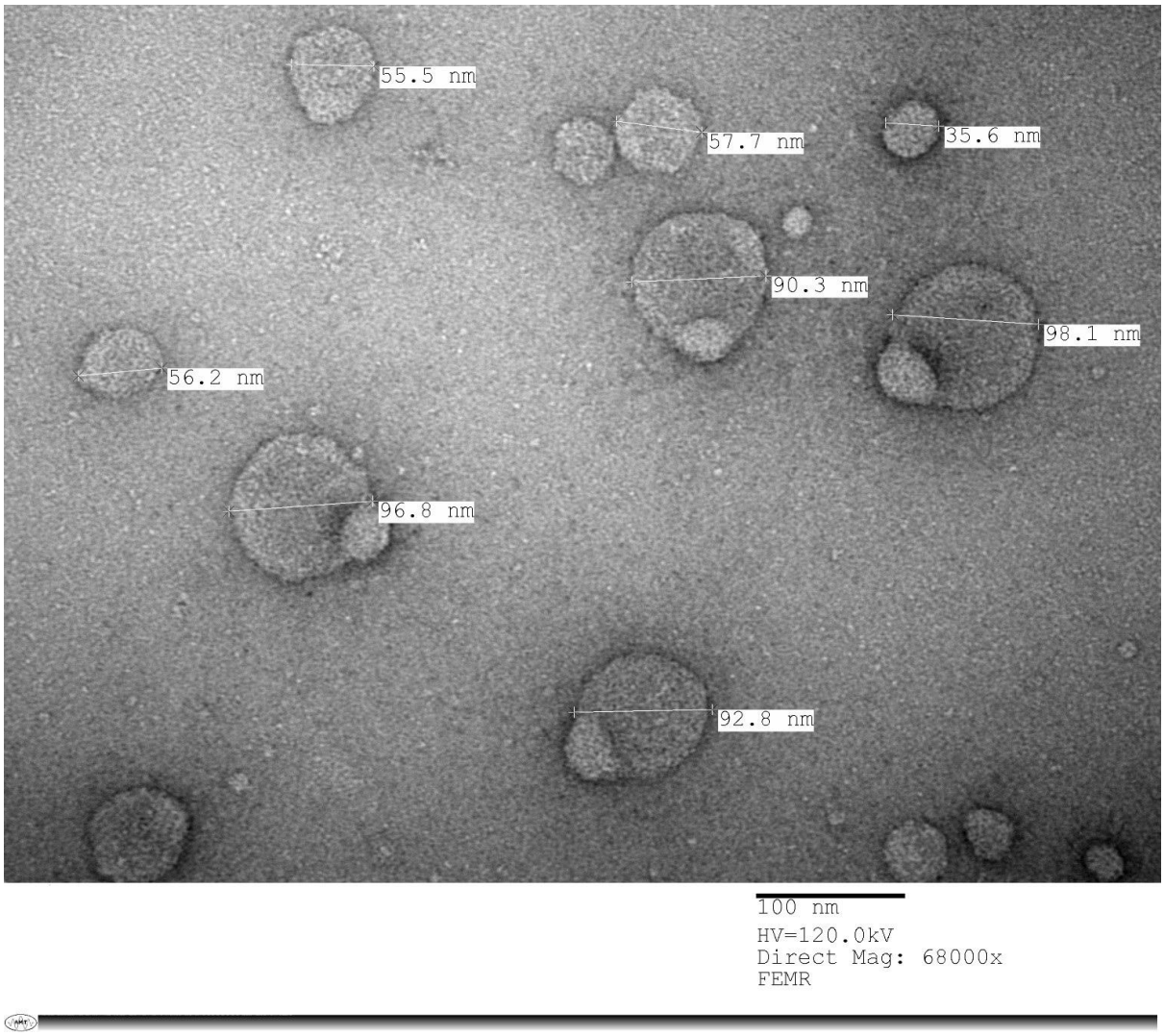

Figure 6.6: TEM image of the nanoliposomes after negative staining (FRR =30, C_{DPPC}= 5 mg/mL)

In Figure 6.6, one can observe than a few of the synthesized liposomes are in fact not completely separated but tend to stick to on another thus forming bigger sized liposomes resembling MLVs. This phenomenon is however not a common occurrence. The captured image in Fig. 6.6 is not statistically significant with the majority of the samples observed under TEM being for the most part SUVs similar to those displayed in Figures 6.3 and 6.5. However, this suggests that careful sonication of the samples for several minutes might be recommended prior to size measurements in order to be able to measure separate liposomes instead of fused ones. Sonication of the samples for 15 mn followed by 1h recuperation of the samples was therefore established prior to DLS and NTA measurements.

Several methods can be used to apply TEM in the evaluation of morphology and architecture of liposomes. The freeze-fracture electron microscopy is an optimal technique for examining the ultrastructure of rapidly frozen biological samples by TEM, but the preparation of the samples (cryo-fixation, fracturation and the following operation of shading

with evaporated platinum or gold) required caution and long time [98]. Negative staining is an easier and faster procedure. According to this procedure, liposomes are surrounded or embedded in a suitable electron dense material providing high contrast and good reproducibility. In our case, a cationic negative stain (uranyl cation) was used that binds the phosphate group of phospholipids, poorly penetrating the lipidic bilayer; nevertheless, it allows the indicative evaluation of the liposomal internal structure without discriminating on the fine details.

The negative staining of our liposomes (Figures 6.3, 6.4, 6.5 and 6.6) confirms the presence of a population of heterogeneous vesicles in which it is possible to emphasize the presence of close bilayer structures spaced by free internal structure. Nevertheless, at high samples concentrations, the shape of liposomes appeared distorted, although this electronic microscopical technique ensures the complete structural analysis of the thin transparent samples [98]. The possible artifacts could be due both to the staining process (the interaction between the sample and the negative stain) and the distortion/alteration induced during the drying steps are caused by the exposition of the samples to a vacuum.

Conclusion:

In conclusion, according to the results obtained from negative stating and TEM imaging, the HFF generated liposomes have under optimal FRR and concentration, a good polydispersity but are not fully monodisperse. Polydispersity increases with a decrease in FRR and an increase in concentration. Also, the liposomes generated are not totally unilamellar as we have MUVs generated under high lipid concentrations and a majority of SUVs under a lower concentration. However, images obtained by negative staining do not mirror completely the reality since the particles are distorted during the staining process. In fact, as part of the drying processes, the particle loses its hydration shell. Often, this shell stabilizes the soluble particle onto a certain configuration and deposition on the carbon can cause it to change shape [93].

6.3 Effect of Experimental Parameters on Liposome Properties

In this section, characterization of liposomes characteristics such as size, charge and concentration are conducted to investigate the effect of fluid parameters such as the flow rate and lipid composition on particles dimensions, size distribution and concentration. As such, the size of the liposomes have been be measured by both dynamic light scattering (DLS) using a Zeta Potential Analyzer and nanoparticles tracking analysis tools (NTA) which also yields valuable information regarding particle concentration.

6.3.1 Effect of Lipid Concentration on Particle Size and Polydispersity

The fate of intravenously injected liposomes is determined by a number of properties. Two of the most important are particle size and zeta potential. Particle size is measured using dynamic light scattering (DLS). This technique measures the time-dependent fluctuations in the intensity of scattered light which occur because the particles are undergoing Brownian motion. Analysis of these intensity fluctuations enables the determination of the diffusion coefficients of the particles which are converted into a size distribution [99].

The size distribution of lipid particle with respect to the flow rate ratio (FRR) between the lipid and water streams has been measured by DLS and plotted for every concentration. Different DPPC concentrations in ethanol have been tested namely (C= 1, 2, 3, 5 and 10 mg/mL). Figure 6.7 shows all the graphs combined and displays the complete size distribution profile for all the lipid concentration of DPPC in ethanol for concentration ranging from 1 to 10 mg/mL.

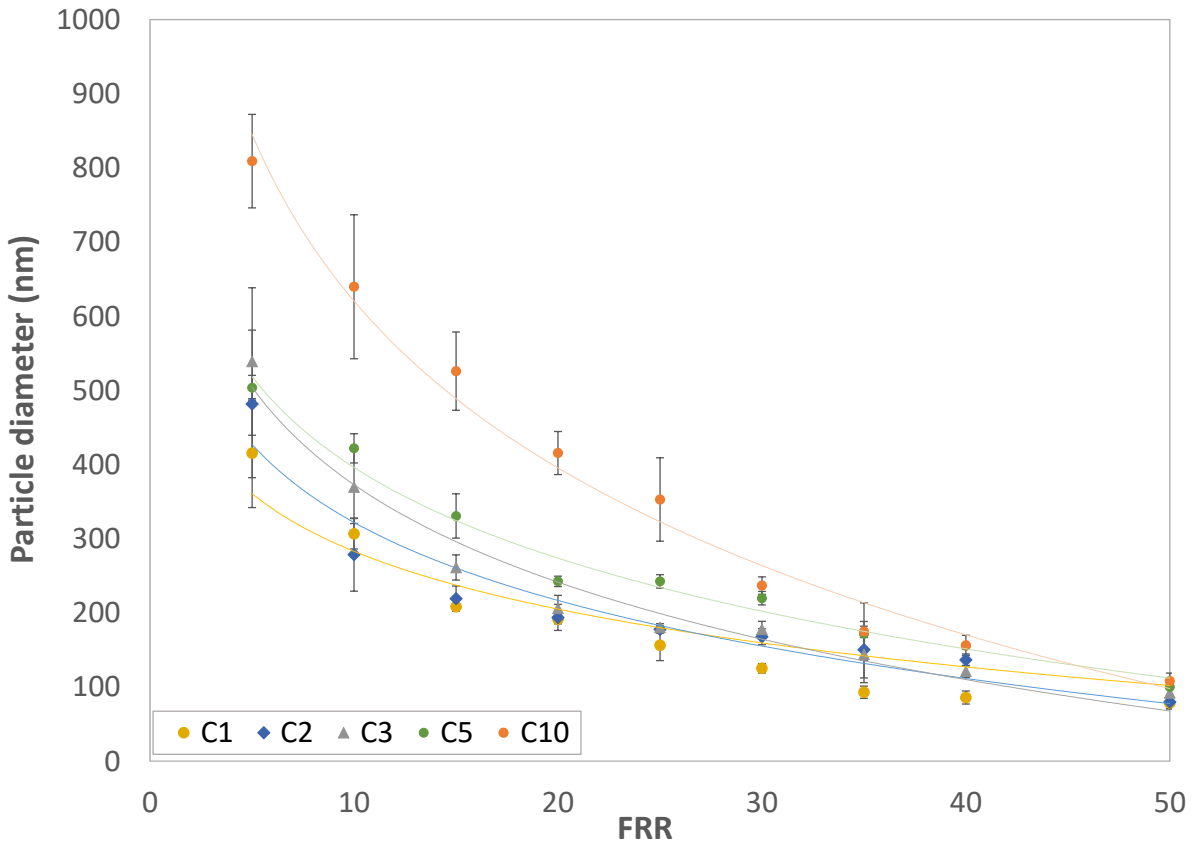

Figure 6.7: Particle size distribution profiles of 2D HFF synthesized liposomes as a function of DPPC lipid concentration at inlet (C=1-10 mg/mL) for various FRRs (5-50) (n⩾15).

A logarithmic tendency curve has been fit to all the concentration profile in Fig. 6.7 with a correlation factor averaging R^2=0.9. At high lipid concentration (C_{DPPC}= 10 mg/mL) and low flow rate ratios (FRRs $\approx 5-10$) , particle sizes reach almost a micron (650-850 nm). However, at high FRR=50, the particle size is significantly smaller (100 nm). As we will see from the next graphs, this is the case for almost every concentration, at the size converges towards 100 nm for FRR= 50 and this is true for every concentration from 1 to 10 mg/mL. We can notice a tendency of a decrease in the correlation factor (R^2) with the decrease in concentration (from 0.985 at C_{DPPC}= 10 mg/mL to 0.71 at C_{DPPC}= 1 mg/mL). At low concentration, the flow and particle formation is less predictable and stable respectively so the standard error is bigger.

Figure 6.8a gives a better representation of how flow rate (or FRR) affects the sizes of the colloidal liposomal dispersions obtained at various DPPC concentrations. The z-average diameter values are the means of at least 50 repeat measurements (standard deviations in brackets) measured 5 times on 10 independent samples of concentrated liposomes.

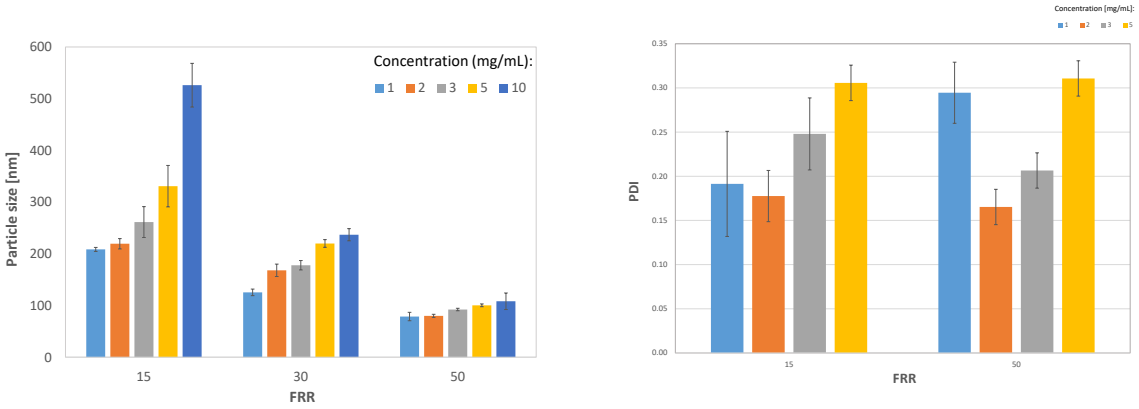

(a) (b)

Figure 6.8: (a) Particle Size Distribution (in nm) of the synthesized liposomes showing a stacked histogram representation of the NPs size distribution at given concentrations (C_{DPPC}= 1-10 mg/mL) and FRRs (15, 30 and 50) (n⩾15). (b) Polydispersity index of the synthesized liposomes as a function of the FRR and DPPc concentration [mg/mL].

From Figure 6.8a, one can observe quite clearly a distinct tendency of an increase of particle size with both a decrease in FRR and an increase in DPPC concentration. In addition, as the flow rate ratio (FRR) increases from 15-50, the differences in particle sizes at various concentrations decreases and are less significant. For example, whereas at FRR=15, particles at C_{DPPC}= 5 mg/mL average ≈ 350 nm, that size is almost doubled at at C_{DPPC}= 10 mg/mL (average ≈ 550 nm). On the other hand, at FRR=50, particle sizes reach a plateau of 100 nm and for every DPPC concentration (1-10 mg/mL).

Average values of the polydispersity index (an estimate of the width of the distribution) for the liposomes prepared at two different FRRs (15 and 50) as various DPPC concentrations (in mg/mL) are given in Figure 6.8b. The polydispersity values are the means of 30 repeat measurements (standard deviations in brackets) measured 5 times on 6 different concentrated liposome samples.
Overall, all liposomal DPPC formulations exhibited homogeneity with a polydispersity index (PDI) of less than 0.35. Overall, the average PDI index was higher at a FRR of 15 than at 50 and was maximum at a concentration of 1 mg/mL at FRR= 15.

6.3.2 Effect of Charge on Particle Size and Stability

The zeta potential of a particle is the overall charge that the particle acquires in a particular medium. Knowledge of the zeta potential of a liposome preparation can help to predict the fate of the liposomes in vivo. Measurement of the zeta potential of samples in the Zetasizer Nano is done using the technique of laser Doppler velocimetry. In this technique, a voltage is applied across a pair of electrodes at either end of a cell containing the particle dispersion. Charged particles are attracted to the oppositely charged electrode

and their velocity is measured and expressed in unit field strength as their electrophoretic mobility [99].

After confirming the core-shell structure of the lipid NPs, and knowing their range of size distribution based on the change in FRR, we investigated the possibility of controlling the NP's physicochemical properties, mainly size and surface charge while keeping other conditions such as lipidic and aqueous flow rates and flow ratios the same. The zeta potential (ZP) of colloidal systems and nano-medicines, as well as their particle size exert a major effect on the various properties of nano-drug delivery systems. Not only the stability of dosage forms and their release rate are affected but also their circulation in the blood stream and absorption into body membranes are dramatically altered by the ZP [100].

Figure 6.9 illustrates a change in zeta potential of the liposomal NPs when molecules with different charges were introduced in the input streams along with DPPC. Generally speaking, the higher the absolute value of the zeta potential, the more stable the system will be. That means it will be better able to withstand additions of salt (which might otherwise destabilize it). It will also usually show a lower viscosity [101]. If one is relying on the electric charge alone to keep the system in a disperse state then the zeta potential will usually need to be kept above 25 mV (positive or negative). Below 10 mV, the suspension is then unstable and the aggregates will quickly settle out from the surrounding medium.

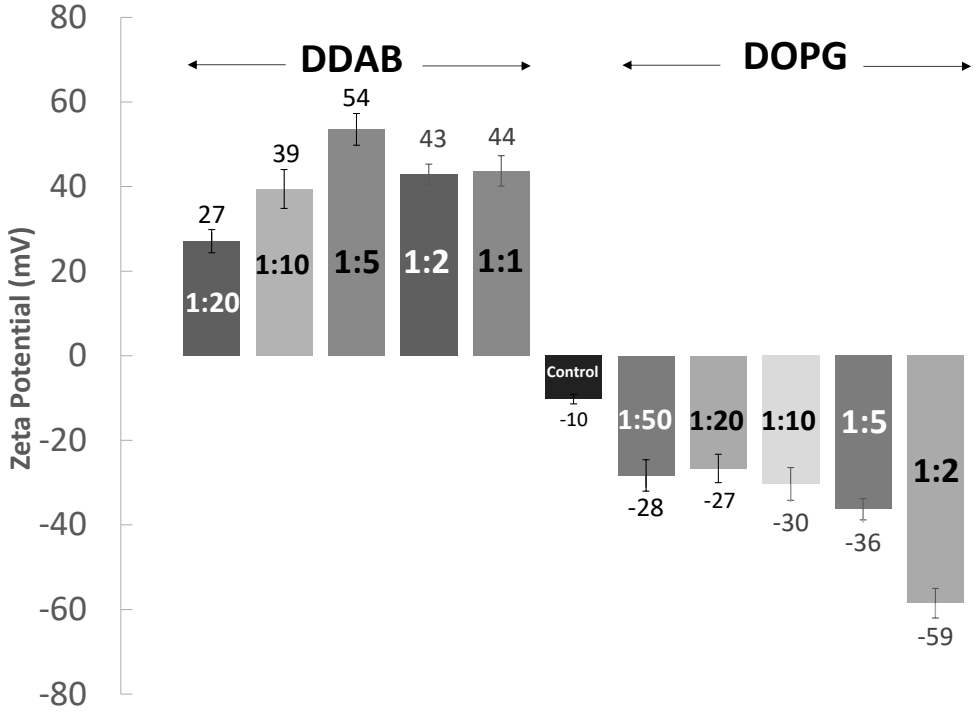

Figure 6.9: Zeta Potential Measurements (in mV) of synthesized liposomes DPPC liposomes with different DOPG/DDAB weight ratios (n⩾10).

From Figure 6.10, we conclude that the zeta potential of the NPs can be controlled. From slightly negative/neutral (ZP ≈ -10 mV) to highly positive (ZP ≈ 54 mV) or negative (ZP ≈ -60 mV) charge by utilizing DDAB or DOPG respectively along with DPPC in the lipidic stream. During this process, the NPs size did not remain unchanged as shown by Figure 6.10.

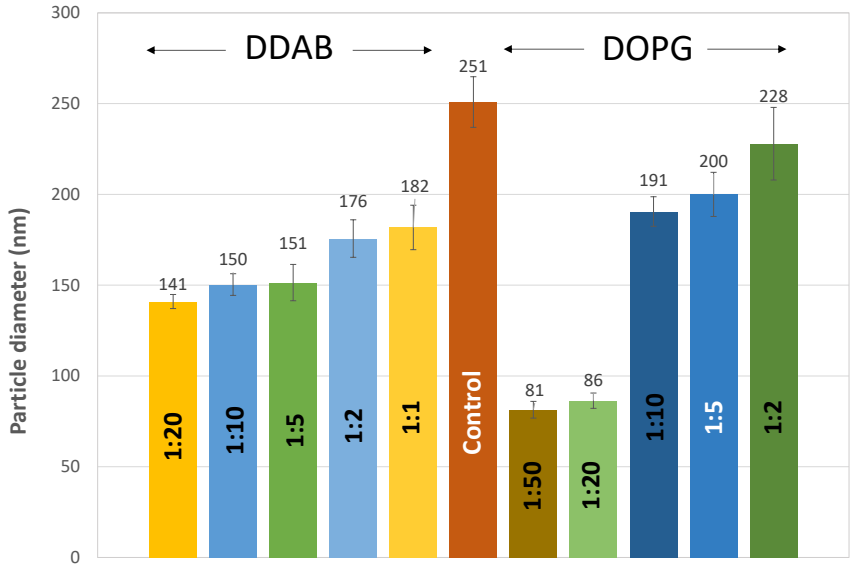

Figure 6.10: Particle Size Distribution (in nm) of the synthesized liposomes (n⩾10).

As shown in Fig.6.9, whereas our control (DPPC: EtOH solution of C=5 mg/mL) has a low -10 mV zeta potential, adding DDAB and DOPG increase either positively or negatively the charge. In fact, adding DDAB at a 1:5 ratio to the control C= 5mg/mL DDAB: ETOH solution give a high zeta potential of approximately 50 mV and results in highly stable lipid particles. On the other hand, adding DOPG gives a highly negative charge to the DPPC: EtOH particles with the maximum being at -30 for a 1:10 ratio which corresponds to a good particle stability. Further studies at higher DOPG: DPPC ratio need to be tested and a compromise between charge and size need to be found as this ratio (1:10 DOPG: DDPC gives the biggest size particles approx. 191 nm).

Conclusion:

Overall, our results show that the surface charge and size of the microfluidic synthesized liposomes can be finely tuned by changing the lipid stream composition and incorporating molecules with positively of negatively charged functional groups. Charge modification of nano-systems offer an opportunity for prolonging the blood circulation time of drugs, enhancing the possibility of its interaction with target cells of interest, and changing the pharmaceutical properties of nanosystems.

6.3.3 Effect of Concentration on Liposomes Yield and Size distribution

Nanoparticle tracking analysis (NTA) was used for the analysis of diluted samples of nanosized lipid particles and liposomes aggregates. A direct comparison with DLS was made in order to gain a more complete estimation of the distribution of liposomes sizes for some conditions. In that case, five measurements of the same sample were performed for every condition.

Qualitative Analysis:

In NTA, particles are visualized rather than imaged. Therefore, particles which are too small to be imaged by the microscope can be visualized in real-time. Figure 6.11 shows our HFF synthesized liposomal particles (C_{DPPC}= 5 mg/mL, FRR=30) visualized by NTA:

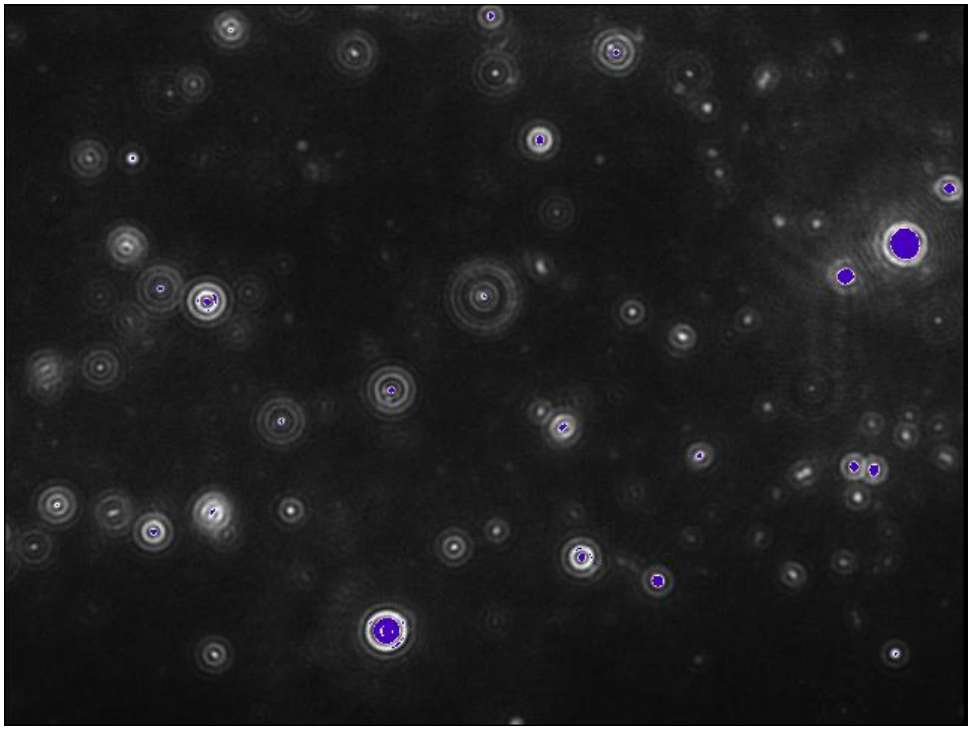

Figure 6.11: NTA video frame showing diluted liposomes particles at C_{DPPC}= 5 mg/mL, FRR= 30 (dilution= 100). Measured size by NTA = 250 nm ±50 nm.

Using the NTA technique, particles are seen as point scatterers moving under Brownian motion, with larger particles scattering significantly more light and appearing bigger. The high resolution of the NTA make us able to get an estimation of the sample polydispersity at any given condition (concentration, FRR) before quantitative capture and measurement. In Figure 6.11, the sample captured is slightly too concentrated. As a consequence some particles are seen to overlap each other (dark blue particles) shown in

Fig. 6.11. By adjusting the sample concentration and diluting the sample to twice more (to 200 x), we are able to proceed with the size measurement and reduce noise prior to quantitative measurements of sample size and concentration. Nonetheless, the sample is fairly mono-disperse, with a polydispersity similar to what was observed by negative TEM microscopy.

Quantitative Analysis:

Nanoparticle Tracking Analysis (NTA) enable the assessment of individual particles, rather than averaging over a bulk sample. This provides a distinct advantage in determining particle size [102]. Figure 6.12 displays the NTA particle concentration measurements at two different concentrations (C_{DPPC}= 5 mg/mL and C_{DPPC}= 10 mg/mL) and for three different flow rate ratios (FRR=15, FRR=30 and FRR=50). The error bars displayed on the NTA graphs were obtained by the standard deviation of five different measurements of each sample (n=5).

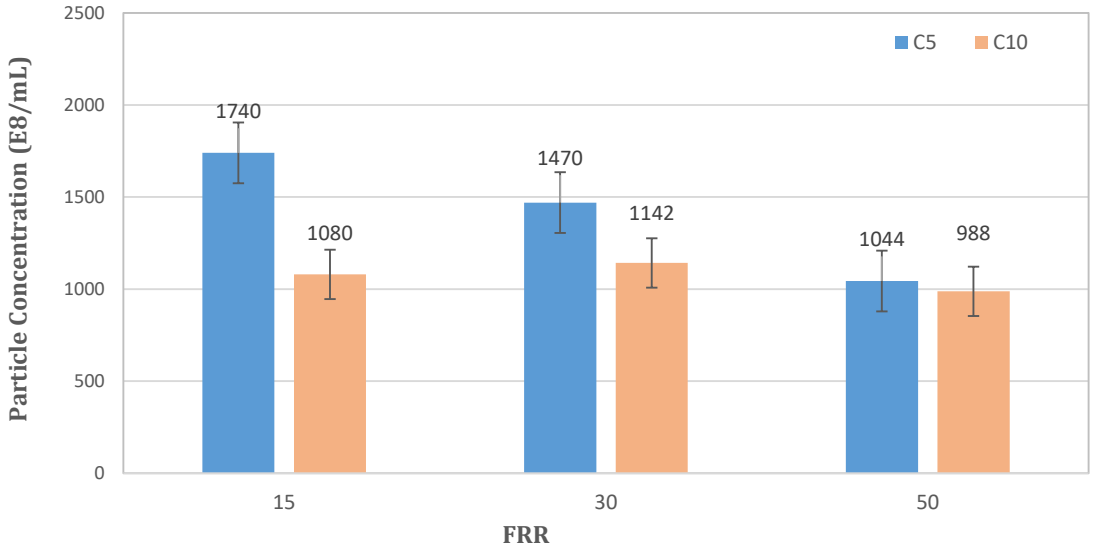

Figure 6.12: Particle Concentration (E8 $particles/mL$) of the synthesized liposomes as a function of DPPC concentration (mg/mL) and FRR.

From Figure 6.12, an inverse correlation between concentrations of lipid DPPC in ethanol and liposome particle concentration can be observed with DPPC solutions at C= 5 mg/mL being 37.9 % more concentrated in liposomes than solutions at C= 5 mg/mL at a FRR=15 and more than 22.3 % concentrated in liposomes at FRR=30. At FRR=50 however, no significant difference of concentration is noted between the two different concentrations (C_{DPPC}= 5-10 mg/mL). Alternatively, for a constant concentration of C_{DPPC}= 10 mg /mL, the difference in liposomal concentration is not significant at the various FRRs. On the other hand, for C_{DPPC} = 5 mg /mL, a tendency of a decrease in sample concentration with an increase in FRR can be observed. This difference amounts to more than 15.5 % between FRR 15-30 and to $\approx$ 29.0% between FRR 30-50.

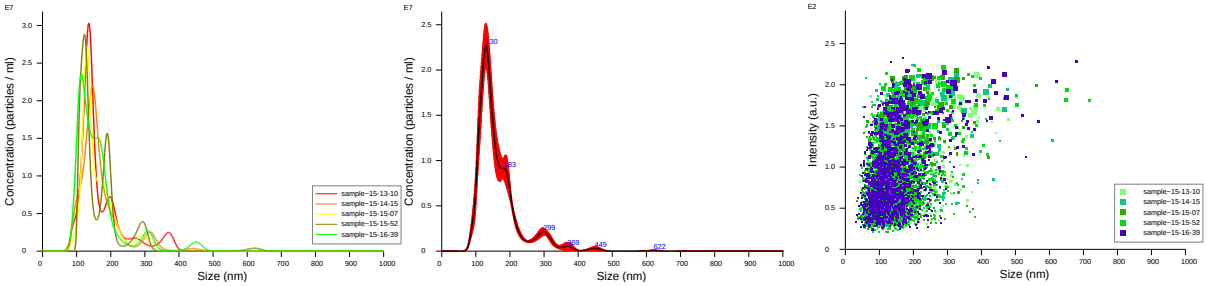

(a) (b)

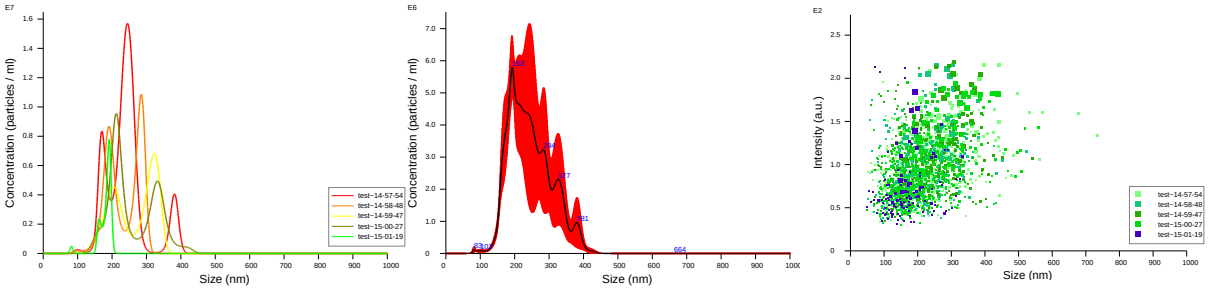

(c) (d)

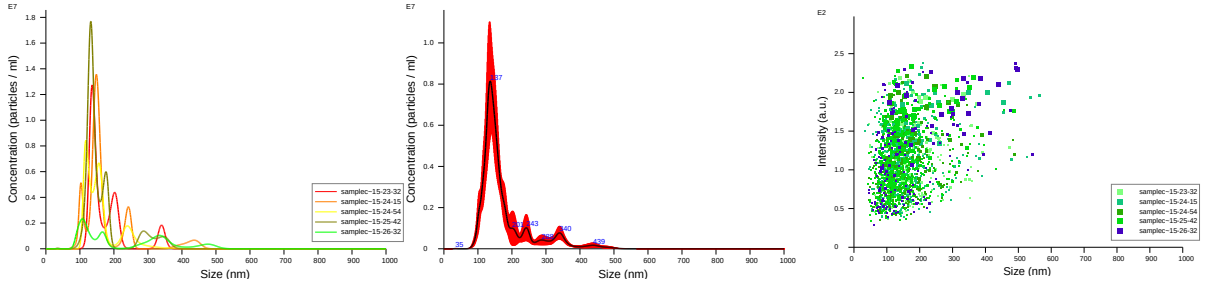

(e) (f)

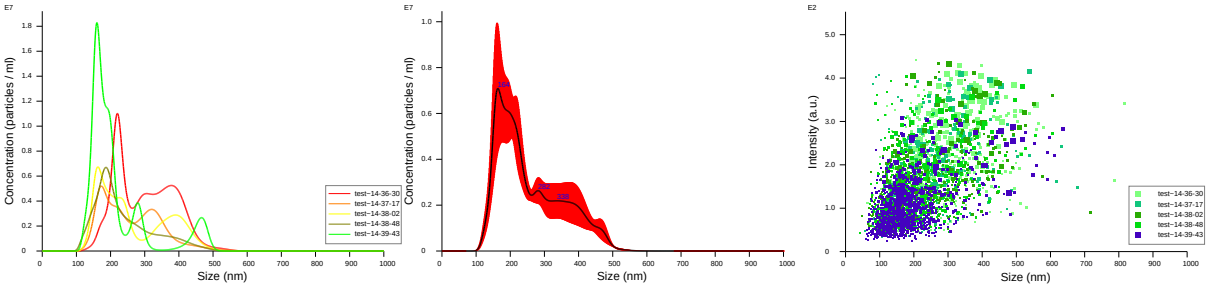

(g) (h)

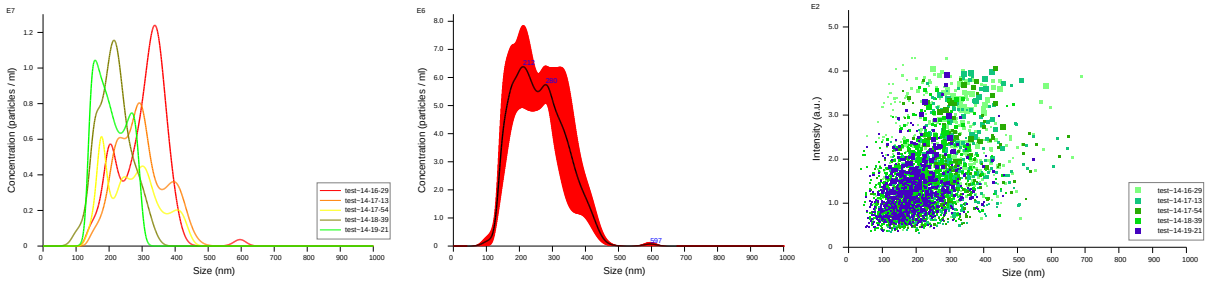

(i) (j)

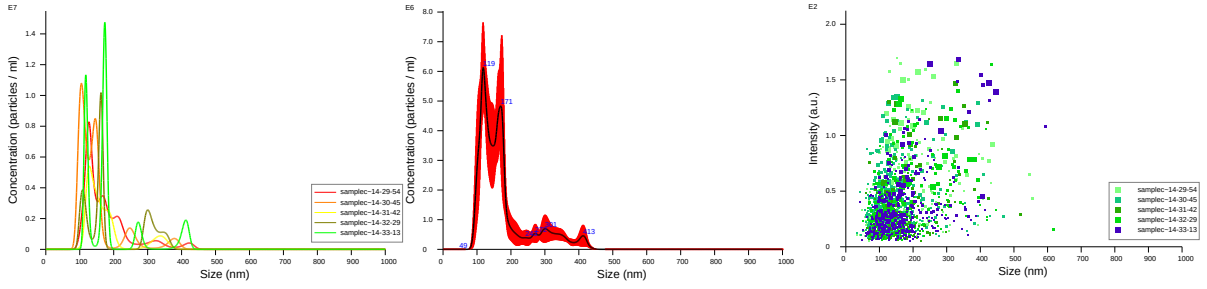

(k) (l)

Figure 6.13: *(Previous page.)* NTA Measurements (n=5) of liposome particles concentration (E8 $particle/mL$) (left) and average concentration (right) as a function of size (nm) (a, c , e, g, i, k). Averaged Intensity/Size graphs (n=5) for liposomes samples (b, d, f, h, j, l). For: C= 5 mg/mL; FRR=15 (a,b), FRR=30 (c,d) FRR=50 (e,f) and at C = 10 mg/mL; FRR=15 (g,h), FRR=30 (i,j), and FRR=50 (k,l). Samples were diluted 200 times prior to NTA measurement.

Overall, the analyzed samples (C_{DPPC}= 5-10 mg/mL, FRR15-50) are not fully mono-diperse. Contrary to the results acquired by DLS which show one main peak at a specific value of particle hydrodynamic diameter, a closer look at the averaged concentration/size peaks (red curves) in Fig. 6.13 (a, c , e, g, i, k) shows more than one peak, a consequence of the sample polydispersity. Therefore, at C= 5 mg/mL, at FRR=15 (a, b), the highest concentration reported is for liposomes particles measuring 130nm, however a secondary peak is observed at 183 nm with half the concentration as well as minor peaks at 299, 369, 449 and 622 nm at a negligible concentration. Alternatively, at C=10 mg/mL, at FRR= 30 (i,j), the highest concentration reported is for liposomes particles measuring at 212 and 280 nm, but no secondary peaks are observed. However, the graph shows a minor peak at 597 nm which is less than ten times the initial concentration. This sample is therefore the most mono-disperse that has been measured. Similarly, at C= 10 mg/mL, at FRR= 15 (g, h), the highest concentration reported is for liposomes particles measuring 164 nm, but two secondary peaks are observed at 282 and 338 nm at a fifth of the maximum concentration. These results however do not necessarily indicate that the samples are heterogeneous and polydisperse. The different peaks measured can be due to the failure of the NTA of resolving and distinguishing between two colliding or neighboring particles (i.e. resolution), thereby giving peaks which are multiple times bigger than the main peak with the highest concentration. For example, at C= 5 mg/mL; FRR=50 (e,f), a main peak of particles at 137 nm is measured, but secondary peaks which are respectively 2 times and almost 4 times the main particles size being measured at 288 and 439 nm respectively. This conclusion is supported by the Intensity/Size graphs (right) shown in Fig.6.13 (b, d, f, h, j, and l), where we see that the samples being measured are not very scattered but in fact located with a 100-200 nm radius on the plots.

Conclusion:

Overall, we conclude that both DPPC concentration and FRR have a significant impact on the concentration of liposomes obtained by HFF synthesis, with the FRR playing a bigger influence on the resulting particle concentration to that played by the inlet concentration of DPPC. NTA was shown to accurately analyze the size distribution of the liposomes samples. Sample visualization and individual particle tracking are features that enabled a thorough size distribution analysis and made possible the characterization of our synthesized liposomal nanoparticles, complementing DLS. Live monitoring of the NPs provided information about potential aggregation and size distribution of liposomes.

Chapter 7

Loading Experiments

Liposomes enable the compartmentalization of compounds making them interesting as drug delivery systems. A drug delivery system (DDS) is a transport vehicle for a drug for in vivo drug administration. Drugs can be encapsulated, bound, or otherwise tethered to the carrier which can vary in size from tens of nanometers to a few micrometers. Liposomal DDSs have shown their capability to deliver drugs in a new fashion, allowing exclusive sales of encapsulated drugs to be extended beyond the initial compound's patent expiration date [44]. However, existing methods to form liposomes and encapsulate drugs are based on bulk mixing techniques with limited process control and the produced liposomes frequently require post-processing steps [24].

In this section, our microfluidic hydrodynamic flow focusing method is demonstrated to control liposome formation and compound encapsulation that guarantees liposome size homogeneity and adjustable encapsulation. The technology utilizes microfluidics for future pharmacy-on-a-chip applications. The microfluidic system allows for precise control of mixing via molecular diffusion with reproducible and controlled physico-chemical conditions compared to traditional bulk-phase preparation techniques (i.e. test tubes and beakers) [37, 38].

7.1 FITC labelled LC-TAT peptide Imaging

TAT is a cell-penetrating peptide (CPP) encompassing a highly cationic cluster composed of 6 arginine and 2 lysine residues in the very middle of the peptide sequence and an α-helical structure on the N-terminal part [103]. The TAT peptide sequence (47YGRKKR-RQRRR57) has been found to be essential for cellular entry [103]. In addition, TAT (Trans-Activator of Transcription) is a protein encoded for by the TAT gene in HIV-1 and stimulates HIV-1 gene expression during transcription initiation and elongation [42]. In addition, by antagonizing the CXCR4 receptor, reports suggest that TAT selectively encourage the reproduction of less virulent M-tropic (macrophage-tropic) strains of HIV early in the course of infection, allowing the more rapidly pathogenic T-cell-tropic strains (which use the CXCR4 receptor) to emerge later after mutating from M-tropic strains [43]. The ability to alter the concentration and control the amount of encapsulated compounds within liposomes in a continuous-flow mode is another interesting feature towards tailored liposomal drug delivery for cancer therapy.Prior to any further investigation, the chosen encapsulation peptide molecule FITC-LC TAT, was observed using light and fluorescence microscopy. As shown in Figures 7.1 and 7.2.

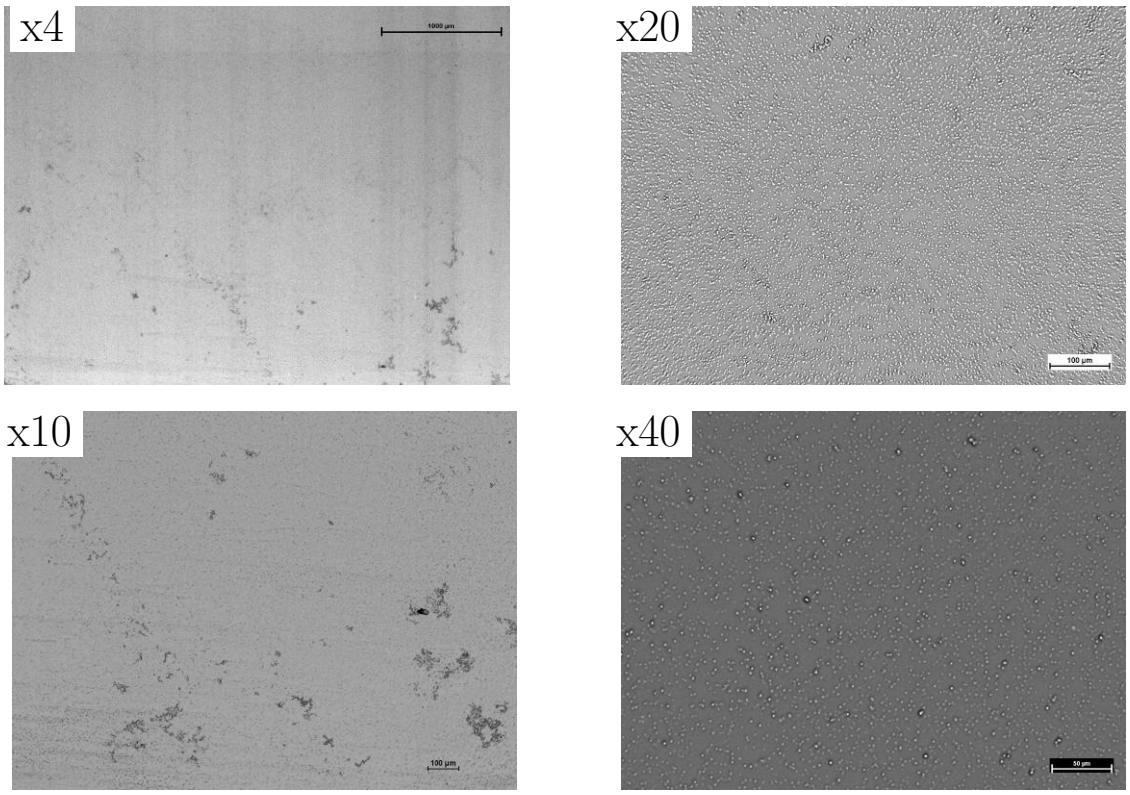

Figure 7.1: Optical imaging of the FITC labeled LC-TAT peptide at different magnifications. Scale bar: 1000 μm (x4), 100 μm (x10 and x20) and 50 μm (x40).

Using optical microscopy capabilities, it is not possible to resolve the FITC-LC-TAT peptide at magnifications of this amplitude. At 20x and 40x we can see a cluster of

peptides aggregating into small groups, but visualization of the peptide itself is beyond our reach. In order to be better able to observe the peptide, we visualize it under florescence as shown in Fig. 7.2.

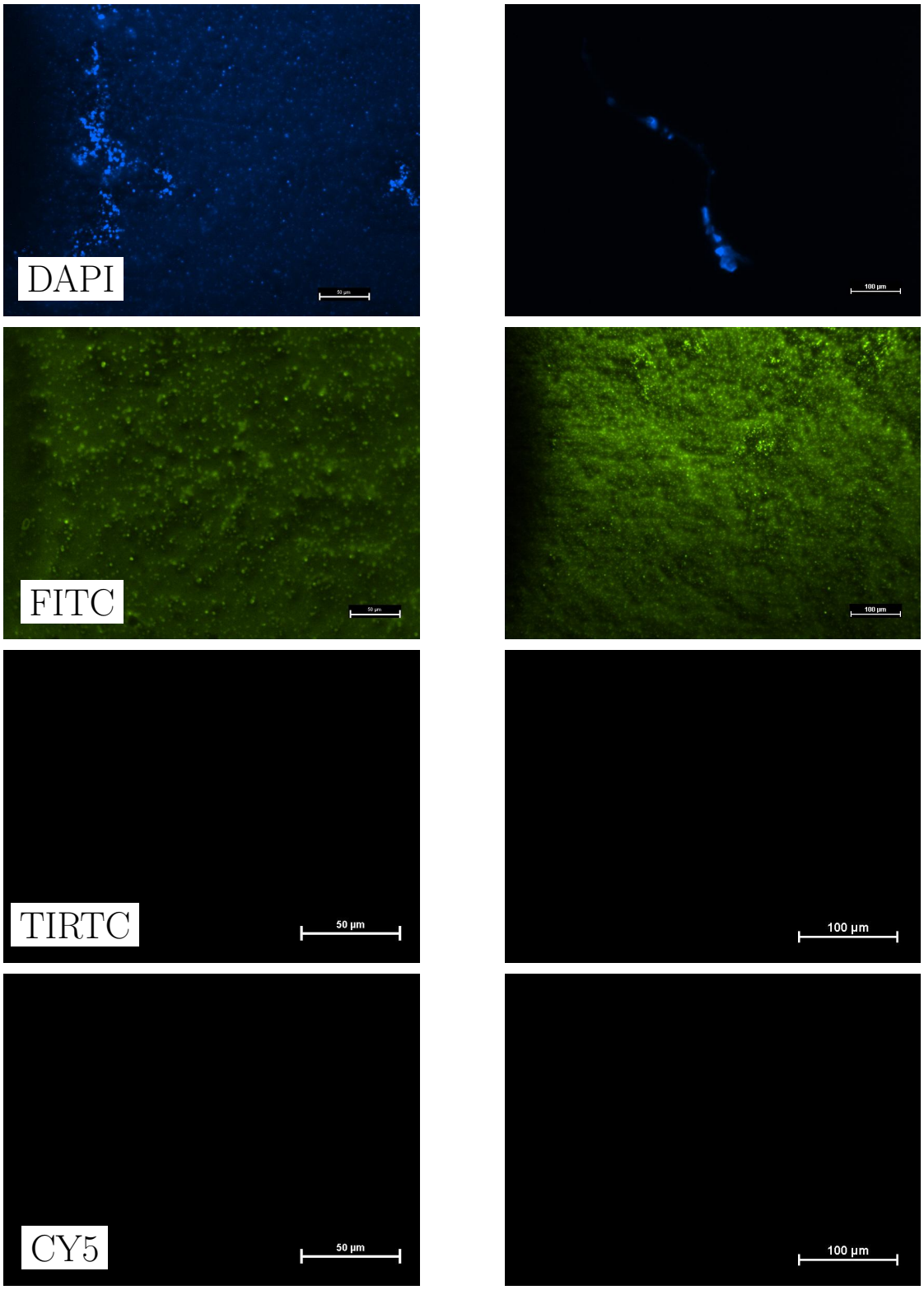

Figure 7.2: Optical imaging of a C = 0.5 mg/mL concentrated FITC labeled LC-TAT peptide in methanol using different filters at 40x (left) and 20x (right).

In Fig. 7.2, FITC-LC TAT was observed under fluorescence with DAPI, FITC, Cy5 and TRITC filters. The molecules have an excitation wavelength of 493 nm and an emission wavelength of 522 nm [104]. Being located in the green range, the FITC-LC TAT molecules were clearly visible using the FITC filter and moderately visible using the DAPI filter given the proximity of the green to the blue range in the UV spectra.

7.2 Characterization of the Encapsulation Process

Subsequently, liposomes containing FITC-LC TAT were observed via microscopy, The representative sets of figures (Fig. 7.3) are visualized under fluorescence with the FITC filter, DAPI and light microscopy, of on-chip, passively loaded liposomes.

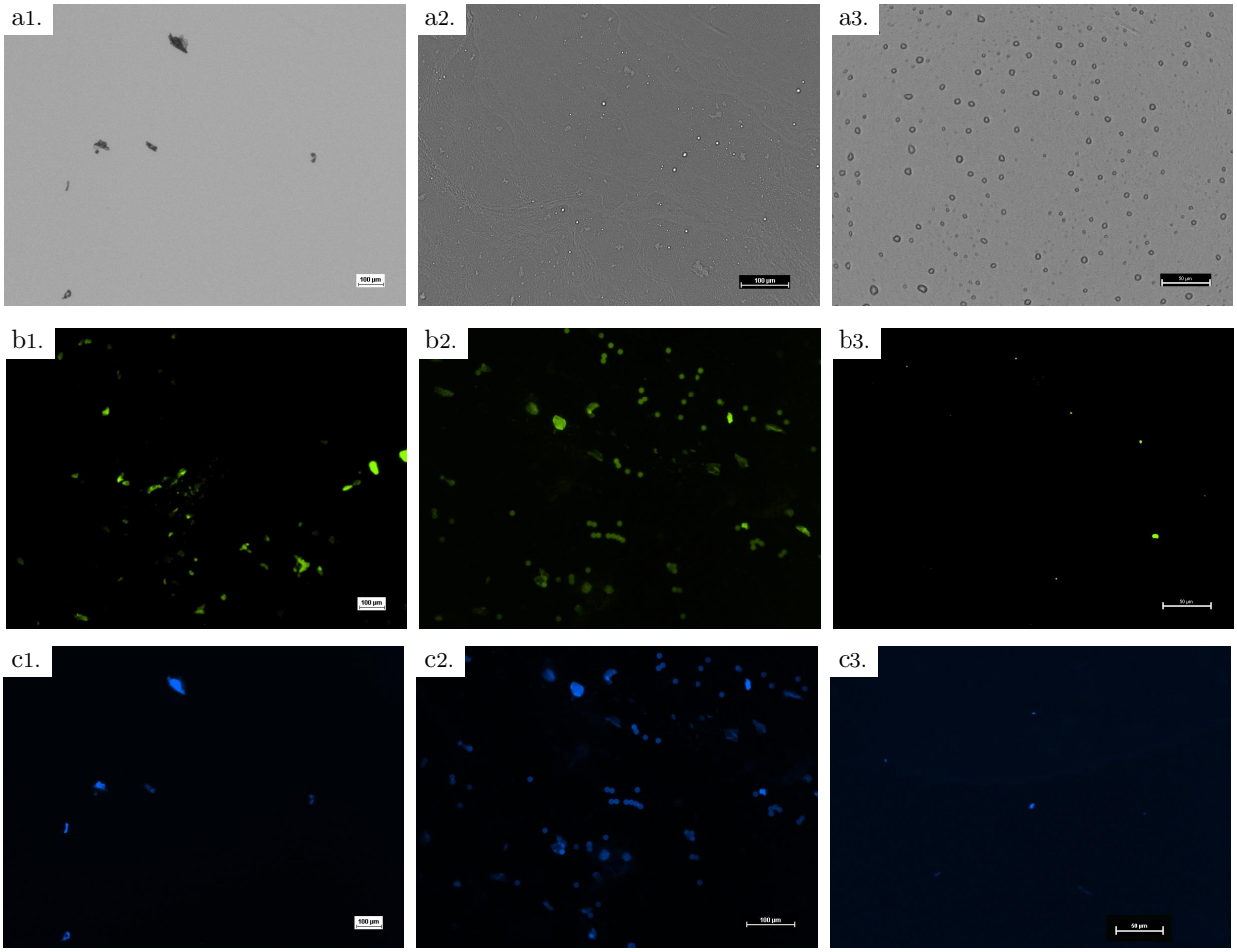

Figure 7.3: Optical imaging of a liposomes encapsulating FITC labeled LC-TAT peptide using different filters: FITC green (b 1, 2 and 3) and DAPI blue (c 1, 2 and 3) at 10 x (a1, b1 and c1), 20x (a2, b2 and c2) and 40x (a3, b3 and c3).

After setting the DPPC concentration and FRR for liposomal synthesis to 3 mg/mL and 30, respectively, FITC-LC-TAT encapsulation was attempted. Approximately 1 ml

of product was obtained in less than three and a half minutes, with larger volumetric outputs, and in turn faster production times, achievable simply by increasing the fluid flow rates. As an example, by increasing the FRR to 50, 1 mL of liposomes encapsulating molecules can be made in approximately 2 minutes. Detailed preparation times for every FRR can be found in Appendix D.

From the figures above, it can be observed that the fluorescence and vesicles overlap. Liposomes should not be affected by the loading time due to the minute volume of solvent present in the mixture [105]. The fluorescence images in Fig. 7.3 imply that the FITC labeled LC-TAT peptide was successfully encapsulated within the liposomes. Optical microscopy (not shown here) comparing batches of encapsulated liposomes with the fluorescent peptide prior and following filtration by dialysis confirmed the absence of any free FITC-LC-TAT peptides. Quantitative image-based particle count of the FITC-encapsulating liposomes has been performed by exploiting the capabilities of Cell Profiler, with a screen-shot of the report of Area C_2 and a plot detailing the particle count over every microscopy view ($B_{1\text{-}3}$, $C_{1\text{-}3}$) in Fig. 7.3 is shown in 7.4 (B). The reports for the remaining microscopy areas can be found in the Appendix, Section D.

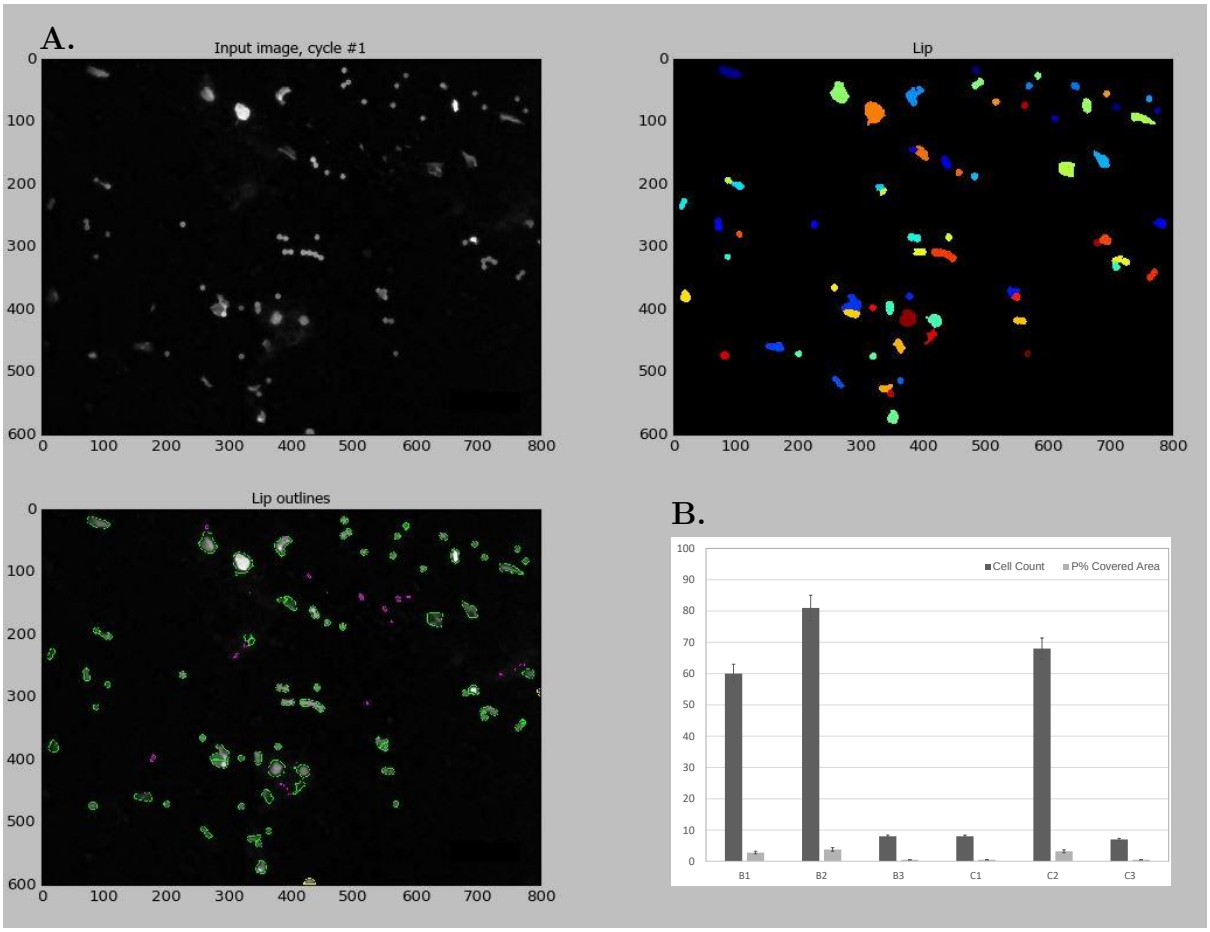

Figure 7.4: (A) Automatic particle counting of Area C_2 in Fig. 7.3 by Cell Profiler, and (B) average particle count over the microscopy areas; ($B_{1\text{-}3}$, $C_{1\text{-}3}$) displayed in Fig. 7.3. Error bars are ± standard errors.

Overall, particle count in the B frames are the highest, with over 80 particles at B_2) and 60 particles at B_1, compared to the C areas; 70 particles at C_2 and 10 particles for B_3 and C_1 respectively. This is to be expected as the B areas encompass an FITC green filter whereas the C frames contain a DAPI blue filter of the fluorescent particles.
After approximately an hour, the particles appear to aggregate, and form large vesicle clumps as shown in Figure 7.5.

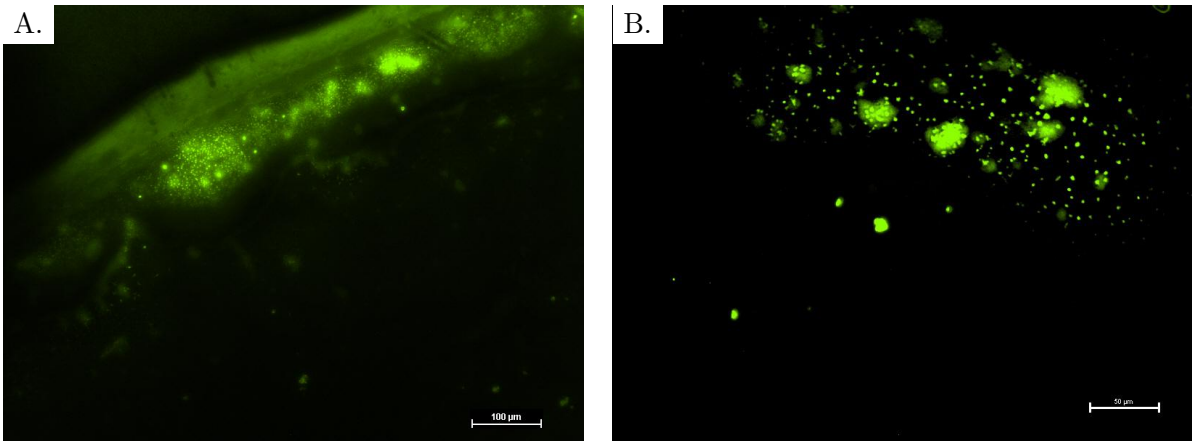

Figure 7.5: Optical imaging showing aggregation of liposomes encapsulating FITC labeled LC-TAT peptide using an FITC filter at x20 (a) and x40 (b) after one hour of deposition into a microscopy glass slide.

Upon deposition on a microscopy glass slide and subsequent evaporation of their aqueous media, interactions occurred spontaneously and large liposomal aggregates were formed, which were now visible with fluorescence optical microscopy, as shown in Figure 7.5. Multiple interactions occur, giving rise to very large aggregates, hundred of microns large. The stability and fusion of liposomes is a phenomenon has has been studied extensively, and investigated either qualitatively using the turbidity method or quantitatively using the calcein florescence method or more recently by atomic force microscopy (AFM) [106].

Conclusion:

In summary, the laminar flow and facile fluidic control in microchannels enabled reproducible self-assembly of lipids into liposomes in a sheathed flow-field. Confining a water-soluble compound to be encapsulated to the immediate vicinity where liposomes formation is expected to occur reduces sample consumption without affecting liposome loading [37]. The ability to alter the concentration and control the amount of encapsulated compounds within liposomes in a continuous-flow mode is another interesting feature towards tailored liposomal drug delivery. The liposome formation strategy demonstrated in this dissertation offers potential for point-of-care drug encapsulation, eliminating shelf-life limitations inherent to current liposome preparation techniques.

Chapter 8

Conclusion

8.1 Summary

In this study, we have developed and demonstrated a straightforward microfluidic geometry incorporating an optimal flow-focusing angle as a proof-of-concept capable of continuous-flow synthesis and loading of DPPC liposomes. A simple, low-cost, and easily scalable in parallel, double flow-focusing device was utilized as a preliminary prototype to provide a high throughput and rapid synthesis of size-tunable nano-liposomes. With our platform, we reduced the number of different apparatus required and reduced the amount of steps needed for the synthesis of liposomes. The initial study revealed an interesting trend regarding increasing the dissolved phospholipid concentration whereby the particle diameter increases with an increase in DPPC concentration. Additionally, we established a correlation between increasing the FRR and the resulting decrease in particle diameter. With further extrapolation, it is posited that the liposome size ultimately achieves a minimal plateau. The platform enabled the synthesis of particles with a range of diameters simply by adjusting the buffer flow rate. Moreover, the platform presents the possibility of multiple encapsulated agents in the synthesis of not only liposomes but also various nano-/microparticulate systems. Using hydrodynamic focusing in microfluidic channels, nanosized liposomes with smaller size and narrower size distribution are easily formed by varying flow parameters. They include flow rate, flow ratio, concentration of lipids solution, as well as characteristic dimensions in microfluidics channels. However, the problem of scaling up liposome production needs to be addressed during the implementation of microfluidics technology for practical applications [24]. Microfluidics provides a new platform for the development and optimization of liposomes in the emerging field of nanomedicine. It can control liposome self-assembly and potentially lead to applications in instant liposome synthesis as part of point-of-care personalized therapeutics [1].

8.2 Limitations and Future Work

Our microfluidic device is characterized by a relatively simple, double 2D HFF configuration for liposomal synthesis. We outline several improvements to incorporate in any future experiments.

Although we were successfully able to visualize FITC molecules following encapsulation and loading into lipsomes, this was done only qualitatively as a proof-of-concept. Future work should include quantifying the encapsulation efficiency of the FITC-LC-TAT loaded liposomes which can be done using several techniques such as High Performance Liquid Chromatography (HPLC) or by flow cytometry. In addition, Cryo-TEM imaging of the microfluidic synthesized liposomes prior to and following encapsulation should give a better visualization of liposomes in solution without the disadvantages of negative straining, and thus yield more accurate images to observe any change in morphology or lamellarity following encapsulation. Visualization of the the loaded and unloaded liposomal samples using cryo-electron microscopy should therefore be considered in order to replace the primary yet simple negative staining method. With Cryo-EM, the sample is always in solution and never comes into contact with an adhering surface. Therefore, the shape that is observed is the true shape of the hydrated molecule in solution and has not been distorted by attaching itself and flattening against any surface. Also, contrary to negative staining there is no stain to distort the sample. Stain does not always lay down evenly, which can generate artifacts and false contrasts when reconstructing the structure of a sample [97]. Furthermore, the staining process requires that the sample be blotted dry. During the drying, the sample can be damaged in many ways, such as by flattening and twisting. Finally, by negative staining, when the sample adheres to the carbon grid, it could stick in a preferential orientation, compromising the resolution of the image in that direction. In our case, however low dose methods have been used, so the electron beam caused less damage to the sample.

We also recommend testing the current DPPC lipidic formulations with a broader range of DDAB and DOPG ratios, possibly with the addition of poly(ethylene glycol) PEG and cholesterol to increase their stability and half-life for future in-vivo studies. A more extensive study of the effect of the incorporation of DOPG and DDAB or any analogous positively and negatively charged molecule onto the DPPC lipid stream at every FRR and its impact on encapsulation efficiency has yet to be investigated. Furthermore, the coating of liposomes with the PEG polymer ensures their stabilization and turns them into sterically stabilized liposomes (SL) characterized by long-circulating blood lifetimes, reduced interaction with and uptake by the reticulo-endothelial system (RES) and enhanced accumulation in tumors [107]. Moreover, the fictionalization of PEG allows subsequent attachment of biologically active or even cell-targeting molecules to prepare sterically stabilized immuno-liposomes, which retain long survival times in circulation

and target recognition [108]. It is possible to efficiently encapsulate biologically active compounds in liposomes produced using microfluidics. Notably, on-chip liposome loading with bioactive compounds (both hydrophilic and lipophilic) has seen a limited number of advancements in recent years, and may represent an exciting avenue of research in the near future [51]. Encapsulation of a range of different therapeutic compounds should be therefore attempted. In addition to synthesizing and loading liposomes, it is hoped that the geometry of this simplistic device could potentially be utilized as a beneficial manufacturing platform for other types of nanoparticles such as polymeric compounds or emulsions.

8.3 Prospects

Microfluidics is a relatively novel technology for the production of micro- and nano-sized liposomes. The characteristics of laminar flow and tunable mixing in microfluidics systems have distinctive advantages in liposome formation over traditional methods, such as thin-film hydration and reverse-phase evaporation. Reproducible control of particle size and size distribution can be implemented in continuous microfluidics flow systems. Using hydrodynamic focusing in microfluidic channels, nanosized liposomes with smaller size and narrower size distribution are easily formed by varying flow parametersb. They include flow rate, flow ratio, concentration of lipids solution, as well as characteristic dimensions in microfluidics channels. However, the problem of scaling up liposome production needs to be addressed during the implementation of microfluidics technology for practical applications. Microfluidics provides a new platform for the development and optimization of liposomes in the emerging field of nanomedicine. It can control liposome self-assembly and potentially lead to applications in instant liposome synthesis as part of point-of-care personalized therapeutics.

Bibliography

[1] Pedro M. Valencia, Omid C. Farokhzad, Rohit Karnik, and Robert Langer. Microfluidic technologies for accelerating the clinical translation of nanoparticles. *Nature Nanotechnology*, 7(10):623–629, 2012.

[2] Chun-Min Lin, Peter Husen, Jonathan Brewer, Luis A. Bagatolli, Per L. Hansen, John H. Ipsen, and Ole G. Mouritsen. Size-dependent properties of small unilamellar vesicles formed by model lipids. *Langmuir*, 28(1):689–700, 2012.

[3] Peter Walde. Preparetion of vesicles (liposomes). *Encyclopedia of Nanoscience and Nanotechnology*, 9(9):43–79, 2004.

[4] P Chattopadhyay, B SHEKUNOV, D YIM, D CIPOLLA, B BOYD, and S FARR. Production of solid lipid nanoparticle suspensions using supercritical fluid extraction of emulsions (sfee) for pulmonary delivery using the aerx system? *Advanced Drug Delivery Reviews*, 59(6):444–453, 2007.

[5] Udaya Sankar Kadimi, Deepan Raja Balasubramanian, Usha Rani Ganni, Manohar Balaraman, and Venkateswaran Govindarajulu. In vitro studies on liposomal amphotericin b obtained by supercritical carbon dioxide mediated process. *Nanomedicine: Nanotechnology, Biology and Medicine*, 3(4):273–280, 2007.

[6] D. Conchouso, D. Castro, S. A. Khan, and I. G. Foulds. Three-dimensional parallelization of microfluidic droplet generators for a litre per hour volume production of single emulsions. *Lab on a Chip*, 14(16):3011, 2014.

[7] Sarinnate Kunastitchai, Lars Pichert, Narong Sarisuta, and Bernd W. Muller. Application of aerosol solvent extraction system (ases) process for preparation of liposomes in a dry and reconstitutable form. *International Journal of Pharmaceutics*, 316(1-2):93–101, 2006.

[8] Mary Cano-Sarabia, Nora Ventosa, Santiago Sala, Cristina Patino, Roco Arranz, and Jaume Veciana. Preparation of uniform rich cholesterol unilamellar nanovesicles using co2-expanded solvents. *Langmuir*, 24(6):2433–2437, 2008.

[9] Sandy Ong, Long Ming, Kah Lee, and Kah Yuen. Influence of the encapsulation efficiency and size of liposome on the oral bioavailability of griseofulvin-loaded liposomes. *Pharmaceutics*, 8(3):25, 2016.

[10] Sheida Shariat, Ali Badiee, Seyed Amir Jalali, Mercedeh Mansourian, Mona Yazdani, Seyed Alireza Mortazavi, and Mahmoud Reza Jaafari. P5 her2/neu-derived peptide conjugated to liposomes containing mpl adjuvant as an effective prophylactic vaccine formulation for breast cancer. *Cancer Letters*, 355(1):54–60, 2014.

[11] Antonio P. Costa, Xiaoming Xu, and Diane J. Burgess. Freeze-anneal-thaw cycling of unilamellar liposomes: Effect on encapsulation efficiency. *Pharmaceutical Research*, 31(1):97–103, 2013.

[12] Bhushan S. Pattni, Vladimir V. Chupin, and Vladimir P. Torchilin. New developments in liposomal drug delivery. *Chemical Reviews*, 115(19):10938–10966, 2015.

[13] Shmuel Batzri and Edward D. Korn. Single bilayer liposomes prepared without sonication. *Biochimica et Biophysica Acta (BBA) - Biomembranes*, 298(4):1015–1019, 1973.

[14] Brian Lohse, Pierre-Yves Bolinger, and Dimitrios Stamou. Encapsulation efficiency measured on single small unilamellar vesicles. *Journal of the American Chemical Society*, 130(44):14372–14373, 2008.

[15] David Olea and Chrystel Faure. Quantitative study of the encapsulation of glucose oxidase into multilamellar vesicles and its effect on enzyme activity. *The Journal of Chemical Physics*, 119(6111-6118), 2003.

[16] A. Kerdudo, A. Dingas, Xavier F., and Chrystel F. Encapsulation of rutin and naringenin in multilamellar vesicles for optimum antioxidant activity. *Food Chemistry*, 159:12–19, 2014.

[17] Louise A. Meure and Fariba Foster, Neil R.and Dehghani. Conventional and dense gas techniques for the production of liposomes: A review. *AAPS PharmSciTech*, 9(3):798, 2008.

[18] M. Reza Mozafari, Chad Johnson, Sophia Hatziantoniou, and Costas Demetzos. Nanoliposomes and their applications in food nanotechnology. *Journal of Liposome Research*, 18(4):309–327, 2008.

[19] Elvin Blanco, Haifa Shen, and Mauro Ferrari. Principles of nanoparticle design for overcoming biological barriers to drug delivery. *Nature Biotechnology*, 33(9):941–951, 2015.

[20] Kristen Bowey, Jean-François Tanguay, and Maryam Tabrizian. Liposome technology for cardiovascular disease treatment and diagnosis. *Expert Opinion on Drug Delivery*, 9(2):249–265, 2012.

[21] Abolfazl Akbarzadeh, Rogaie Rezaei-Sadabady, Soodabeh Davaran, Sang Woo Joo, Nosratollah Zarghami, Younes Hanifehpour, Mohammad Samiei, Mohammad Kouhi, and Kazem Nejati-Koshki. Liposome: classification, preparation, and applications. *Nanoscale Research Letters*, 8(1):102, 2013.

[22] M Brandl. Liposomes as drug carriers: a technological approach. *Biotechnology Annual Review*, 7:59 – 85, 2001.

[23] Renee R. Hood and Don L. DeVoe. High-throughput continuous flow production of nanoscale liposomes by microfluidic vertical flow focusing. *Small*, 11(43):5790–5799, 2015.

[24] Lorenzo Capretto, Dario Carugo, Stefania Mazzitelli, Claudio Nastruzzi, and Xunli Zhang. Microfluidic and lab-on-a-chip preparation routes for organic nanoparticles and vesicular systems for nanomedicine applications. *Advanced Drug Delivery Reviews*, 65(11-12):1496–1532, 2013.

[25] Bo Yu, Robert J. Lee, and L. James Lee. Chapter 7 - microfluidic methods for production of liposomes. In *Methods in Enzymology*, volume 465 of *Methods in Enzymology*, pages 129 – 141. Academic Press, 2009.

[26] Theresa M. Allen and Pieter R. Cullis. Liposomal drug delivery systems: From concept to clinical applications. *Advanced Drug Delivery Reviews*, 65(1):36 – 48, 2013. Advanced Drug Delivery: Perspectives and Prospects.

[27] Wafa' T. Al-Jamal and Kostas Kostarelos. Liposomes: From a clinically established drug delivery system to a nanoparticle platform for theranostic nanomedicine. *Accounts of Chemical Research*, 44(10):1094–1104, 2011.

[28] Hongwei Zhang. *Thin-Film Hydration Followed by Extrusion Method for Liposome Preparation*, pages 17–22. Springer New York, New York, NY, 2017.

[29] M. J. Valle and A. Navarro. Liposomes prepared in absence of organic solvents: Sonication versus lipid film hydration method. *Current Pharmaceutical Analysis*, 11(2):86–91, 2015.

[30] Salima Varona, Angel Martin, and Maria Jose Cocero. Liposomal incorporation of lavandin essential oil by a thin-film hydration method and by particles from gas-saturated solutions. *Industrial & Engineering Chemistry Research*, 50(4):2088–2097, 2011.

[31] Catherine Charcosset, Audrey Juban, Jean-Pierre Valour, Sébastien Urbaniak, and Hatem Fessi. Preparation of liposomes at large scale using the ethanol injection method: Effect of scale-up and injection devices. *Chemical Engineering Research and Design*, 94:508 – 515, 2015.

[32] Chiraz Jaafar-Maalej, Roudayna Diab, Veronique Andrieu, Abdelhamid Elaissari, and Hatem Fessi. Ethanol injection method for hydrophilic and lipophilic drug-loaded liposome preparation. *Journal of Liposome Research*, 20(3):228–243, 2009.

[33] Yoshie Maitani. *Lipoplex Formation Using Liposomes Prepared by Ethanol Injection*, pages 393–403. Humana Press, Totowa, NJ, 2010.

[34] Yoshie Maitani, Saki Igarashi, Mamiko Sato, and Yoshiyuki Hattori. Cationic liposome (dc-chol/dope=1:2) and a modified ethanol injection method to prepare liposomes, increased gene expression. *International Journal of Pharmaceutics*, 342(1):33 – 39, 2007.

[35] F. Szoka and D. Papahadjopoulos. Procedure for preparation of liposomes with large internal aqueous space and high capture by reverse-phase evaporation. *Proceedings of the National Academy of Sciences*, 75(9):4194–4198, 1978.

[36] Wim Jiskoot, Tom Teerlink, E. Coen Beuvery, and Daan J. A. Crommelin. Preparation of liposomes via detergent removal from mixed micelles by dilution. *Pharmaceutisch Weekblad*, 8(5):259–265, Oct 1986.

[37] Andreas Jahn, Wyatt N. Vreeland, Michael Gaitan, and Laurie E. Locascio. Controlled vesicle self-assembly in microfluidic channels with hydrodynamic focusing. *Journal of the American Chemical Society*, 126(9):2674–2675, 2004.

[38] Andreas Jahn, Wyatt N. Vreeland, Don L. DeVoe, Laurie E. Locascio, and Michael Gaitan. Microfluidic directed formation of liposomes of controlled size. *Langmuir*, 23(11):6289–6293, 2007.

[39] Mounir Traikia, Dror E. Warschawski, Michel Recouvreur, Jean Cartaud, and Philippe F. Devaux. Formation of unilamellar vesicles by repetitive freeze-thaw cycles: characterization by electron microscopy and 31 p-nuclear magnetic resonance. *European Biophysics Journal*, 29(3):184–195, 2000.

[40] Ruthairat Benjakul, Busaba Panyarachun, and Narong Sarisuta. Preparation of dry reconstituted liposomal powder by freeze-drying at room temperature. *Journal of Liposome Research*, 21(1):28–37, 2011.

[41] Zhenjun Huang, Xuan Li, Ting Zhang, Yanzhi Song, Zhennan She, Jing Li, and Yihui Deng. Progress involving new techniques for liposome preparation. *Asian Journal of Pharmaceutical Sciences*, 9(4):176 – 182, 2014.

[42] Liang Hui, Xuesong Chen, Norman J Haughey, and Jonathan D Geiger. Role of endolysosomes in hiv-1 tat-induced neurotoxicity. *ASN Neuro*, 4(4):AN20120017, 2012.

[43] H. Xiao, C. Neuveut, H. L. Tiffany, M. Benkirane, E. A. Rich, P. M. Murphy, and K.-T. Jeang. Selective cxcr4 antagonism by tat: Implications for in vivo expansion of coreceptor use by hiv-1. *Proceedings of the National Academy of Sciences*, 97(21):11466–11471, 2000.

[44] Gokhan Dikmen, Lutfi Genc, and Gamze Guney. Advantage and disadvantage in drug delivery systems. *Journal of Material Science and Engineering*, 5:468–472, 2011.

[45] Chrystel Faure, Marie-Edith Meyre, Sylvain Trepout, Olivier Lambert, and Eric Lebraud. Magnetic multilamellar liposomes produced by in situ synthesis of iron oxide nanoparticles: Magnetonions. *The Journal of Physical Chemistry B*, 113(25):8552–8559, 2009.

[46] Antonin Prevoteau and Chrystel Faure. Effect of onion-type multilamellar liposomes on trametes versicolor laccase activity and stability. *Biochimie*, 94(1):59 – 65, 2012.

[47] Tripta Bhatia, Peter Husen, Jonathan Brewer, Luis A. Bagatolli, Per L. Hansen, John H. Ipsen, and Ole G. Mouritsen. Preparing giant unilamellar vesicles (guvs) of complex lipid mixtures on demand: Mixing small unilamellar vesicles of compositionally heterogeneous mixtures. *Biochimica et Biophysica Acta (BBA) - Biomembranes*, 1848(12):3175 – 3180, 2015.

[48] Umar Iqbal, Homam Albaghdadi, Mu-Ping Nieh, Ursula I Tuor, Zoltan Mester, Danica Stanimirovic, John Katsaras, and Abedelnasser Abulrob. Small unilamellar vesicles: a platform technology for molecular imaging of brain tumors. *Nanotechnology*, 22(19):195102, 2011.

[49] Meng-Hsuan Chao, Yen-Ting Lin, Namasivayam Dhenadhayalan, Hsin-Lung Lee, Hsin-Yen Lee, and King-Chuen Lin. 3d probed lipid dynamics in small unilamellar vesicles. *Small*, 13(13):3160–3408, 2017.

[50] Liza Mouret, Grégory Da Costa, and Arnaud Bondon. Sterols associated with small unilamellar vesicles (suvs): intrinsic mobility role for 1h nmr detection. *Magnetic Resonance in Chemistry*, 52(7):339–344, 2014.

[51] Dario Carugo, Elisabetta Bottaro, Joshua Owen, Eleanor Stride, and Claudio Nastruzzi. Liposome production by microfluidics: potential and limiting factors. *Scientific Reports*, 6(1), 2016.

[52] Lawrence D. Mayer, Linda C. L. Tai, Dicken S. C. Ko, Dana Masin, Richard S. Ginsberg, Pieter R. Cullis, and Marcel B. Bally. Influence of vesicle size, lipid composition, and drug-to-lipid ratio on the biological activity of liposomal doxorubicin in mice. *Cancer Research*, 49(21):5922–5930, 1989.

[53] A.D. Bangham, M.M. Standish, and J.C. Watkins. Diffusion of univalent ions across the lamellae of swollen phospholipids. *Journal of Molecular Biology*, 13(1):238 – IN27, 1965.

[54] Mozafari Mohammed Reza. Liposomes: An overview of manufacturing techniques. *Cell Molecular Biology*, 10(4):711–719, 2005.

[55] M.R. Galani C. Maherani, B. Mozafari. Liposomes: A review of manufacturing techniques and targeting strategies. *Current Nanoscience*, 7(3):2674–2675, 2011.

[56] R. Schubert R. Peschka, T. Purmann. Cross-flow filtration—an improved detergent removal technique for the preparation of liposomes. *Int J Pharm*, 162:176 – 182, 1998.

[57] Sinil Kim and George M. Martin. Preparation of cell-size unilamellar liposomes with high captured volume and defined size distribution. *Biochimica et Biophysica Acta (BBA) - Biomembranes*, 646(1):1 – 9, 1981.

[58] R. R. C. NEW. Preparation of liposomes. *Liposomes: a practical approach.*, pages 33–104, 1990.

[59] Stephan Hauschild, Ute Lipprandt, Anja Rumplecker, Uwe Borchert, Anja Rank, Rolf Schubert, and Stephan Forster. Direct preparation and loading of lipid and polymer vesicles using inkjets. *Small*, 1(12):1177–1180, 2005.

[60] Evaporation of solvents using a rotary evaporator, 2017.

[61] Subin R. C. K. Rajendran, Chibuike C. Udenigwe, and Rickey Y. Yada. Nanochemistry of protein-based delivery agents. *Frontiers in Chemistry*, 4, 2016.

[62] S. Moazam Mortazavi, M. Reza Mohammadabadi, Kianoush Khosravi-Darani, and M. Reza Mozafari. Preparation of liposomal gene therapy vectors by a scalable method without using volatile solvents or detergents. *Journal of Biotechnology*, 129(4):604–613, 2007.

[63] J. Zhong. Liposomal preparation by supercritical fluids technology. *African Journal of Biotechnology*, 10(73), 2011.

[64] E. Badens, C. Magnan, and G. Charbit. Microparticles of soy lecithin formed by supercritical processes. *Biotechnology & Bioengineering*, 72(2):194–204, 2000.

[65] L. Lesoin, C. Crampon, O. Boutin, and E. Badens. Preparation of liposomes using the supercritical anti-solvent (sas) process and comparison with a conventional method. *The Journal of Supercritical Fluids*, 57(2):162–174, 2011.

[66] Zhen Wen, Bo Liu, Zongkun Zheng, Xinkui You, Yitao Pu, and Qiong Li. Preparation of liposomes entrapping essential oil from atractylodes macrocephala koidz by modified ress technique. *Chemical Engineering Research and Design*, 88(8):1102–1107, 2010.

[67] Lene Frederiksen, Klaus Anton, Peter van Hoogevest, Hans Rudolf Keller, and Hans Leuenberger. Preparation of liposomes encapsulating water-soluble compounds using supercritical carbon dioxide. *Journal of Pharmaceutical Sciences*, 86(8):921–928, 1997.

[68] Katsuto Otake, Tomohiro Imura, Hideki Sakai, and Masahiko Abe. Development of a new preparation method of liposomes using supercritical carbon dioxide. *Langmuir*, 17(13):3898–3901, 2001.

[69] T.P Castor and L Chu. Methods and apparatus for making liposomes containing hydrophobic drugs, 1998.

[70] L. Lesoin, C. Crampon, O. Boutin, and E. Badens. Development of a continuous dense gas process for the production of liposomes. *The Journal of Supercritical Fluids*, 60:51–62, 2011.

[71] Kenichi Aburai, Nobuhiro Yagi, Yuusaku Yokoyama, Hiroaki Okuno, Kenichi Sakai, Hideki Sakai, Kazutami Sakamoto, and Masahiko Abe. Preparation of liposomes modified with lipopeptides using a supercritical carbon dioxide reverse-phase evaporation method. *Journal of Oleo Science*, 60(5):209–215, 2011.

[72] Ramon Barnadas-Rodriguez and Manuel Sabes. Factors involved in the production of liposomes with a high-pressure homogenizer. *International Journal of Pharmaceutics*, 213(1–2):175 – 186, 2001.

[73] Ulrich Massing, Sanja Cicko, and Vittorio Ziroli. Dual asymmetric centrifugation (dac)—a new technique for liposome preparation. *Journal of Controlled Release*, 125(1):16 – 24, 2008.

[74] Chunlei Li and Yingjie Deng. A novel method for the preparation of liposomes: Freeze drying of monophase solutions. *Journal of Pharmaceutical Sciences*, 93(6):1403 – 1414, 2004.

[75] N Nguyen and S Wereley. *Fundamentals and Applications of Microfluidics*. Artech House Publishers, 1 edition, 2002.

[76] Andrew Evan Kamholz and Paul Yager. Theoretical analysis of molecular diffusion in pressure-driven laminar flow in microfluidic channels. *Biophysical Journal*, 80(1):155–160, 2001.

[77] C. Cruickshank Miller. The stokes-einstein law for diffusion in solution. *Proceedings of the Royal Society of London.*, 106(740):724–749, 1924.

[78] Lung-Hsin Hung Abraham Phillip Lee. Microfluidic devices for the synthesis of nanoparticles and biomaterials. *The Journal of Medical and Biological Engineering*, 1-6(1):724–749, 2007.

[79] Bingcheng Lin. *Microfluidics: Technologies and Applications.* Springer Berlin, 1 edition, 2013.

[80] Todd Thorsen, Richard W. Roberts, Frances H. Arnold, and Stephen R. Quake. Dynamic pattern formation in a vesicle-generating microfluidic device. *Phys. Rev. Lett.*, 86:4163–4166, Apr 2001.

[81] Mariano Michelon, Davi Rocha Bernardes Oliveira, Guilherme de Figueiredo Furtado, Lucimara Gaziola de la Torre, and Rosiane Lopes Cunha. High-throughput continuous production of liposomes using hydrodynamic flow-focusing microfluidic devices. *Colloids and Surfaces B: Biointerfaces*, 156:349 – 357, 2017.

[82] James B. Knight, Ashvin Vishwanath, James P. Brody, and Robert H. Austin. Hydrodynamic focusing on a silicon chip: Mixing nanoliters in microseconds. *Physical Review Letters*, 80(17):3863–3866, 1998.

[83] C. G. Hebert, S. J. R. Staton, T. Q. Hudson, S. J. Hart, C. Lopez-Mariscal, and A. Terray. Dynamic radial positioning of a hydrodynamically focused particle stream enabled by a three-dimensional microfluidic nozzle. *Biomicrofluidics*, 9(2):024106, 2015.

[84] N. Sundararajan, M. S. Pio, L. P. Lee, and A. A. Berlin. Three-dimensional hydrodynamic focusing in polydimethylsiloxane (pdms) microchannels. *Journal of Microelectromechanical Systems*, 13(4):559–567, Aug 2004.

[85] Peter B. Howell Jr, Joel P. Golden, Lisa R. Hilliard, Jeffrey S. Erickson, David R. Mott, and Frances S. Ligler. Two simple and rugged designs for creating microfluidic sheath flow. *Lab Chip*, 8:1097–1103, 2008.

[86] Xiaole Mao, John Robert Waldeisen, and Tony Jun Huang. "microfluidic drifting"-implementing three-dimensional hydrodynamic focusing with a single-layer planar microfluidic device. *Lab Chip*, 7:1260–1262, 2007.

[87] Myung Gwon Lee, Sungyoung Choi, and Je-Kyun Park. Three-dimensional hydrodynamic focusing with a single sheath flow in a single-layer microfluidic device. *Lab Chip*, 9:3155–3160, 2009.

[88] Joel P. et al. Golden. Multi-wavelength microflow cytometer using groove-generated sheath flow. *Lab Chip*, 9:1942–1950, 2009.

[89] Jong-Min Lim, Nicolas B., P. M. Valencia, M. Rhee, R. Langer, S. Jon, Omid C. Farokhzad, and R. Karnik. Parallel microfluidic synthesis of size-tunable polymeric nanoparticles using 3d flow focusing towards in vivo study. *Nanomedicine: Nanotechnology, Biology and Medicine*, 10(2):401–409, 2014.

[90] Andreas Jahn, Samuel M. Stavis, Jennifer S. Hong, Wyatt N. Vreeland, Don L. DeVoe, and Michael Gaitan. Microfluidic mixing and the formation of nanoscale lipid vesicles. *ACS Nano*, 4(4):2077–2087, 2010. PMID: 20356060.

[91] Simon Attwood, Youngjik Choi, and Zoya Leonenko. Preparation of dopc and dppc supported planar lipid bilayers for atomic force microscopy and atomic force spectroscopy. *International Journal of Molecular Sciences*, 14(2):3514–3539, 2013.

[92] Application builder comsol multiphysics, 2017. https://www.comsol.com/release/5.1/application-builder.

[93] Melanie Ohi, Ying Li, Yifan Cheng, and Thomas Walz. Negative staining and image classification: powerful tools in modern electron microscopy. *Biological Procedures Online*, 6(1):23–34, 2004.

[94] Gwo-Bin Lee, Chih-Chang Chang, Sung-Bin Huang, and Ruey-Jen Yang. The hydrodynamic focusing effect inside rectangular microchannels. *Journal of Micromechanics and Microengineering*, 16(5):1024, 2006.

[95] Marek Dziubinski. *Hydrodynamic Focusing in Microfluidic Devices*. INTECH Open Access Publisher, 1 edition, 2012.

[96] P. J. CROSLAND-TAYLOR. A device for counting small particles suspended in a fluid through a tube. *Nature*, 171(4340):37–38, 1953.

[97] Lei Zhang, Huimin Tong, Mark Garewal, and Gang Ren. Optimized negative-staining electron microscopy for lipoprotein studies. *Biochimica et Biophysica Acta (BBA) - General Subjects*, 1830(1):2150–2159, 2013.

[98] Barbara Ruozi, Daniela Belletti, Andrea Tombesi, Giovanni Tosi, Lucia Bondioli, Flavio Forni, and Maria Angela Vandelli. Afm, esem, tem, and clsm in liposomal characterization: a comparative study. *International Journal of Nanomedicine*, page 557, 2011.

[99] Size and zeta potential characterisation of anionic and cationic liposomes on the zetasizer nano, 2017. http://www.azonano.com/article.aspx?ArticleID=1220.

[100] S Honary and F Zahir. Effect of zeta potential on the properties of nano-drug delivery systems - a review (part 2). *Tropical Journal of Pharmaceutical Research*, 12(2), 2013.

[101] Electroacoustics tutorials: The zeta potential, 1999. http://www.colloidal-dynamics.com.

[102] Vasco F., Andrea H., and Wim J. Critical evaluation of nanoparticle tracking analysis (nta) by nanosight for the measurement of nanoparticles and protein aggregates. *Pharmaceutical Research*, 27(5):796–810, 2010.

[103] Buddhadev Layek, Lindsey Lipp, and Jagdish Singh. Cell penetrating peptide conjugated chitosan for enhanced delivery of nucleic acid. *International Journal of Molecular Sciences*, 16(12):28912–28930, 2015.

[104] Fitc-lc-tat peptide, anaspec technical data sheet, 2017. http://http://www.tenovapharma.com/TAT-(47-57)-FITC-LC-labeled.

[105] Ryan V. Tien Sing Young and Maryam Tabrizian. Rapid, one-step fabrication and loading of nanoscale dspc liposomes in a simple, double flow-focusing microfluidic device. *Biomicrofluidics*, 9(4):046501, 2015.

[106] Alexandros Pantos, Zili Sideratou, and Constantinos M. Paleos. Complementary liposomes based on phosphatidylcholine: Interaction effectiveness vs protective coating. *Journal of Colloid and Interface Science*, 253(2):435–442, 2002.

[107] C Carrion, J.C Domingo, and M.A de Madariaga. Preparation of long-circulating immunoliposomes using peg–cholesterol conjugates. *Chemistry and Physics of Lipids*, 113(1–2):97 – 110, 2001.

[108] Mastrobattista E., Koning G. A., and Storm G. Immunoliposomes for the targeted delivery of antitumor drugs. *Advanced Drug Delivery Reviews*, 40(1):103 – 127, 1999.

Appendices

Appendix A

CFD Simulations

I. Simulation Parameters

Table A.1: Computational Parameters used for Mesh Modeling (in 2D) and their Values.

Parameters	**Value(s)**
Maximum Element Size	0.0025 $[m]$
Minimum Element Size	2.32 x 10^{-4} $[m]$
Maximum Element Growth Rate	1.08
Curvature Factor	0.25
Resolution of Narrow Regions	1.00

II. 2D Simulations

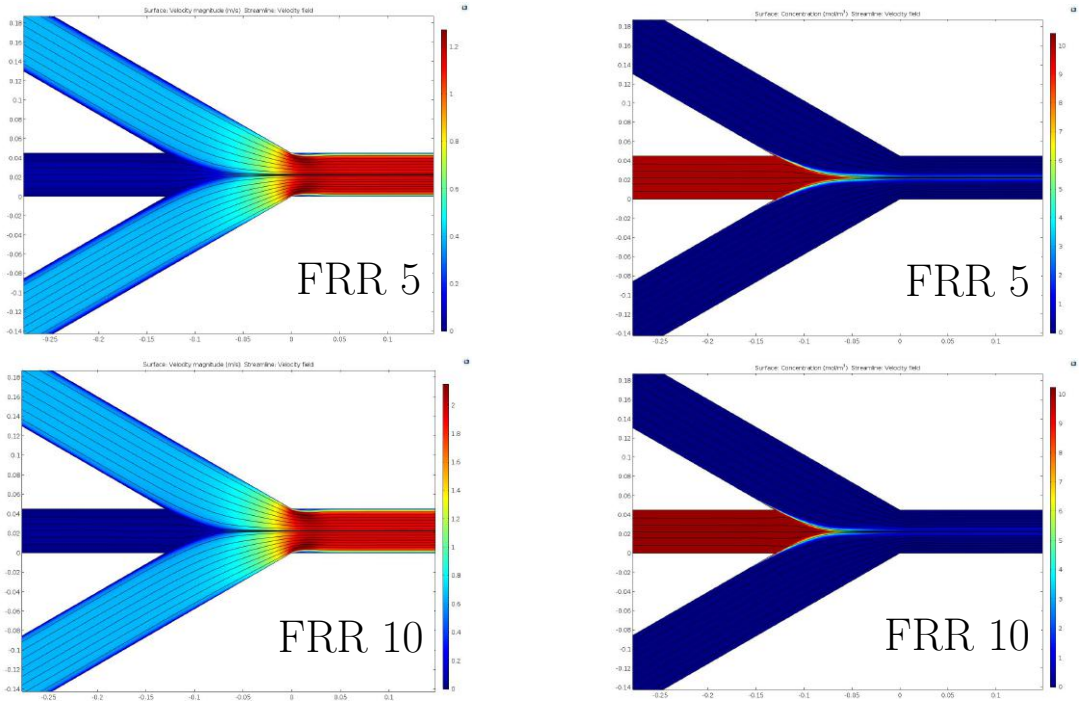

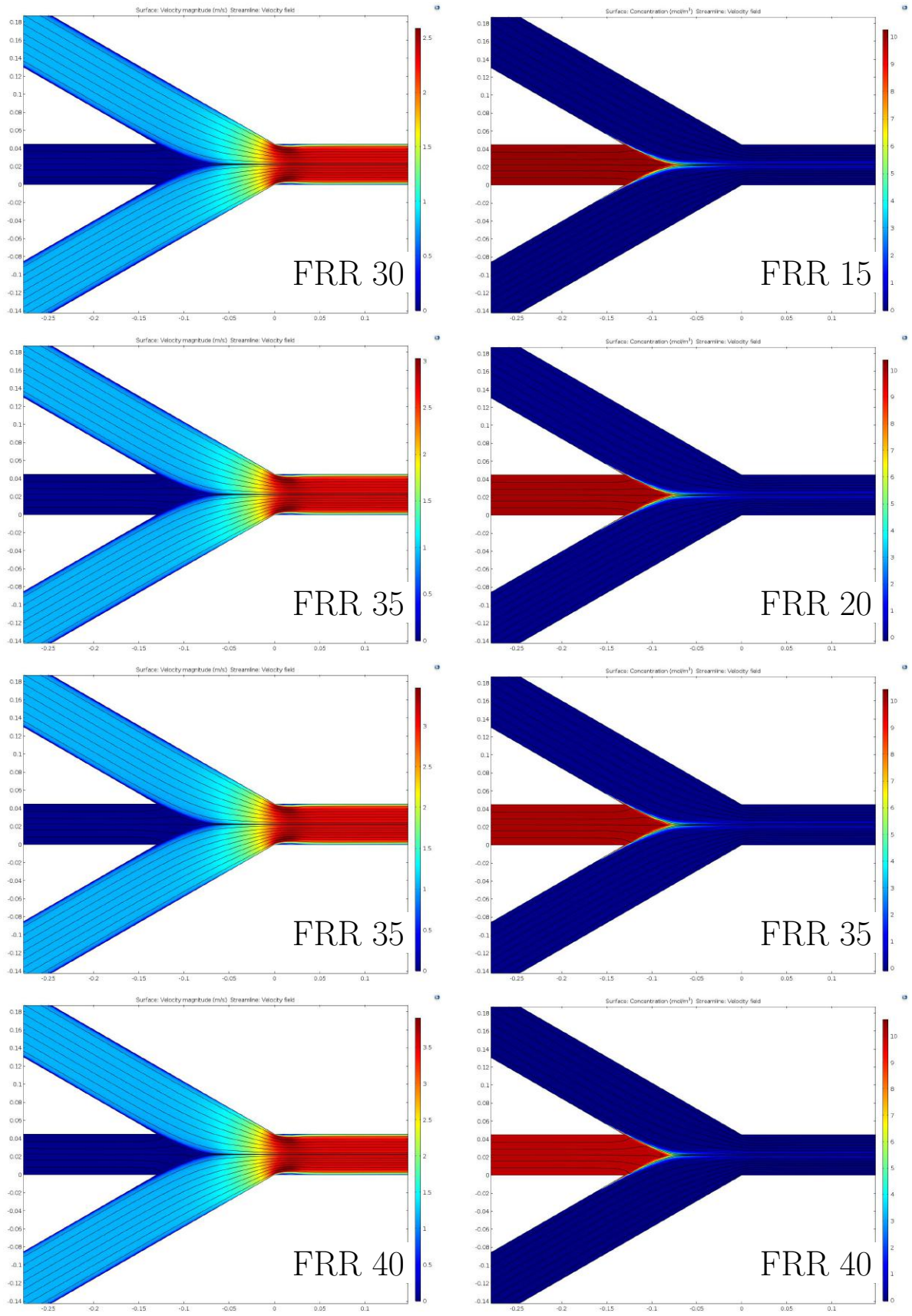

Figure A.1: CFD Simulations of the flow focusing junction of different flow rate ratios (FRRs:15-50) using COMSOL Multiphysics. Other FRR conditions (5,10, 20 and 50) can be found in Fig.5.3.

III. Application Builder:

A.3.1. Algorithm

```
function: Reset_Param % Resets parameters to their default values and prompts a
message box before continuing %
String answer = confirm("Are you sure you want to reset parameters to their
default value?");
if (answer.equals("Yes")){model.param().set("Q1inlet", 10);
model.param().set("Q2inlet", 10);
model.param().set("Cin", 10);
model.param().set("Cdrug", 10);
model.param().set("statusp", 0);
zoomExtents("Plot_Mesh/graphics1");
zoomExtents("Plot_Velocity/graphics1");
zoomExtents("Plot_Concentration/graphics1");}
function: Statusp % Flow Rate Selection %
model.param().set("statusp", 1);
double Q1= model.param().evaluate("Q1inlet");
double Q2= model.param().evaluate("Q2inlet");
double A1= model.param().evaluate("A1");
double A2= model.param().evaluate("A2");
if(Q1<100)
{model.param().set("statusp",0);}
if(Q1>101)
{model.param().set("statusp",0);}
if(Q2<100)
{model.param().set("statusp",0);}
if(Q2>101)
{model.param().set("statusp",0);}
function Ser % Syringe Selection %
model.param().set("ser_a","A1");
model.param().set("ser_a","A2");
model.param().set("statusp", 0);

function: pumps_rbutton
double Nx= model.param().evaluate ("Nx");
if(Nx<=1);{model.param().set("Q2inlet", 0);
model.param().set("statusp", 0);
model.param().set("FRR_exp", "FRR_EXP"); }
if(Nx>=2) {model.param().set("statusp", 0);
alert("Please enter a value for both Q1 and Q2");}
```

A.3.2. Other Applications

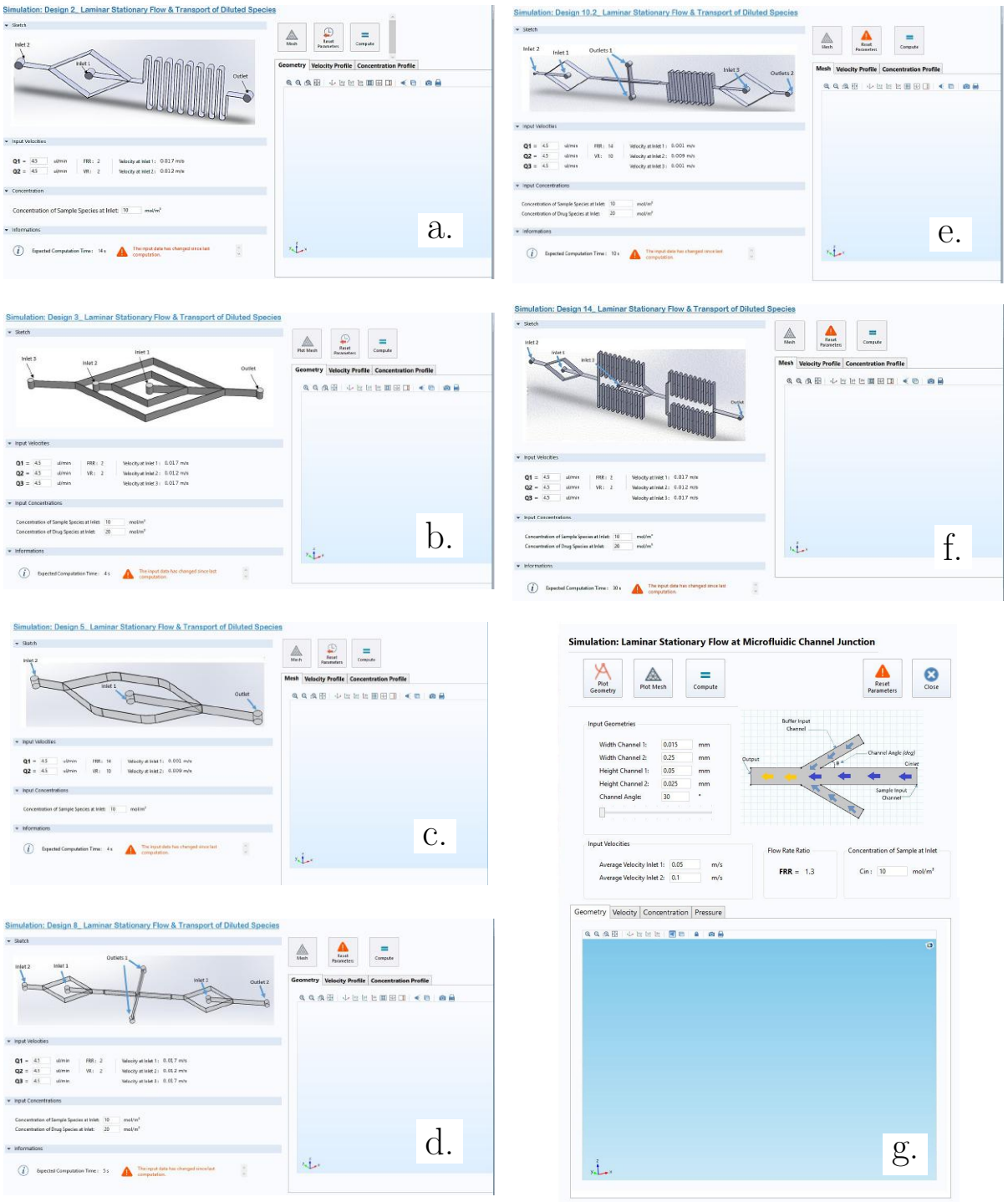

Figure A.2: Applications for the study and simulation of the effect of microfluidic chip design and geometry (a-f) and (g) microfluidic focusing angle (in deg.°) at junction and its effect on the velocity, concentration and pressure profiles.

Appendix B

Flow Visualization

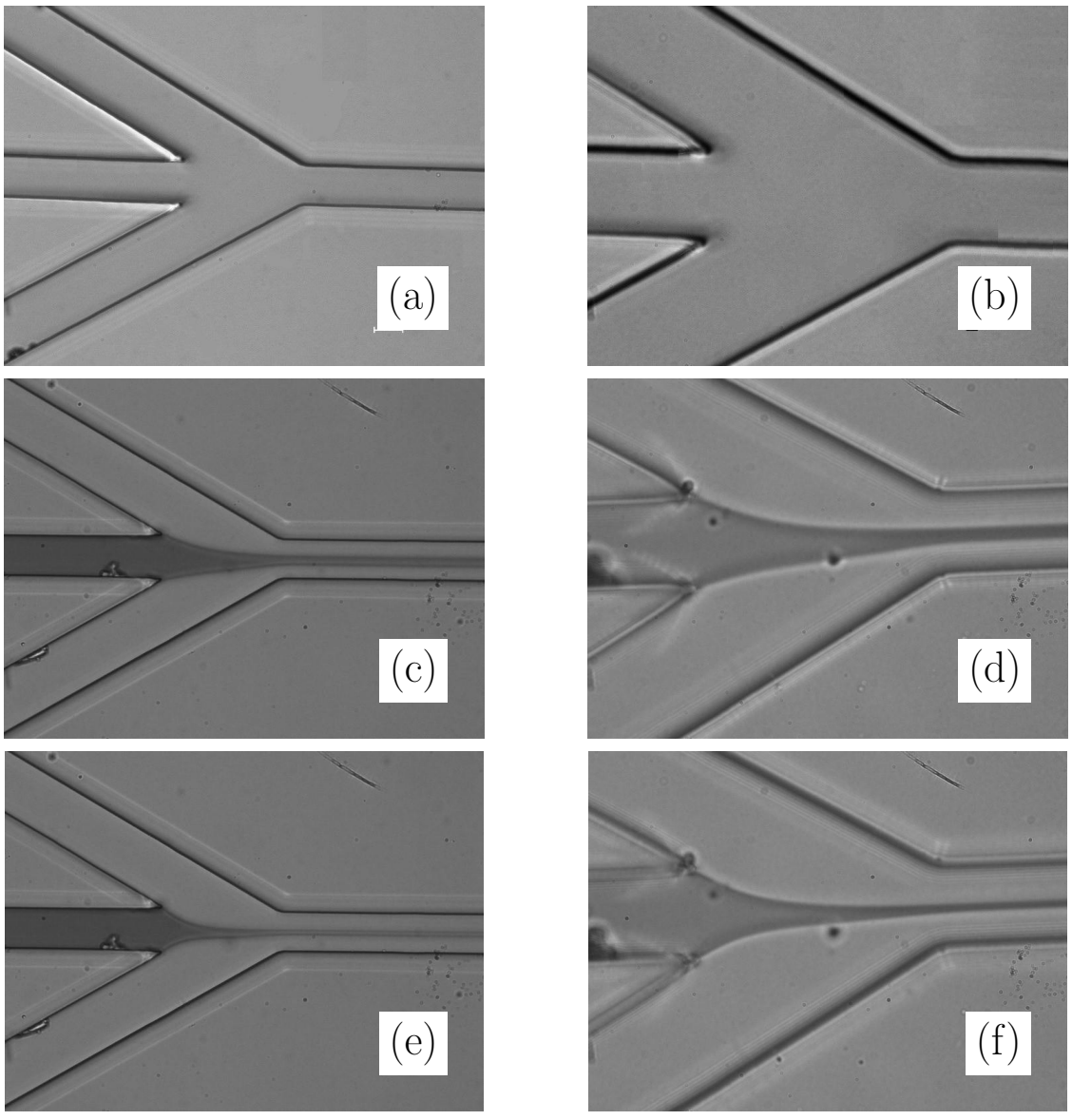

Figure B.1: Optical images of the flow focusing junction at (x20) and (x40): (a)–(b) Control, (c)–(d) FRR5 and (e)–(f) FRR10

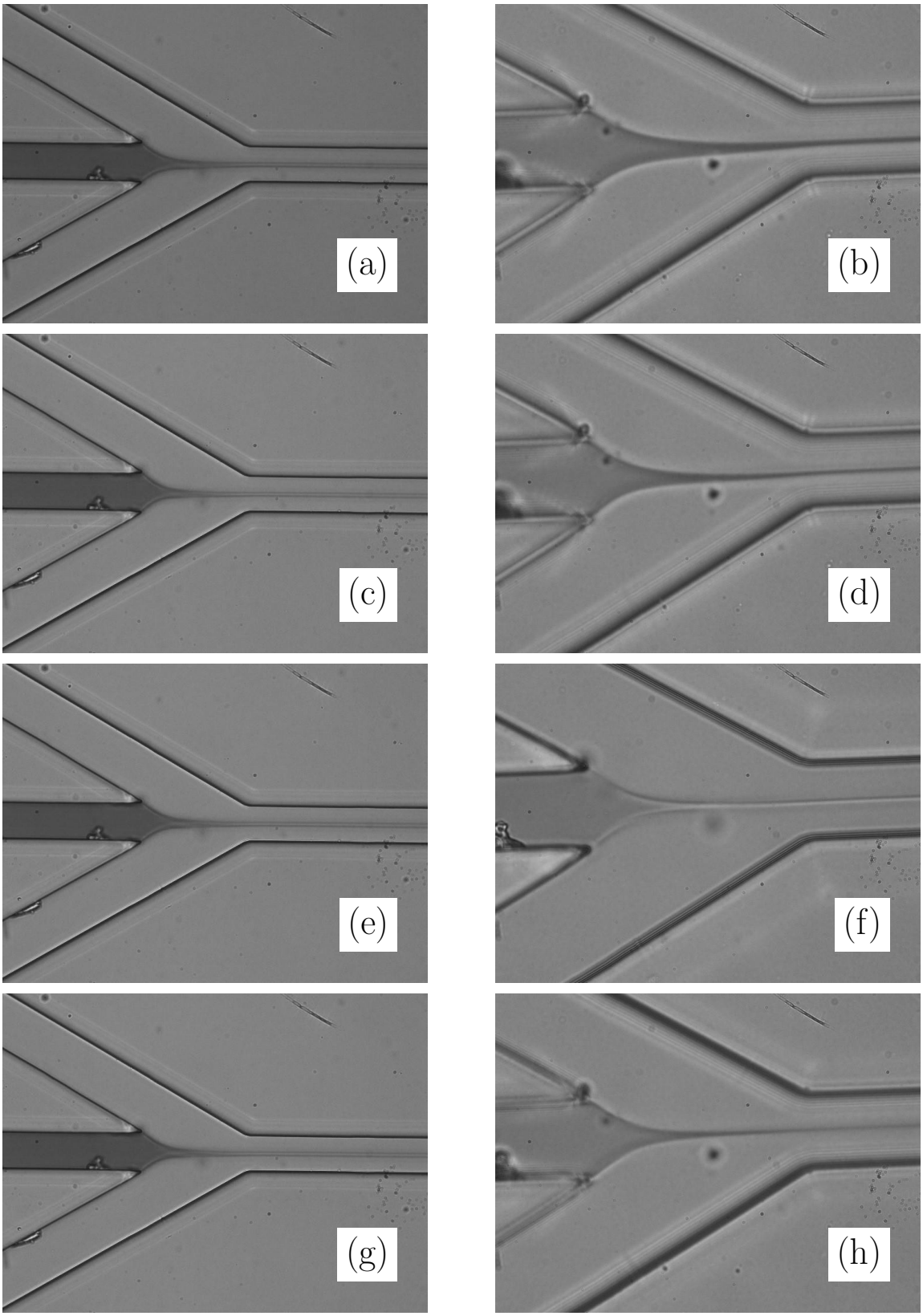

Figure B.2: Optical images of the flow focusing junction at (x20) and (x40): (a)–(b) FRR15, (c)–(d) FRR20, (e)–(f) FRR25, and (g)-(h) FRR30

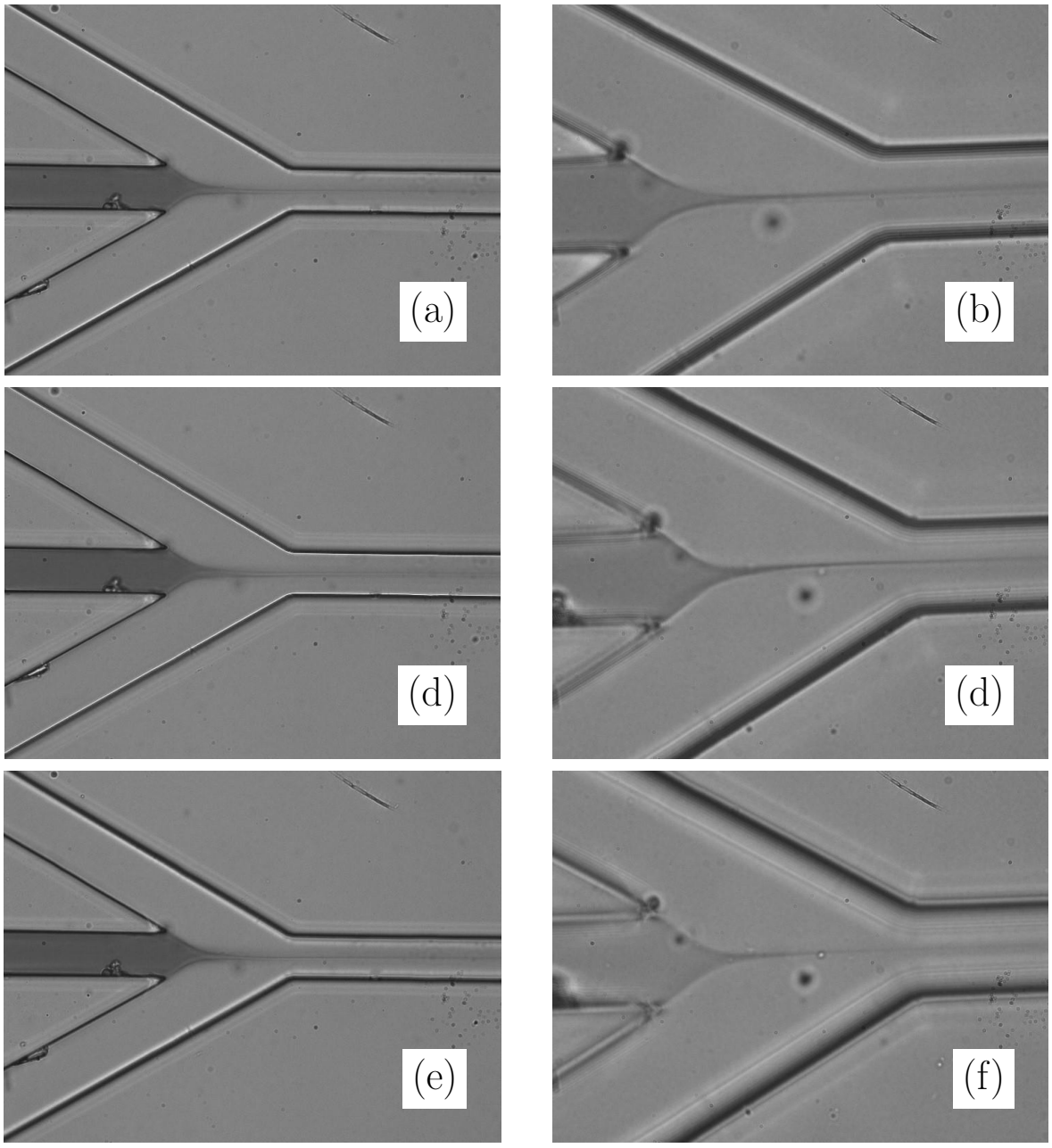

Figure B.3: Optical images of the flow focusing junction at (x20) and (x40): (a)–(b) FRR35, (c)–(d) FRR40, and (e)–(f) FRR50

Appendix C

Microfabrication

I. Microfabrication Protocols:

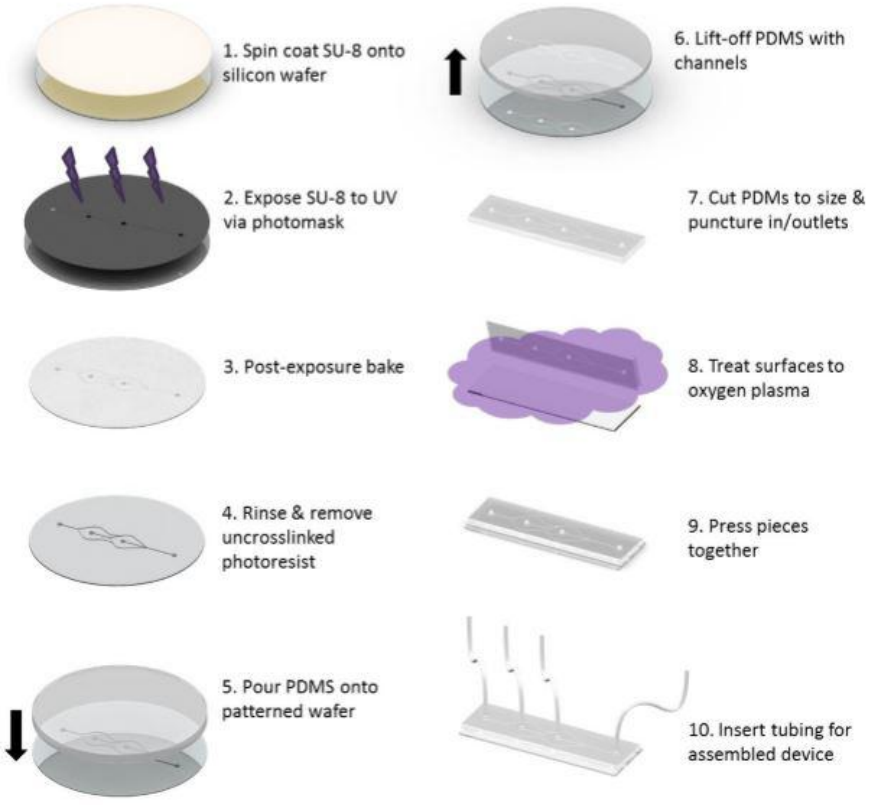

Figure C.1: Photo- and soft- lithography procedures for MHF chip fabrication [105].

Protocol: 1) Spin at 1700 rpm for 100 μ thickness. Soft bake to evaporate solvent. 2) Exposure energy requires: 317 mJ/cm^2. 3) Bake at 65°C for 4 min., then 95°C for 9 min. 4) Develop for 8 min., rinse with fresh solution for 10 sec., rinse with IPA for 10 sec. 5) Mould silanized prior to this step. Cured for 1 h at 70°C. 6) Gently lift-off so as to not damage channels. 7) Protect channel side with tape to avoid contamination. 8) Plasma treatment for 1 min at 50 W. 9) Gently press together, eliminating all air bubbles between surfaces. 10) Insert tubing approximately 3/4 down into PDMS (*Adapted from* [105]).

II. Photomasks and Drawings:

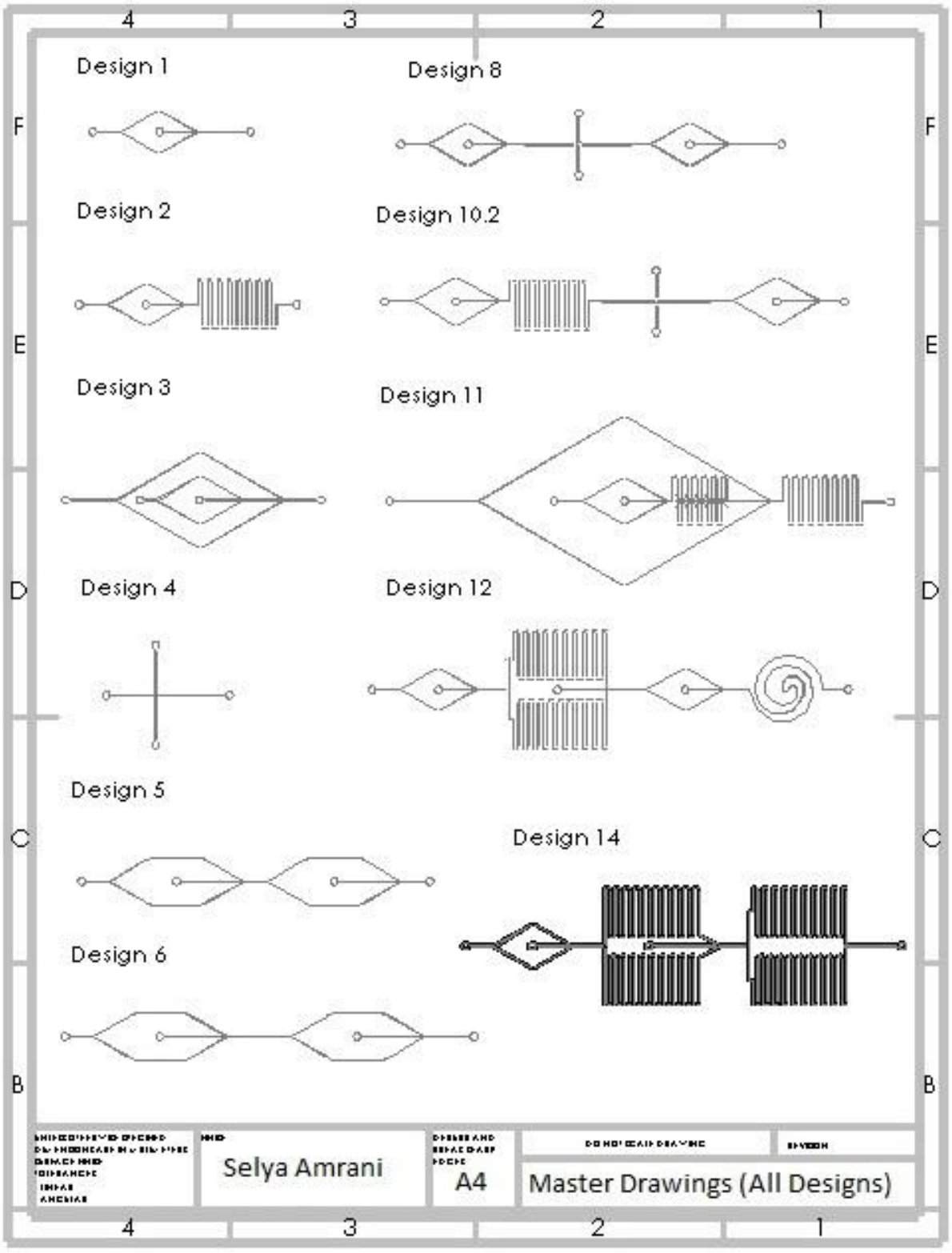

Figure C.2: Sketch drawing showing all the CAD Designs developed for the microfluidic device.

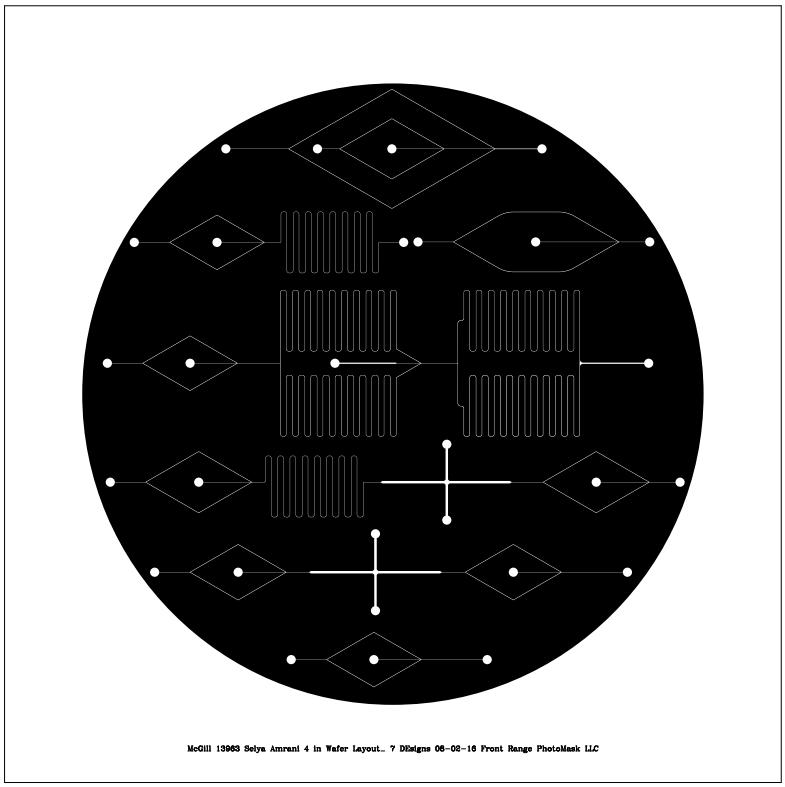

(a)

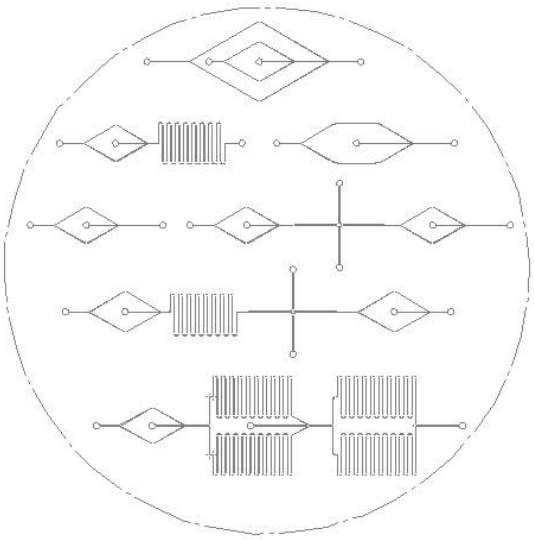

(b)

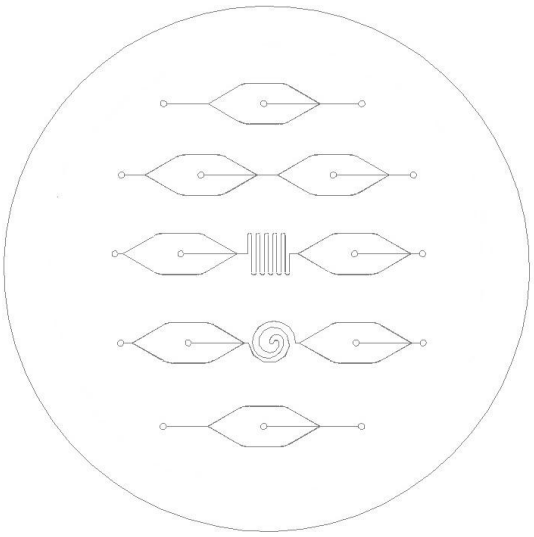

(c)

Figure C.3: Dark-field four inch (4 in) photo-mask (a) and 2-D sketch drawings showing the designs of the two (4 in) masks (b) and (c) respectively, used for the fabrication of the master via photo-lithography.

III. Si Mask Imaging:

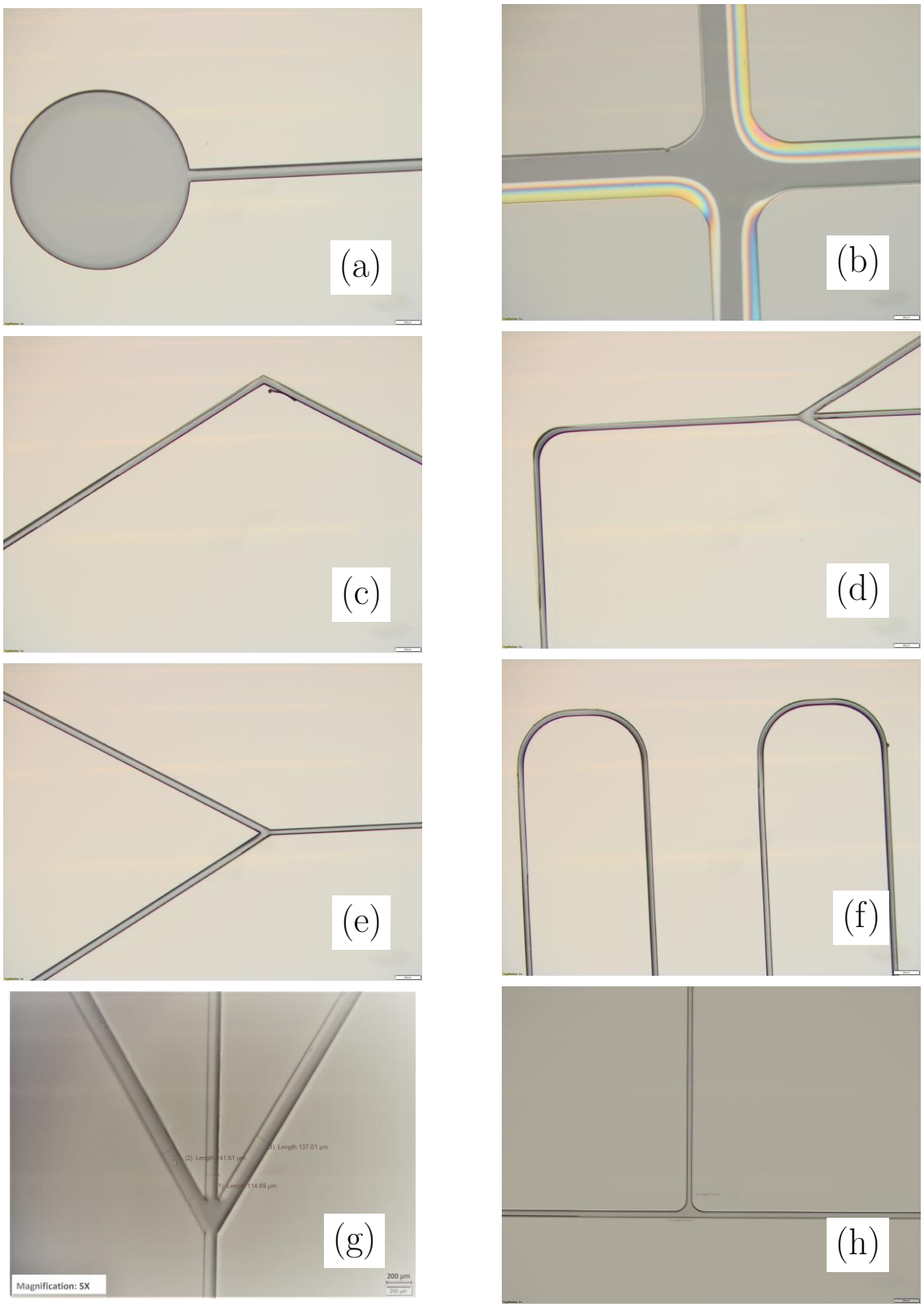

Figure C.4: Fabricated silicon master design geometries: (a) Inlet, (b) Double T-junction, (c) 120° junction, (d) Y-junction with 90° curvature, (e) 120° flow focusing curvature, (f) Serpentine channels, (g) Y-junction (h) T-junction.

Appendix D

Liposomes Preparation

I. Unloaded Liposomes Formulations

Table D.1: Experimental Values for the time required to synthesize 1 mL of loaded/unloaded liposomes at corresponding FRRs.

FRR	**Time**
5	25 min 00 s
10	11 min 07 s
15	07 min 09 s
20	05 min 16 s
25	04 min 10 s
30	03 min 27 s
35	02 min 56 s
40	02 min 34 s
50	02 min 02 s

Table D.3: Composition of samples used for the DDAB/DPPC based liposomes synthesis experiments.

DDAB [mg]	**DPPC[mg]**	**Weight Ratio**
0.00	5.00	Control
5.00	5.00	1:1
0.50	5.00	1:2
1.00	5.00	1:5
0.50	5.00	1:10
0.25	5.00	1:20

Table D.4: Composition of samples used for the DOPG/DPPC based liposomes synthesis experiments.

DOPG [mg]	**DPPC[mg]**	**Weight Ratio**
0.00	5.00	Control
2.50	5.00	1:2
1.00	5.00	1:5
0.50	5.00	1:10
0.25	5.00	1:20
0.01	5.00	1:50

II. Encapsulation & Cell Profiler Reports

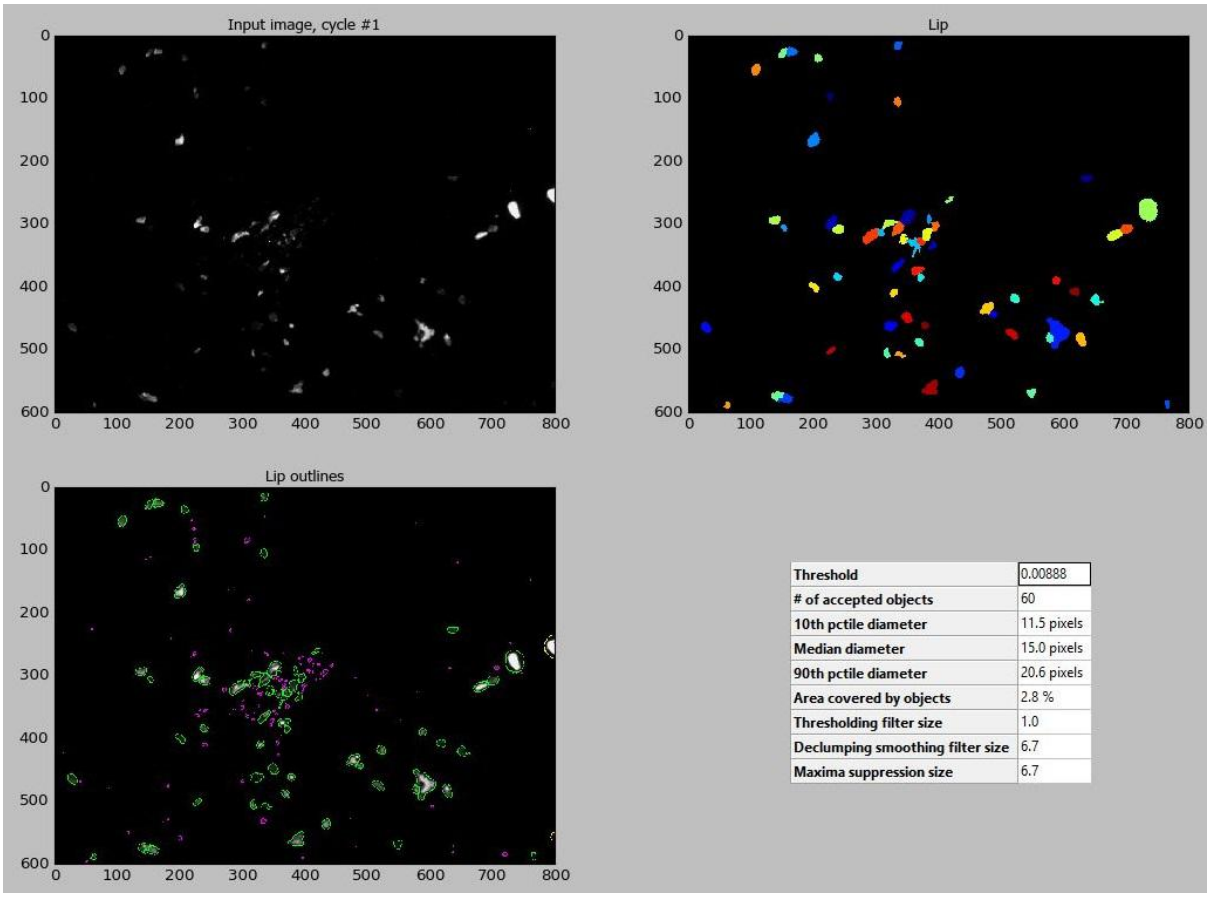

Figure D.1: Cell Profiler Report for liposomes samples measurements of Area B1.

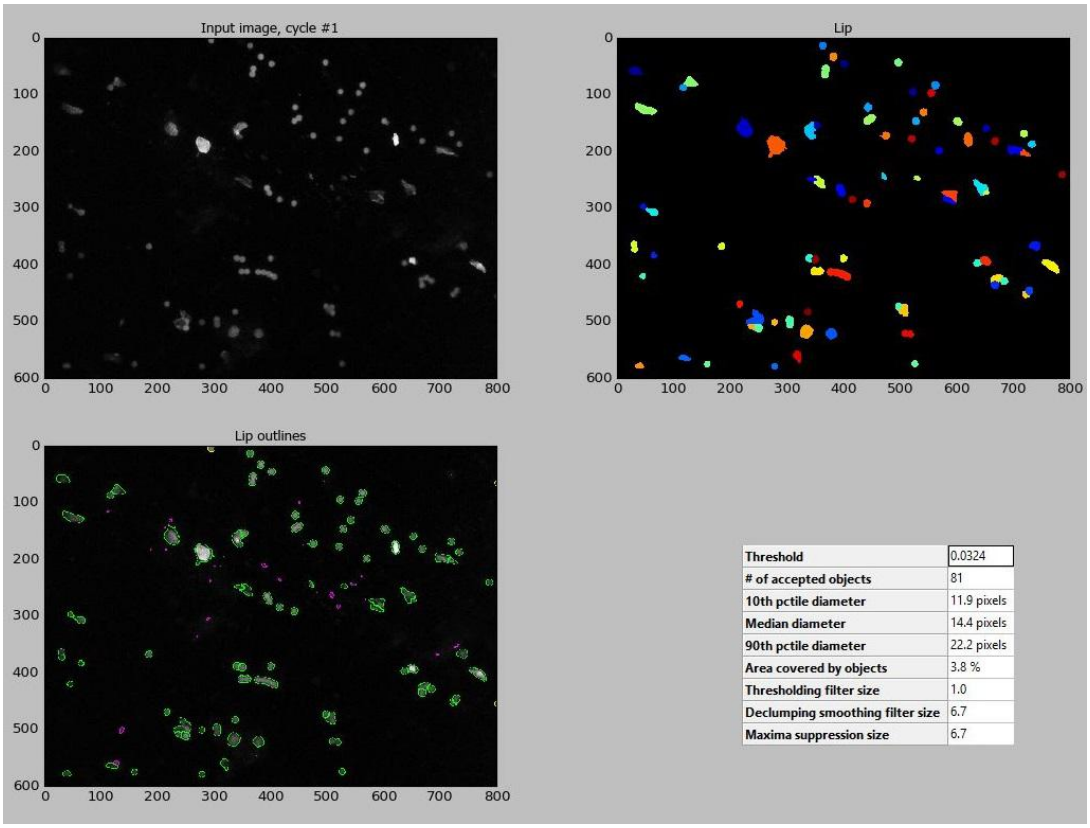

Figure D.2: Cell Profiler Report for liposomes samples measurements of Area B2.

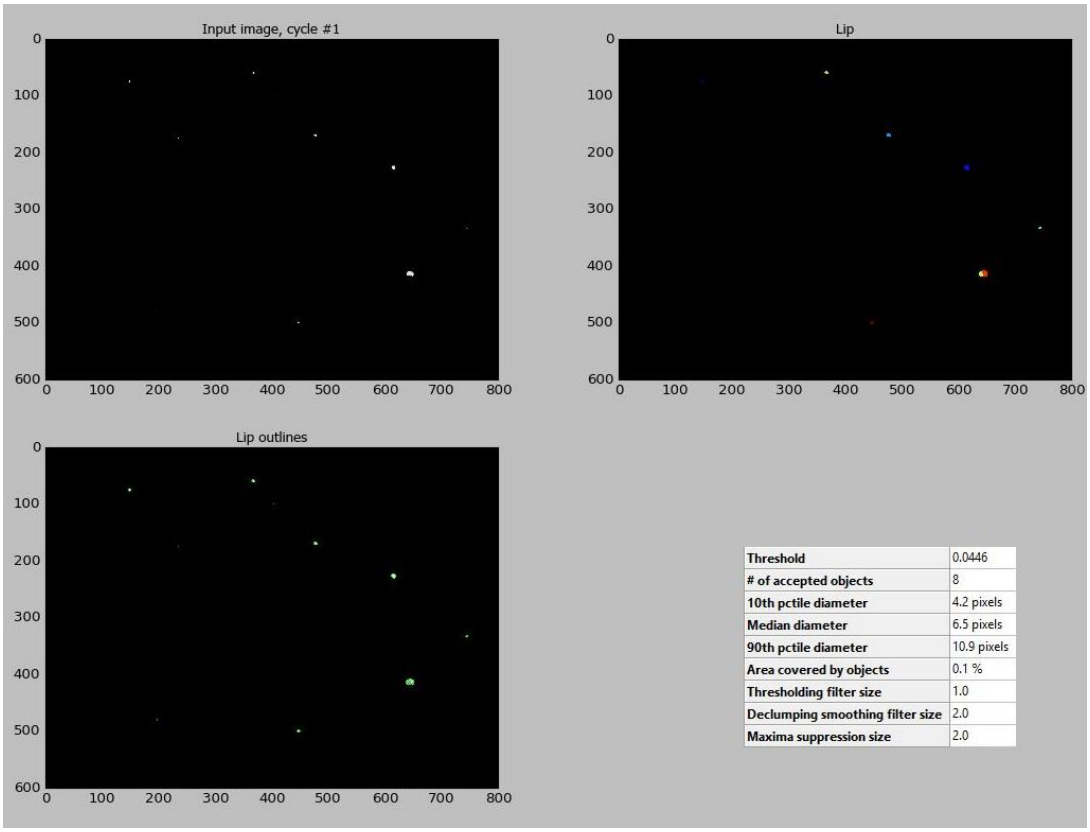

Figure D.3: Cell Profiler Report for liposomes samples measurements of Area B3.

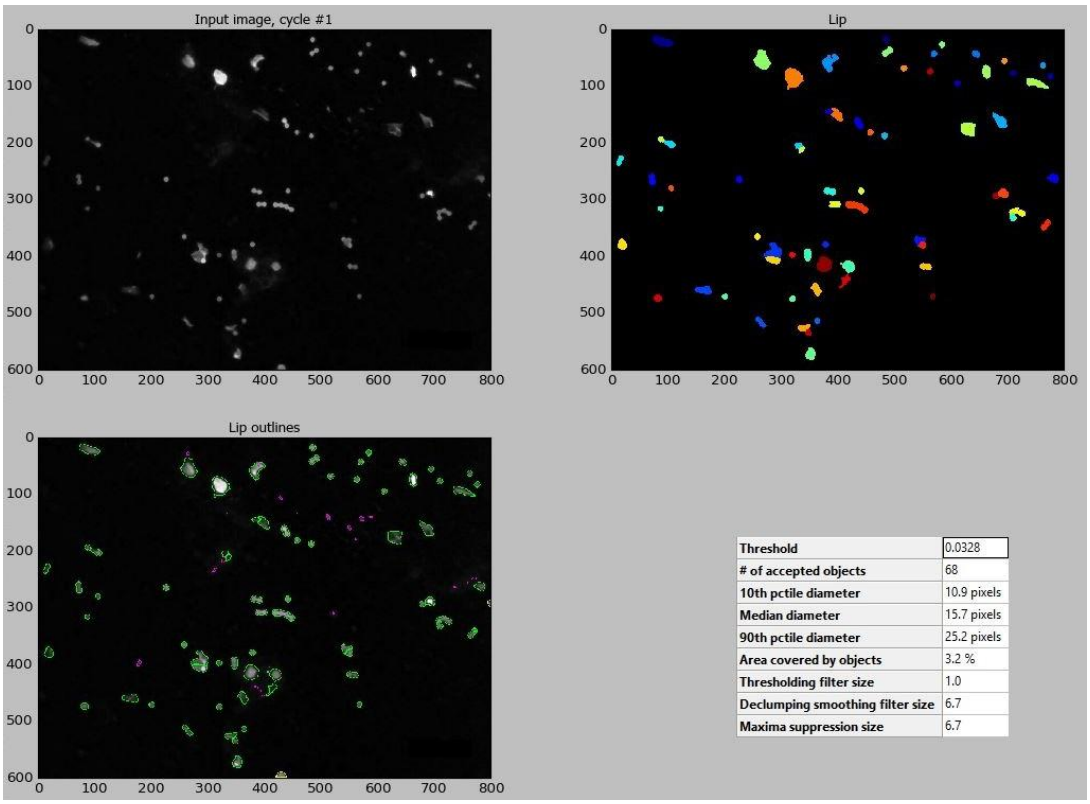

Figure D.4: Cell Profiler Report for liposomes samples measurements of Area C2.

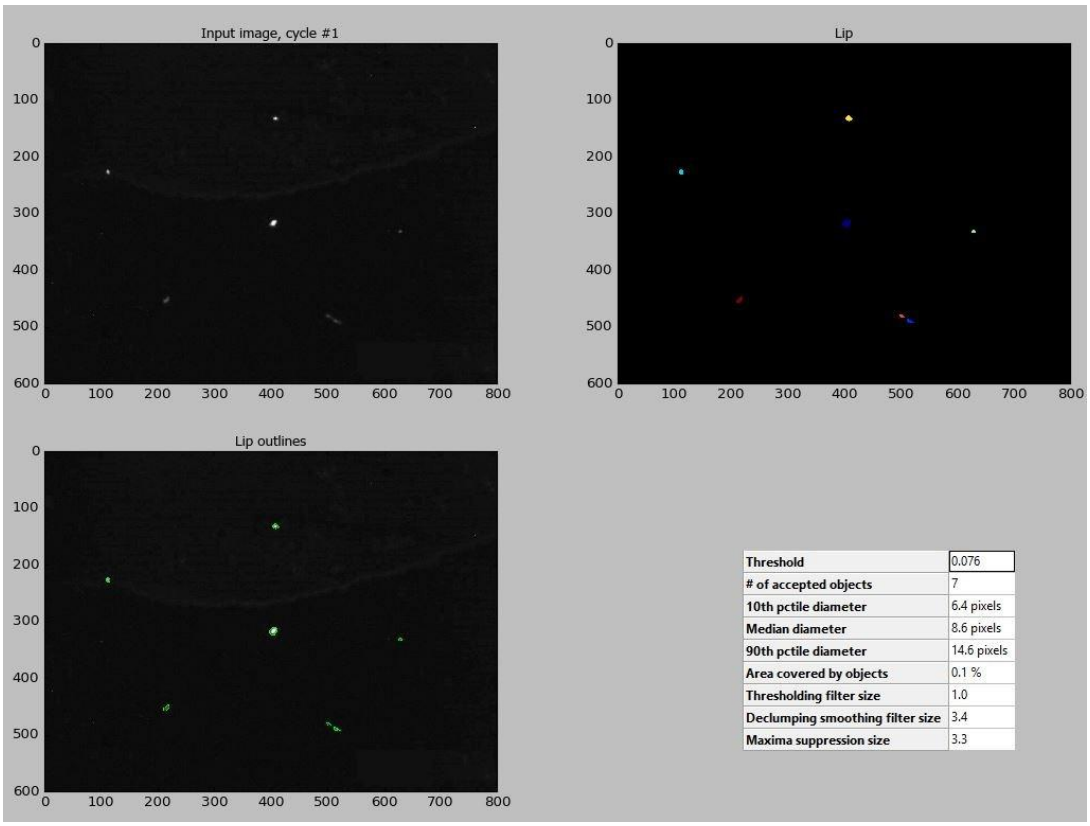

Figure D.5: Cell Profiler Report for liposomes samples measurements of Area C3.

Appendix E

NTA Reports

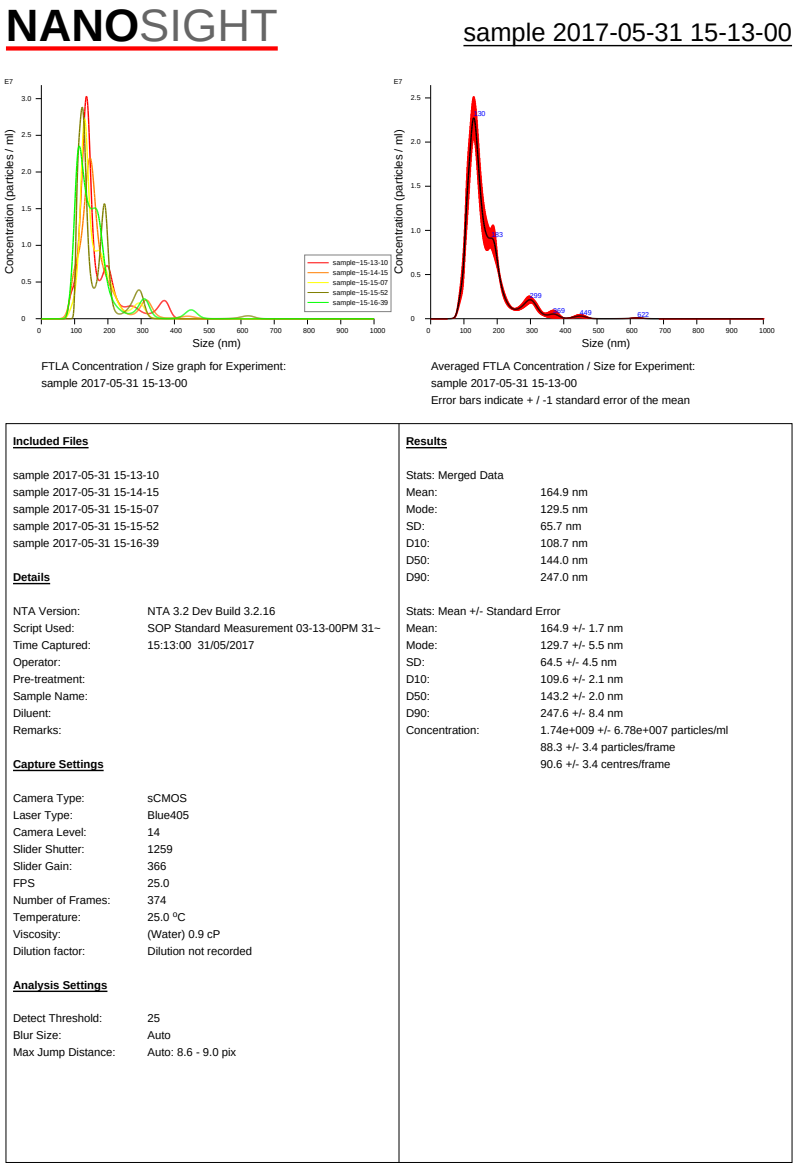

Figure E.1: NTA Report for liposomes samples measurements at a DPPC:EtOH lipid concentration of C=5 mg/mL and FRR=15 (dilution=100x).

NANOSIGHT sample2c5frr30 2017-06-02 15-10-51

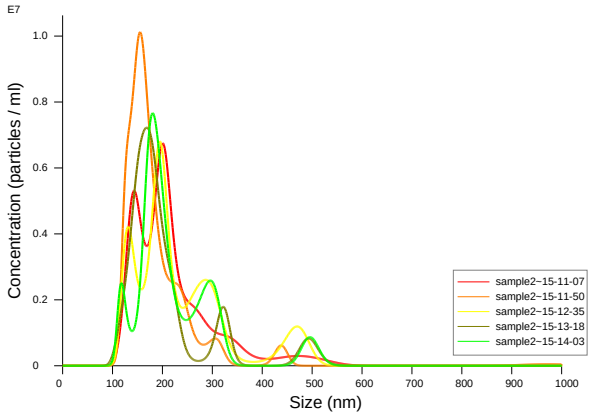

FTLA Concentration / Size graph for Experiment:
sample2c5frr30 2017-06-02 15-10-51

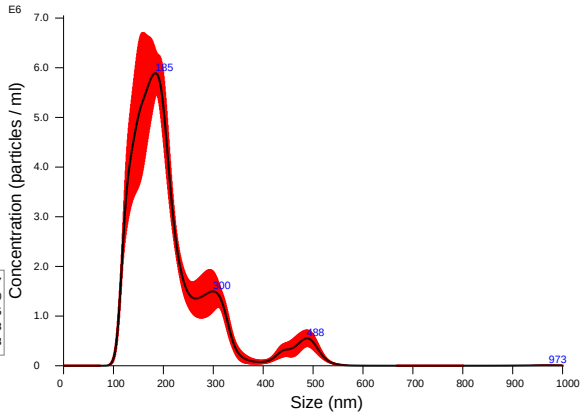

Averaged FTLA Concentration / Size for Experiment:
sample2c5frr30 2017-06-02 15-10-51
Error bars indicate + / -1 standard error of the mean

Included Files

sample2c5frr30 2017-06-02 15-11-07
sample2c5frr30 2017-06-02 15-11-50
sample2c5frr30 2017-06-02 15-12-35
sample2c5frr30 2017-06-02 15-13-18
sample2c5frr30 2017-06-02 15-14-03

Details

NTA Version:	NTA 3.2 Dev Build 3.2.16
Script Used:	SOP Standard Measurement 03-10-51PM 02J~
Time Captured:	15:10:51 02/06/2017
Operator:	
Pre-treatment:	
Sample Name:	
Diluent:	
Remarks:	

Capture Settings

Camera Type:	sCMOS
Laser Type:	Blue405
Camera Level:	15
Slider Shutter:	1206
Slider Gain:	366
FPS	25.0
Number of Frames:	374
Temperature:	25.0 °C
Viscosity:	(Water) 0.9 cP
Dilution factor:	Dilution not recorded

Analysis Settings

Detect Threshold:	31
Blur Size:	Auto
Max Jump Distance:	Auto: 7.6 - 8.4 pix

Results

Stats: Merged Data

Mean:	214.3 nm
Mode:	184.1 nm
SD:	89.5 nm
D10:	133.4 nm
D50:	188.7 nm
D90:	315.8 nm

Stats: Mean +/- Standard Error

Mean:	214.7 +/- 8.2 nm
Mode:	180.0 +/- 8.3 nm
SD:	87.8 +/- 2.5 nm
D10:	135.7 +/- 2.6 nm
D50:	188.7 +/- 7.4 nm
D90:	324.2 +/- 24.2 nm
Concentration:	7.35e+008 +/- 2.40e+007 particles/ml
	37.3 +/- 1.2 particles/frame
	39.2 +/- 1.4 centres/frame

Figure E.2: NTA Report for samples measurements at a DPPC:EtOH lipid concentration of C=5 mg/mL and FRR= 30 (dilution=100x).

NANOSIGHT

samplec5frr50 2017-06-02 15-23-24

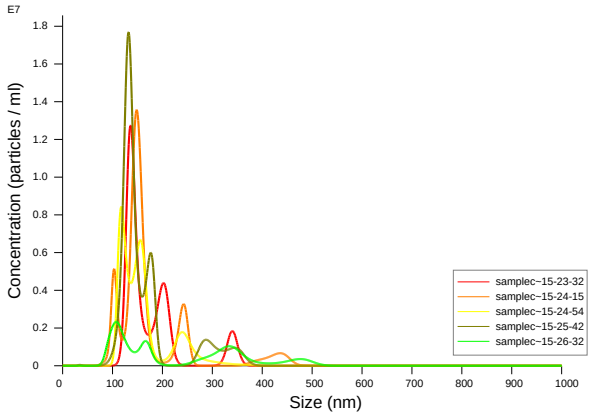

FTLA Concentration / Size graph for Experiment:
samplec5frr50 2017-06-02 15-23-24

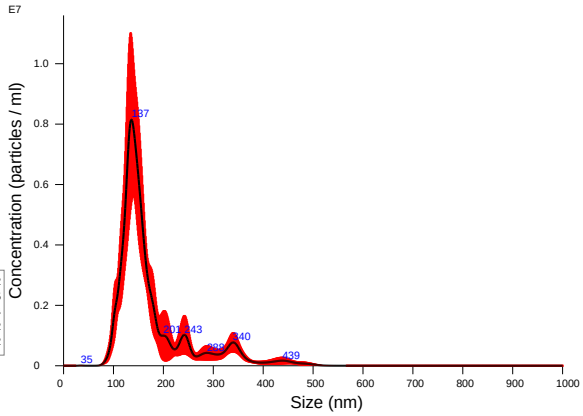

Averaged FTLA Concentration / Size for Experiment:
samplec5frr50 2017-06-02 15-23-24
Error bars indicate + / -1 standard error of the mean

Included Files

samplec5frr50 2017-06-02 15-23-32
samplec5frr50 2017-06-02 15-24-15
samplec5frr50 2017-06-02 15-24-54
samplec5frr50 2017-06-02 15-25-42
samplec5frr50 2017-06-02 15-26-32

Details

NTA Version:	NTA 3.2 Dev Build 3.2.16
Script Used:	SOP Standard Measurement 03-23-24PM 02J~
Time Captured:	15:23:24 02/06/2017
Operator:	
Pre-treatment:	
Sample Name:	
Diluent:	
Remarks:	

Capture Settings

Camera Type:	sCMOS
Laser Type:	Blue405
Camera Level:	14
Slider Shutter:	1259
Slider Gain:	366
FPS	25.0
Number of Frames:	374
Temperature:	25.0 ^{o}C
Viscosity:	(Water) 0.9 cP
Dilution factor:	Dilution not recorded

Analysis Settings

Detect Threshold:	31
Blur Size:	Auto
Max Jump Distance:	Auto: 8.2 - 8.8 pix

Results

Stats: Merged Data

Mean:	175.0 nm
Mode:	136.0 nm
SD:	75.1 nm
D10:	115.5 nm
D50:	147.0 nm
D90:	294.4 nm

Stats: Mean +/- Standard Error

Mean:	181.5 +/- 12.6 nm
Mode:	128.3 +/- 7.2 nm
SD:	75.8 +/- 13.3 nm
D10:	113.1 +/- 5.0 nm
D50:	151.0 +/- 5.2 nm
D90:	283.2 +/- 34.4 nm
Concentration:	5.22e+008 +/- 8.01e+007 particles/ml
	26.5 +/- 4.1 particles/frame
	28.9 +/- 4.4 centres/frame

Figure E.3: NTA Report for samples measurements at a DPPC:EtOH lipid concentration of C=5 mg/mL and FRR= 50 (dilution=200x).

NANOSIGHT

test 2017-05-31 14-36-20

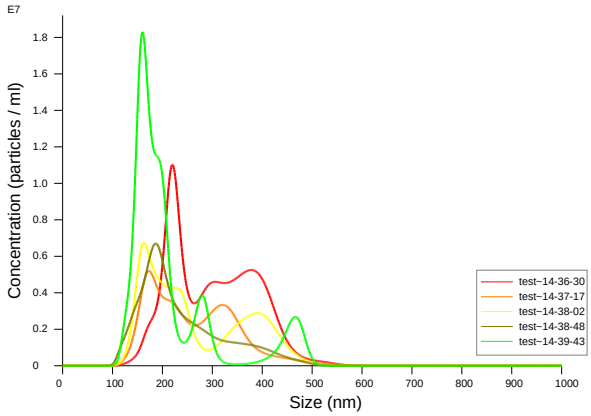

FTLA Concentration / Size graph for Experiment:
test 2017-05-31 14-36-20

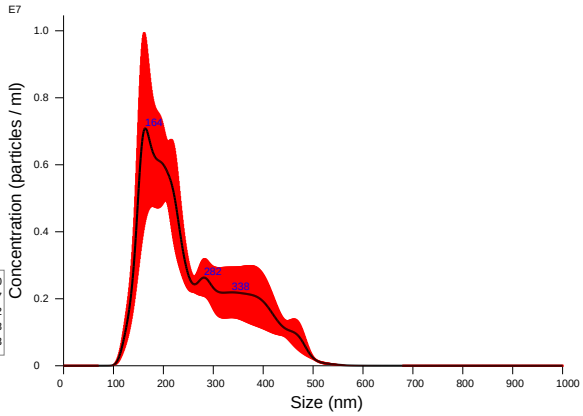

Averaged FTLA Concentration / Size for Experiment:
test 2017-05-31 14-36-20
Error bars indicate + / -1 standard error of the mean

Included Files

test 2017-05-31 14-36-30
test 2017-05-31 14-37-17
test 2017-05-31 14-38-02
test 2017-05-31 14-38-48
test 2017-05-31 14-39-43

Details

NTA Version:	NTA 3.2 Dev Build 3.2.16
Script Used:	SOP Standard Measurement 02-36-20PM 31~
Time Captured:	14:36:20 31/05/2017
Operator:	
Pre-treatment:	
Sample Name:	
Diluent:	
Remarks:	

Capture Settings

Camera Type:	sCMOS
Laser Type:	Blue405
Camera Level:	12 - 13
Slider Shutter:	1200 - 1232
Slider Gain:	146 - 219
FPS	25.0
Number of Frames:	374
Temperature:	25.0 °C
Viscosity:	(Water) 0.9 cP
Dilution factor:	Dilution not recorded

Analysis Settings

Detect Threshold:	13 - 19
Blur Size:	Auto
Max Jump Distance:	Auto: 6.8 - 7.8 pix

Results

Stats: Merged Data

Mean:	256.5 nm
Mode:	163.8 nm
SD:	95.0 nm
D10:	154.3 nm
D50:	225.0 nm
D90:	402.1 nm

Stats: Mean +/- Standard Error

Mean:	255.5 +/- 14.0 nm
Mode:	180.5 +/- 10.9 nm
SD:	89.4 +/- 3.1 nm
D10:	161.9 +/- 10.0 nm
D50:	231.8 +/- 18.7 nm
D90:	394.7 +/- 10.5 nm
Concentration:	1.08e+009 +/- 1.34e+008 particles/ml
	55.0 +/- 6.8 particles/frame
	58.9 +/- 6.8 centres/frame

Figure E.4: NTA Report for samples measurements at a DPPC:EtOH lipid concentration of C=10 mg/mL and FRR=15 (dilution=100x).

NANOSIGHT

test 2017-05-31 14-16-00

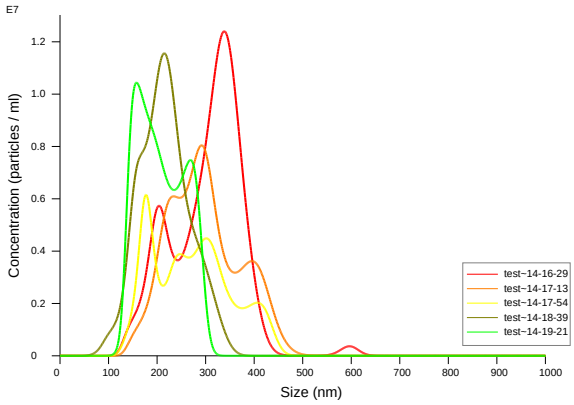

FTLA Concentration / Size graph for Experiment:
test 2017-05-31 14-16-00

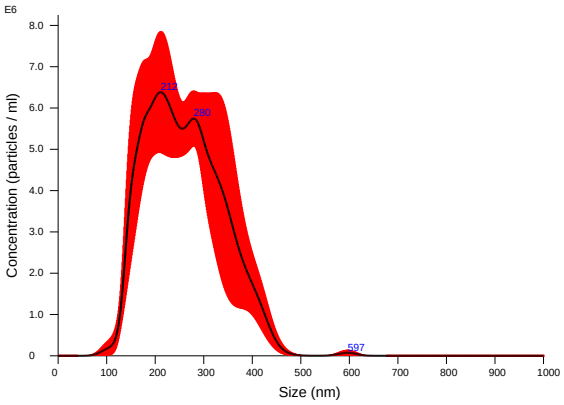

Averaged FTLA Concentration / Size for Experiment:
test 2017-05-31 14-16-00
Error bars indicate + / -1 standard error of the mean

Included Files

test 2017-05-31 14-16-29
test 2017-05-31 14-17-13
test 2017-05-31 14-17-54
test 2017-05-31 14-18-39
test 2017-05-31 14-19-21

Details

NTA Version:	NTA 3.2 Dev Build 3.2.16
Script Used:	SOP Standard Measurement 02-16-00PM 31May2017.txt
Time Captured:	14:16:00 31/05/2017
Operator:	
Pre-treatment:	
Sample Name:	
Diluent:	
Remarks:	

Capture Settings

Camera Type:	sCMOS
Laser Type:	Blue405
Camera Level:	12
Slider Shutter:	1200
Slider Gain:	146
FPS	25.0
Number of Frames:	374
Temperature:	25.0 ºC
Viscosity:	(Water) 0.9 cP
Dilution factor:	Dilution not recorded

Analysis Settings

Detect Threshold:	13
Blur Size:	Auto
Max Jump Distance:	Auto: 6.4 - 8.8 pix

Results

Stats: Merged Data

Mean:	260.4 nm
Mode:	211.1 nm
SD:	78.0 nm
D10:	162.6 nm
D50:	252.5 nm
D90:	366.2 nm

Stats: Mean +/- Standard Error

Mean:	259.0 +/- 19.9 nm
Mode:	236.0 +/- 34.4 nm
SD:	65.7 +/- 6.5 nm
D10:	173.2 +/- 11.9 nm
D50:	257.2 +/- 21.8 nm
D90:	347.3 +/- 27.1 nm
Concentration:	1.33e+009 +/- 1.14e+008 particles/ml
	67.7 +/- 5.8 particles/frame
	76.9 +/- 7.1 centres/frame

Figure E.5: NTA Report for samples measurements at a DPPC:EtOH lipid concentration of C=10 mg/mL and FRR= 30 (dilution=100x).

NANOSIGHT samplec10frr50 2017-06-02 14-29-34

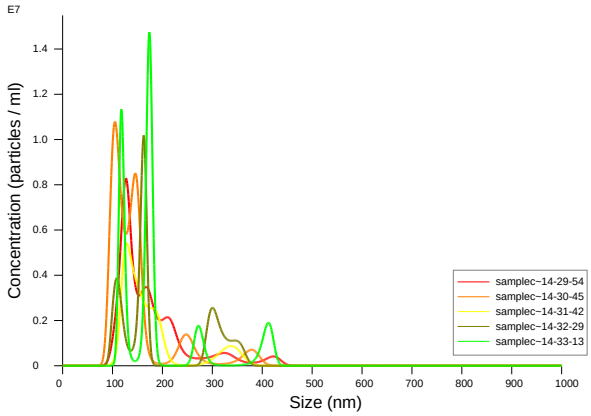

FTLA Concentration / Size graph for Experiment:
samplec10frr50 2017-06-02 14-29-34

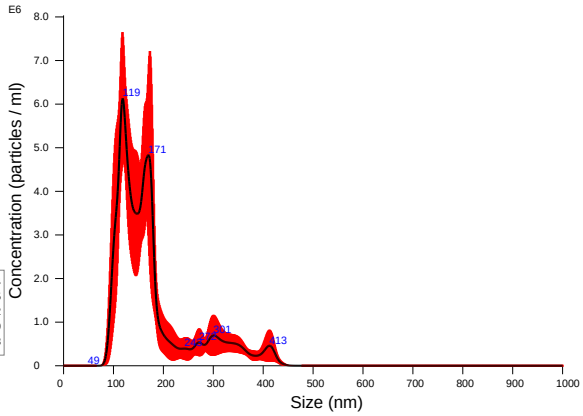

Averaged FTLA Concentration / Size for Experiment:
samplec10frr50 2017-06-02 14-29-34
Error bars indicate + / -1 standard error of the mean

Included Files

samplec10frr50 2017-06-02 14-29-54
samplec10frr50 2017-06-02 14-30-45
samplec10frr50 2017-06-02 14-31-42
samplec10frr50 2017-06-02 14-32-29
samplec10frr50 2017-06-02 14-33-13

Details

NTA Version:	NTA 3.2 Dev Build 3.2.16
Script Used:	SOP Standard Measurement 02-29-34PM 02J~
Time Captured:	14:29:34 02/06/2017
Operator:	
Pre-treatment:	
Sample Name:	
Diluent:	
Remarks:	

Capture Settings

Camera Type:	sCMOS
Laser Type:	Blue405
Camera Level:	15
Slider Shutter:	1206
Slider Gain:	366
FPS	25.0
Number of Frames:	374
Temperature:	25.0 °C
Viscosity:	(Water) 0.9 cP
Dilution factor:	Dilution not recorded

Analysis Settings

Detect Threshold:	20
Blur Size:	Auto
Max Jump Distance:	Auto: 8.7 - 10.1 pix

Results

Stats: Merged Data

Mean:	175.6 nm
Mode:	118.5 nm
SD:	78.0 nm
D10:	107.6 nm
D50:	151.9 nm
D90:	308.3 nm

Stats: Mean +/- Standard Error

Mean:	178.2 +/- 8.6 nm
Mode:	139.3 +/- 12.6 nm
SD:	75.9 +/- 4.4 nm
D10:	110.9 +/- 4.0 nm
D50:	153.3 +/- 6.9 nm
D90:	312.7 +/- 23.9 nm
Concentration:	4.94e+008 +/- 5.14e+007 particles/ml
	25.1 +/- 2.6 particles/frame
	26.6 +/- 2.7 centres/frame

Figure E.6: NTA Report for samples measurements at a DPPC:EtOH lipid concentration of C=5 mg/mL and FRR= 50 (dilution=200x).

Appendix F

Submitted Manuscript

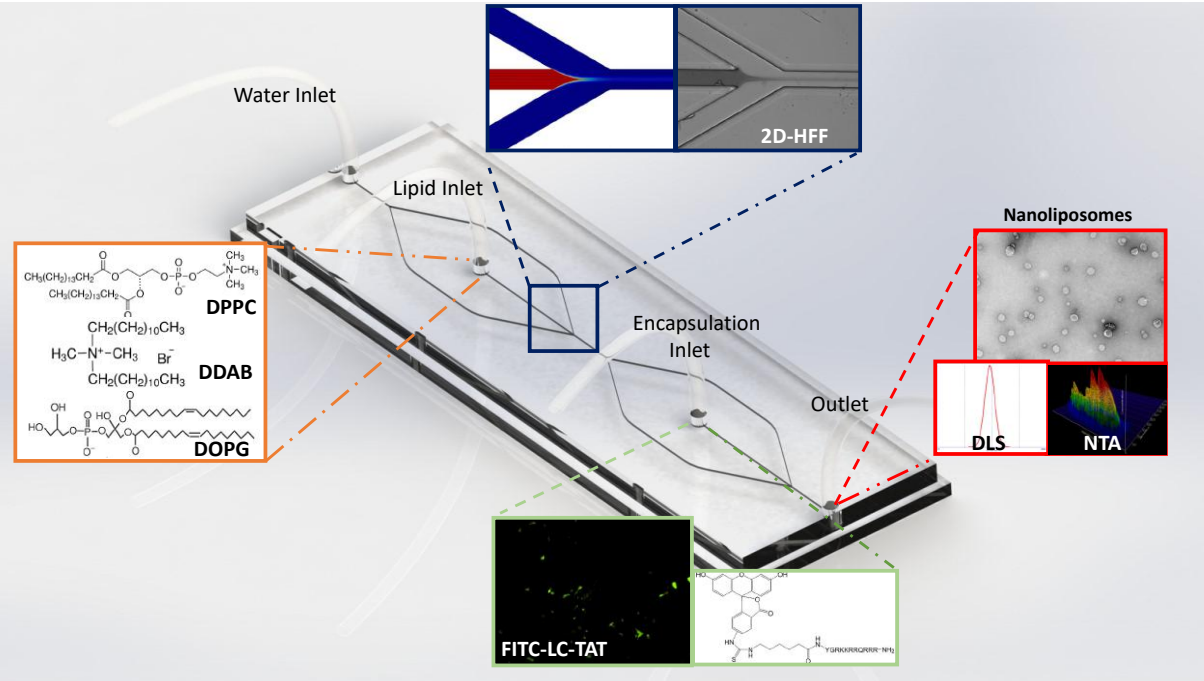

Figure F.1: Cover Page of the Manuscript Submitted to ACS Biomaterials and Engineering (*Paper under Review*).

Passive Encapsulation and Characterization of Nanoscale Liposomes Produced by 2-D Hydrodynamic Flow Focusing

Selya Amrani[1] and Maryam Tabrizian[1,2]

[1] *Faculty of Medicine, Department of Biomedical Engineering, McGill University, Duff Medical Building, Montreal, Quebec H3A 2B4, Canada.*
[2] *Faculty of Dentistry, McGill University, Strathcona Anatomy & Dentistry Building, Montreal, Quebec H3A 2B2, Canada.*

Email: *selya.amrani@mail.mcgill.ca, maryam.tabrizian@mcgill.ca*

ABSTRACT

This paper presents the continuous flow formation by two dimensional (2-D) hydrodynamic flow focusing (HFF) of nano-sized liposomes in microfluidic systems. We introduced the use of nanoparticle tracking analysis (NTA) to estimate for the first time the throughput of synthesized liposomal NPs by measuring quantitatively the concentration of the synthesized particles directly at the outlet. The size distribution and concentration of the nano-sized liposomes, as well as the polydispersity and zeta potential (ZP) of the liposomal dispersions were investigated under various flow rate ratios (FRRs) and lipid formulations, by the selective incorporation of either positively charged DDAB (didodecyl-dimethyl-ammonium bromide) or negatively charged DOPG (1,2 dioleoyl-sn-glycero-3- phosphoglycerol) lipids to the main bilayer DPPC (1,2-dipalmitoyl-sn-glycero-3-phosphocholine) constituent. The challenges of encapsulating labeled LC-TAT peptide, which plays a direct role in the HIV regulation and transcription, overcame and could be achieved via one-step nanoliposomes synthesis, in order to validate the potential of this device as an all-in-one nanoparticle synthesis and loading platform. Liposomes with sizes ranging between 60 nm to 800 nm were produced with low polydispersity and high particle throughput from alteration of the flow rate ratio and lipid concentration. Stable and unilamellar liposomes were generated at a maximum concentration of 1740 x E8 $particles/mL$ in less than two minutes, with higher FRR enabling the most rapid generation of liposomes with similar diameter and significant lower polydispersity index than those obtained by other batch techniques.

1 INTRODUCTION

A major challenge in the development of nanoparticles (NPs) for drug delivery is the control of size and size distribution[1,2]. To avoid measurements perturbed by polydispersity in vesicle size, a solution of vesicles of uniform diameters is a prerequisite for studying size-dependent properties[2]. In addition, NPs diameters have been shown to play an important role on their circulation time within the body and their elimination[3]. Traditional bulk methods of NPs preparation are however limited by difficulty in controlling size[4], as well as by problems of scale-up[5–8], inconsistent encapsulation efficiency[9–11], along with difficulty in effective sterilization[12]. In addition, long processing times, difficulty in obtaining relatively monodisperse products, large reagent volumes[13], and the multiple and lengthy steps necessary for encapsulation[14–16], make bulk synthesis methods time-consuming and uneconomical[1,17]. The production of nano/microsized liposomes is mostly based on the formation of a dried lipid film[18,19], and include processes such as thin-film hydration[20–22], ethanol injection[23–26], and detergent dialysis methods[27,28]. Because these processes rely on the self-assembly of lipids in a bulk phase, which is heterogeneous and uncontrolled[29–31], the resultant liposomes are polydispersed in size and often multilamellar. Further post-processing by extrusion[21,20], freeze–thaw[11,32,33], sonication[21], and/or high-pressure homogenization[34,32] is often required, in order to obtain liposomes with specific size and conformations[35].

Compared to their non-organic nanoparticles counterparts, the use of liposomes as a delivery vehicle offers many advantages including longer circulation times within the body[29], protection and controlled release

of the encapsulated molecules[36,37], and the ability to overcome biological barriers to achieve targeted delivery[38,39]. The search for new strategies to alleviate the current issues facing liposome fabrication and provide control over both lipid aggregation and particle size while enabling encapsulation of various compounds, continues to remain a challenge in the field of liposome technology. In this context, drug-loaded nano-liposomes can be produced in one step only with a microfluidic continuous process with many advantages over classical methods. This includes reducing the use of organic solvents, as well as providing fast, single-stage production and producing stable, uniform liposomes[40,34].

Jahn et al.[30] first reported on the controlled synthesis of submicrometer-sized liposomes through microfluidic flow focusing (MHF). New iterations of the MHF device containing five-inlet channels and three-outlet channels were later introduced[31], which produced relatively high liposome concentration and catalyzed the formation of more stable liposomes along the interfacial region[34]. Since then, several flow focusing microfluidic devices have been developed for the production of micro/nanoscale lipid-based vesicular systems[41–44]. With efforts being deployed to define the parameters determining particle size distribution of the liposomal preparation. Pradhan et al.[44] exploited a syringe pump-driven microfluidic injection device to produce liposomes under different conditions. They observed a decrease in particle size of the liposomes with a decrease in needle diameter (or increase in hydrodynamic pressure), a decrease in lipid concentration in the alcohol solution, a decrease in phase transition temperature (T_m) of the lipid bilayer and the absence of cholesterol (or decrease in membrane rigidity[44]. The effect of microfluidic chip design and lipid formulations were also notably evaluated by Carugo et al.[45] in terms of the size and homogeneity of the end product, where the role of lipid formulation, lipid concentration, residual amount of solvent, production method (including microchannel architecture), and drug loading was evaluated in determining liposome characteristics[45]. Devices with mixing channel displaying distinct architectural features (i.e., straight, serpentine-like, and containing micro-pillar structures) and scaled-up versions of microscale flow focusing architectures in the millimeter range were introduced, citing the effects of operating parameters (especially the FRR) on liposomes dimensions[45].

However, while a variety of techniques for liposome synthesis have been reported that take advantage of microfluidic flow elements to achieve precise control over the size and polydispersity of nanoscale liposomes, with important implications for nanomedicine applications, these methods suffer from extremely limited throughput, making them impractical for large-scale nanoparticle synthesis[41]. As an alternative to enhance the throughput of liposome synthesis, Michelon et al.[46] performed a systematic study of the effect of channel aspect-ratios for nanoscale liposome formation. A simple T-junction plan focusing design for liposome formation using planar (2-D) HFF microfluidic devices was presented. More complex high aspect ratio microfluidic vertical flow focusing has also been developed by Hood et al[41] as an attempt to overcome the throughput limits of established microfluidic nanoparticle synthesis techniques[41]. Vertical flow focusing technique was utilized to generate populations of small, unilamellar, and nearly monodisperse liposomal nanoparticles with exceptionally high production rates and sample homogeneity.

Building upon previous HFF work[47], in which we developed a double flow-focusing microfluidic geometry capable of sub-hour synthesis and controlled loading of DSPC tunable liposomes, this new platform addresses some of the issues previously encountered with the last prototype, including the low particle yield and diluted liposomal solutions at the outlet. In this work, we therefore address the high throughput synthesis of liposomal particles bellow the 500 nm range without compromising the final particle concentration at the outlet. In addition, since the through-put of microfluidic devices is generally expressed in terms of mg per minute, this gives limited information as to the particle count/ concentration of liposomes in solution. As such, this work represents the first attempt to estimate quantitatively the throughput of hydrodynamic flow-focusing microfluidic devices for liposome formation, expressed in terms of the concentration of the produced liposome nanoparticles directly at the outlet. Using *1,2-dipalmitoyl-sn-glycero-3-phosphocholine* (DPPC) as the main bilayer constituent, particle diameters and concentrations were evaluated with respect to phospholipid concentration, composition and flow rates. In addition, by adding either positively and negatively charged lipid particles to the bilayer DPPC constituent, by incorporating DDAB (*didodecyldimethylammonium bromide*) and DOPG (*1,2 dioleoyl-sn-glycero-3-phosphoglycerol*) respectively, the effect of the lipid charge and the colloidal stability on liposome size is investigated at different FRRs. Finally, as a demonstration of the generality of the microfluidic mixing encapsulation process, encapsulation of a bioactive molecule; an FITC labeled LC-TAT cell-penetrating peptide is demonstrated. TAT (Trans-Activator of Transcription) is a protein encoded for by the TAT gene in HIV-1 and stimulates HIV-1 gene

expression during transcription initiation and elongation[48]. In addition, by antagonizing the CXCR4 receptor, reports suggest that TAT selectively encourage the reproduction of less virulent M-tropic (macrophage-tropic) strains of HIV early in the course of infection, allowing the more rapidly pathogenic T-cell-tropic strains (which use the CXCR4 receptor) to emerge later after mutating from M-tropic strains[49].

2 Materials and Methods

2.1 Materials

Negative photoresist, SU-8 2050, was purchased from Microchem Corp. (Boston, MA, USA). Sylgard 184 elastomer kits, consisting of a prepolymer and a curing agent of PDMS, were purchased from Dow Corning Corp. (Saint-Laurent, QC, Canada). Tygon 0.020" ID microbore tubing was purchased from Cole-Parmer Canada Inc. (Montreal, QC, Canada). A quick setting epoxy adhesive was purchased from LePage-Henkel (Mississauga, ON, Canada). 2-propanol (IPA), acetone, methanol (MeOH), all analytical grade, and glass microscope slides were purchased from Fisher Scientific (Waltham, MA, USA). Anhydrous ethyl alcohol (EtOH) was purchased from GreenField Specialty Alcohols Inc. (Brampton, ON, Canada). Trichloro(1H,1H,2H,2H-perfluorooctyl) silane, DOPG (1,2-Dioleoyl-sn-glycero-3-phosphoglycerol) and DDAB (Didodecyldimethylammonium bromide) were purchased from Sigma Aldrich (Oakville, ON, Canada). FITC-LC-TAT fluorescent peptide was purchased from AnaSpec Inc. (Fremont, CA, USA). 1,2-Dipalmitoyl-sn-glycero-3-phosphocholine (DPPC) was purchased from Avanti Polar Lipids Inc. (Alabaster, AL, USA). Glass vials were purchased from VWR International (Radnor, PA, USA), 1 mL and 10 mL Hamilton glass syringes were obtained from Fisher Scientific (Ottawa, ON, Canada). Ultrapure water (MilliQ) from a Millipore filtration system (resistivity above 18.2 MΩ-cm) was used for all experiments.

2.2 Methods

2.2.1 Computer-Assisted Design (CAD):

The design was modeled using a computer aided design (CAD) software (SolidWorks 2016 - Dassault S.A., Vélizy, France) and the 2D geometry was exported to be used in computational fluid dynamics (CFD) studies using the "CAD Import Module" in COMSOL. The same design was then used to fabricate the photo-mask for subsequent micro-fabrication in the cleanroom.

2.2.2 Numerical Flow Simulations:

The microfluidic channel geometry used for simulation (Fig. 1) originated from the SolidWorks 2016 sketch used for the experimental fabrication; however, the microfluidic channels leading to and from the flow focusing junction area were truncated to leave only the Y junction of interest. Numerical simulations were then conducted using COMSOL Multiphysics 5.2a (COMSOL Inc., Burlington, MA, USA). The "COMSOL Multiphysics", "CAD Import" as well as the "Microfluidics" Modules were selected. Laminar Flow Models include both 2D "Time-Dependent" and "Steady-State" Analyses. Stationary Steady state studies are governed by "Incompressible Navier-Stokes" (1) and "Continuity" (2) equations where the final forms assuming incompressible Newtonian fluids, are presented below:

$$\rho\left[\frac{\delta u}{\delta t}+(u\cdot\nabla)u\right]=-\nabla p+\mu\nabla^2+F \tag{1}$$

$$\rho\left[\nabla\cdot(u)\right]=0 \tag{2}$$

Where: u is the flow velocity, ρ is the fluid density, p is the pressure, μ is the dynamic viscosity and F represents outer forces.

For mass transport of dissolved (solute) species, concentration gradients will cause diffusion[50]. In addition, convection will also contribute to the flux of chemical species by bulk fluid motion. Therefore, we were interested in solving for the combined effect of both convection and diffusion. For a dilute species:

$$N_i=-D_i\nabla C_i+c_i u \tag{3}$$

$$\frac{\delta c_i}{\delta t}+(\nabla\cdot N_i)=R_i \tag{4}$$

Where: c_i is the species concentration (in $mol.m^{-3}$), N_i is the molar flux (in $m^{-2}s^{-1}$, R is a net volumetric source for c: $R>0$ assumes that a chemical reaction is creating more of the species, and $R<0$ that a chemical reaction is destroying the species. D_i is the diffusion coefficient of the species (in m^2/s).

With water as the working fluid, the flow focusing device is characterized by the Flow Rate Ratio (FRR), which is defined as follows:

$$FRR = \frac{Q_1 + Q_2}{Q_1} \tag{5}$$

Where: Q_1 and Q_2 represent flow rate of the lipid stream dissolved in ethanol and the water flow rates respectively (in μL/min).
A no-slip boundary condition for the walls was applied, to ensure that the modeled fluid comes to rest at the channel walls. The inlets and outlets were defined as the openings at the extremities of the solid model, contrary to the configuration of the actual device, whereby the inlets and outlets are through the upper surface of the channels. The outlet boundary was set to a function of pressure, with p = 0 Pa. Tetrahedral elements were used to mesh the 2D flow-focusing geometry with COMSOL Multiphysics for adaptive mesh refinement. Mesh refinement was manually adjusted around the central flow focusing region and around the edges to get more accurate velocity/concentration profiles. Detailed information regarding the computational parameters used for meshing the flow focusing region and their values can be found in the Supplemental Information under the CFD section.

2.2.3 Device Manufacturing and Assembly:

The microfluidic channels were manufactured via negative photolithography onto a silicon wafer, followed by soft lithography in PDMS. The initial step consists of utilizing the previously constructed CAD geometry to create a chrome photomask comprised of a top view of the channels. For this negative lithographic process, a dark field photomask was created. The pattern or channels to be created are transparent, and everything else was covered in chrome. The photomasks was obtained from the Center of Microfluidic Systems (CMC, Toronto Ontario, Canada) and used to create a positive mold onto a silicon wafer. Firstly, the process consists of spinning a negative photoresist, SU-8 2050, at 1700 rpm for 30s to achieve a thickness of 100 μm. Conventional ultraviolet photolithography was performed using the aforementioned photomask, whereby the exposed negative photoresist was cross-linked and thus becomes insoluble to the developer. The mould was then treated with PFOTS (trichloro(1H, 1H, 2H, 2H perfluorooctyl)silane) via chemical vapor deposition to aid with the demolding process. Vacuum is applied for about 1-1.30 h, resulting in the vaporization of the silane. After silanizing the PDMS master, pouring of an elastomer, PDMS, onto the previously silanized mould. The elastomer kit was composed of a pre-polymer and a curing agent, which was mixed in a 10:1 w/w ratio, as per the manufacturer's protocol. The prepared mixture was poured onto the wafer, which was then degassed in the vacuum desiccator to remove any bubbles within the elastomer and cured at 70 °C for 3 hours. Once cured, the channels are carefully cut and removed from the cured polymer with a surgical scalpel or razor blade. The bottom face, containing the channels, was temporarily covered with transparent packing tape so as to avoid any contamination or dust deposits. A 1.2 mm biopsy punch was then used to puncture the inlet and outlet ports. A representative view of the assembled microfluidic device and its geometry is depicted in Figure 1.

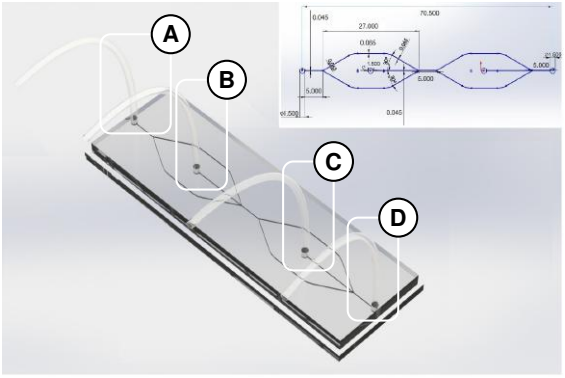

Figure 1: Schematic representation of the different components of the planar 2-D flow focusing microfluidic device: (A) Water inlet, (B) Lipid/alcohol inlet (DPPC +/- DOPG/DDAB in ethanol) (C) Loaded molecule for encapsulation (including FITC-LC TAT peptide) and (D) Outlet. The upper left insert represents a 2-D technical diagram of the design pattern of the device geometry (all dimensions in mm).

2.3 Liposome Fabrication and Loading

The phospholipid-solvent mixtures (DPPC:EtOH) were prepared using DPPC dissolved directly into EtOH at various concentrations. They were prepared in glass vials (VWR International Radnor, PA, USA) and stored at 4°C until use. For the encapsulation studies, a 0.5 mg/ml stock solution of fluorescent FITC-LC-TAT peptide was prepared as per the manufacturer's protocol by adding 2 ml of MeOH to a 1 mg of FITC-LC-TAT and stored at 20°C.
For the bare liposomes fabrication, inlet 1 was blocked, MilliQ water flowed through inlet 2, and

DPPC:EtOH flowed through inlet 3. For the runs correlating diameter with lipid concentration, DPPC:EtOH solutions at concentrations of 1, 2, 3, 5, and 10 mg/ml were prepared. The flow rate ratios (FRRs), defined as the total volumetric flow rate divided by the focused sheath flow rate, investigated were ranging between 5-50. For the peptide encapsulation investigation, the FRR was set to 50 and the DPPC:EtOH concentration was 3 mg/ml. The control batch was prepared by flowing MilliQ water, 3 mg/ml DPPC:EtOH, and MeOH through inlets 1, 2, and 3, respectively. The same setup was used for encapsulation, with the exception of the incorporation of 0.5 mg/ml FITC-LC-TAT:MeOH flowing through inlet 3, i.e., loaded. Detailed batch descriptions can be found in the Supplementary Information.

2.4 Characterization

2.4.1 Zeta Potential Measurements

In order to quantify their colloidal stability, the zeta potential of the liposomes was measured using a Zetasizer Nano ZS (Malvern, UK). The samples were analyzed for ten cycles with a voltage of 4 mV.

2.4.2 Size/ Concentration Measurements

In order to evaluate the size of the loaded and unloaded liposomes (both prior and following FITC-LC-TAT peptide encapsulation), dynamic light scattering (DLS) measurements were coupled with nanoparticle tracking analysis (NTA) measurements in order to characterize the particles size, size distribution, polydispersity index (PDI) and concentration.

Dynamic Light Scattering (DLS): The particle diameters were determined by use of dynamic light scattering (DLS) via a ZetaPALS Zeta Potential Analyzer (Brookhaven Instruments Corp. - Holtsville, NY, USA). DLS relies on the Brownian motion of particles suspended in a solution to obtain a diffusion coefficient, from which the particle size is determined. A red laser (675 nm) is emitted at a 90° angle, with the recording chamber temperature set to 6°C. Each run consisted of ten 10 second readings.

Nanoparticle Tracking Analysis (NTA): NTA was also used for detecting simultaneously sub-micron particle size distributions and particle concentrations of multiples samples. Measurements were performed with a NanoSight LM14 (NanoSight, Amesbury, United Kingdom), equipped with a sample chamber with a 640-nm laser and a Viton fluoro-elastomer O-ring. The samples were injected in the sample chamber with sterile syringes (BD Discardit II, New Jersey, USA) until the liquid reached the tip of the nozzle. The samples were measured for 40 s with manual shutter and gain adjustments. All measurements were performed at room temperature (T=25 °C). Data was processed by the NTA 3.2 Build 127 software.

2.4.3 Imaging and Visualization

Negative Staining: Samples for negative staining were prepared using the Single-droplet method[51]. After preparing a 2% aqueous solution of an uranyl acetate stain (and adjusting the pH to 7.0 with 1M KOH when required), formvar-carbon coated grids were glow discharged in order to increase their hydrophilicity prior to their use. A volume of 5 μl was then pipetted on the grid so as to cover the entirety of the grid surface. After approximately 10 seconds, 5 μl of the uranyl acetate stain was slowly pipetted on to sample, and the stain absorbed from the opposite side using a wedge of filter paper. The grid was then allowed to dry and then examined by TEM (transmission electron microscopy). Samples were imaged at a magnification of 50,000x at room temperature using a Philips Tecnai T12 electron microscope equipped with an LaB6 filament and operated at an acceleration voltage of 120 kV.

Device Flow Visualization: The fluid flow rates were controlled with a Nexus 3000 syringe pump (Chemyx Inc. – Stafford, TX, USA) in conjunction with syringes of various volumes (BD Medical – Mississauga, ON, Canada). The image acquisition setup consisted of an inverted microscope (Eclipse TE 2000-U, Nikon Corp.—Mississauga, ON, Canada), with fluorescence capabilities, which was used to visualize the liposomes as well as the fluorescence emission from the FITC-LC-TAT peptide . All images were captured using a CCD camera (Retiga-2000R, Qimaging—Surrey, BC, Canada) and Nikon NIS-Elements D software. MilliQ water, colored with readily available food dyes, was used as the working fluid. The pumps were set to flow at various flow rates and images of the flow focusing junctions were obtained at low (x20) and high (x40) magnifications.

Particle Count: An open-source software; CellProfiler, was used to quantitatively measure the fluores-

cent particles count. A pipeline was custom developed for detection of drug encapsulating liposomes. The pipeline has four major steps: 1) Background correction, 2) Colony detection & Filtering, 3) Measuring Colony parameters, and 4) Overlaying images. Background correction was done through its own inherent modules- Color to Gray, Correct Illumination calculation, and Correct Illumination Apply-. Modules for object detection (Identify Primary Objects) were based on thresholding and are available in Cell Profiler.

2.5 Statistical Analysis

Data are expressed as mean $\pm$ standard deviation (SD) of at least five replicates per group. Statistical analyses were performed for multiple comparisons via one-way ANOVA and Student's t-test was used for direct result comparison. Differences were considered significant at $p < 0.05$.

3 Results and Discussion

In order to fully characterize the HFF device and its liposomes synthesis and loading capabilities, flow visualization of the flow focusing junction was first conducted to qualitatively visualize the effect of varying the FRR on the width and behavior of the focused stream at the focusing junction. A comparison between the simulated flows, computed using Comsol Microfluidics and the experimental flows inside the platform as imaged by optical microscopy is therefore provided. Next, visualization of the synthesized liposomes was conducted by negative stating TEM microscopy thus offering both a quantitative and qualitative representation of the shape and morphology as well as the size of synthesized liposomes in aqueous conditions. Finally, the effect of varying both the lipid composition and flow parameters for the synthesis of DPPC nano-sized liposomes within the platform was assessed with regards to size, concentration, charge and polydispersity of the resulting nanoliposomes.

3.1 Comparison between Experimental and Simulated Flows

Initial attempts at hydrodynamic focusing were aimed at confining sample flow to a narrow, planar column, which is now commonly referred to as two 2-D flow focusing[52]. The possibility of significant microfluidic focusing in 2-D was first demonstrated by confining a sample flow from a 10 μm nozzle to a width of only 50 nm[53].

Liposomes formation in HFF occurs by a diffusively driven process, when a stream of lipids dissolved in an organic solvent such as ethanol, is hydrodynamically sheathed between two oblique aqueous streams in a microfluidic channel[30]. Light microscopy images of the focusing stream at magnifications of (x20) and (x40) are shown for different flow rate ratios (FRRs) in Figure 2 which depicts the focusing of a central lipid stream (dark stream) by two aqueous water streams (not visible).

The main concept of HFF is to reduce the stream width and consequently the mixing path length of the focused stream. A stream of lipids resolubilized in ethanol is hydrodynamically focused into a very narrow sheet with a thickness varying from a few micrometers down to sub-micrometers depending on the respective water-to-ethanol volumetric flow rate ratios (FRRs)[54]. The focused stream at the center of the flow focusing junction is not always centered along the midline of the channel or symmetrical as shown in Figure 2. For low Reynolds numbers ($Re < 5$), a slightly convex shape of the focused streams is generated and is to be expected in microfluidic channels due to viscous forces dominating inertial ones at low Re numbers[55]. This can cause flow disturbances in a way reminiscent of that of a turbulent flow at high Re numbers. This phenomenon can be observed in this flow focusing device at low FRRs (such as FRR 5), where one can see that the flow is not symmetrical but in fact leans slightly towards the upper side of the central channel wall. Retrospectively, a higher polydispersity and SD of the particles diameters at low FRRs compared to high FRRs is therefore expected, where a better control of the flow focusing enables a constant more laminar flow.

Flow-focusing was first examined from the plan view (Figure 2), to compare the focused alcohol stream in a the 65 μm wide central micro-channel and the two 45 μm wide side micro-channels, imaged with an optical microscope and the 2-D model simulation for the respective FRRs of 5, 10, 20 and 50 for flow rates corresponding to 40, 90, 190 and 490 $\mu L/min$. Overall, the 2-D simulation results were well substantiated with the experimental findings. The shape and width of the focused ethanol stream was well represented in the simulation with a tendency to decrease its thickness with an increase in the FRR. Experimental investigations indicated that in the case of symmetric side streams focused flow sheet was not necessarily uniform with undesirable thickening close to the walls of a microchannel observed in the case of low FRRs (Figure 2). By manipulating flow rates of the focusing flows, location of the focused sheet could be deformed and moved

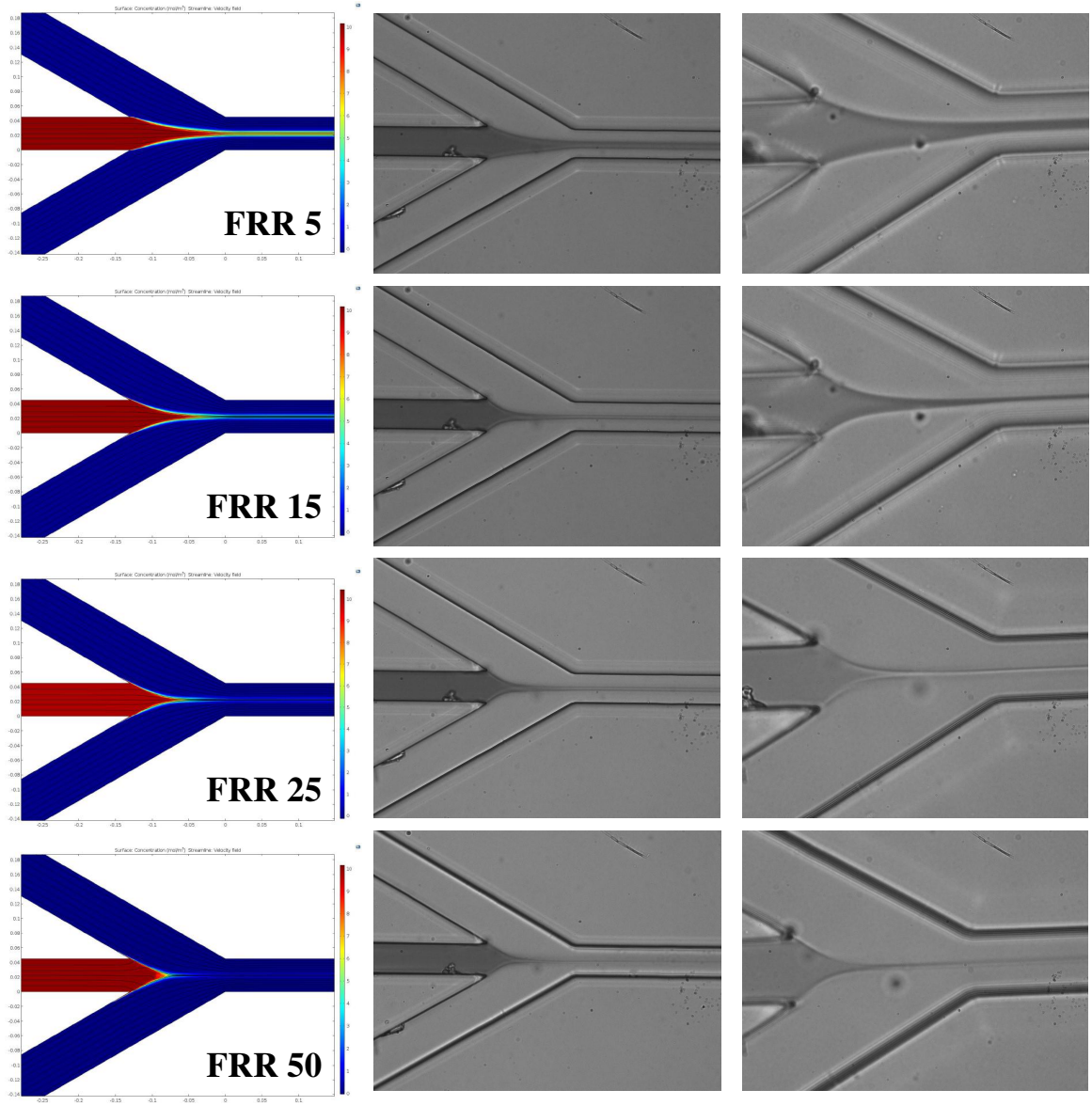

Figure 2: Comparison between 2-dimensional model simulations of the concentration profile at the focusing junction for the respective FRRs of 5, 10, 20 and 50 and the focused stream imaged with an optical microscope at (x20) and (x40) respectively.

out of the symmetry plane and most importantly, a precise control of the width of the focused stream, on which the size and polydispersity of the generated liposomes depend on, was achieved. Maintaining a precise control of the focused stream width is crucial in various applications of the flow focusing systems[56].

3.2 Visualization of Liposomes by Negative Staining Electron Microscopy

Figure 3 shows the DPPC:EtOH lipsoomes formed at a flow rate ratio of FRR=30 and a concentration of C_{DPPC}= 10 mg/mL and C_{DPPC}= 5 mg/mL respectively. At the former condition (FRR=30, C_{DPPC}= 10 mg/mL,) the liposomes particles are spherical and mostly unilamellar. Although no clear correlation between the concentration of DPPC and the size of the liposomes could be drawn from TEM images alone, re-

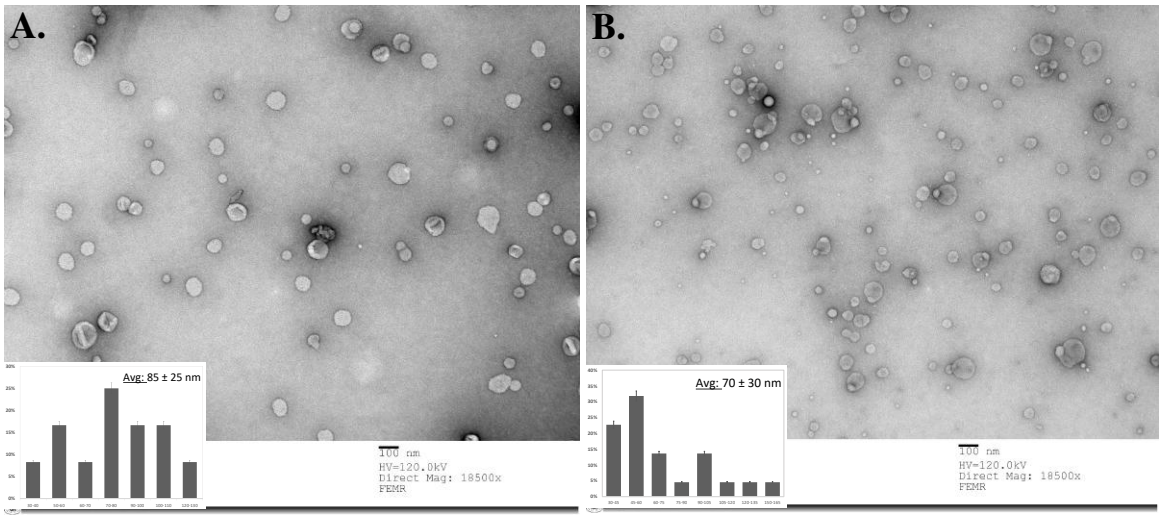

Figure 3: Transmission Electron Microscopy (TEM) image of the DPPC:EtOH liposomes after negative staining at FRR =30 for: (A) C= 5 mg/mL, and (B) C= 10 mg/mL. The small inserts show the size distribution of the particles as measured by Cell Profiler with the average value (in nm $\pm$ SD).

gardless, at high samples concentrations (C_{DPPC}= 10 mg/mL; Fig. 3A), liposomal population appear bigger in size, with lesser particles below 30 nm observed than at C_{DPPC}= 5 mg/mL (Fig. 3B). In some cases, the shape of liposomes appeared distorted. This could be attributed to both the HFF process and to the negative staining technique as well[57]. Although the electronic microscopy technique ensures the complete structural analysis of the thin transparent samples[58], possible artifacts could be due both to the staining process (the interaction between the sample and the negative stain) and the distortion/alteration induced during the drying steps caused by the exposition of the samples to a vacuum[51]. In fact, as part of the drying processes, the particle loses its hydration shell. Often, this shell stabilizes the soluble particle onto a certain configuration and deposition on the carbon can cause it to change shape[51].

3.3 Effect of Experimental Parameters on Liposome Size and Size Distribution:

The size distribution of lipid particle with respect to the FRR between the lipid and water streams has been measured by DLS and plotted for every concentration. Different DPPC concentrations in ethanol have been tested namely (C_{DPPC}= 1, 2, 3, 5 and 10 mg/mL). Figure 4A. shows all the graphs combined and displays the complete size distribution profile for all the lipid concentration of DPPC in ethanol for concentration ranging from 1 to 10 mg/mL. A logarithmic tendency curve has been fit to all the concentration profiles.

Different microfluidic techniques have been shown to produce uniformly dispersed liposomes and allow for direct control of liposome size via fine adjustments to the FRR. Decreasing the sample stream width to micrometer length scales allows for controlled and reproducible mechanical and chemical conditions across the stream width, especially compared to more traditional bulk-phase preparation techniques (i.e., test tubes and beakers).[30]. It has been found that the mean diameter of the liposomes produced to be directly related to lipid concentration and inversely related to the FRR[30,31]. Both lipid and ethanol concentration have been proven to have a significant effect on liposome properties (in both bulk and microfluidic methods)[45]. The mean diameter of the liposomes produced is directly related to lipid concentration[34].

From Figures 4A. and B., we observe that at high DPPC lipid concentration (10 mg/mL) and low flow rate ratios (FRRs $\approx 5-10$), particle sizes reach almost a micron (650-850 nm). However, at high FRR=50, the particle size is significantly smaller, in the range of 100 nm for almost every concentration (C_{DPPC}= 1 to 10 mg/mL). At low concentration, the flow and particle formation is less predictable and stable respectively so the standard error is bigger. A better illustration of the effect of FRR on the sizes of the colloidal liposomal dispersions as a function of DPPC concentrations is presented in Figure 4B. A distinct tendency of an in-

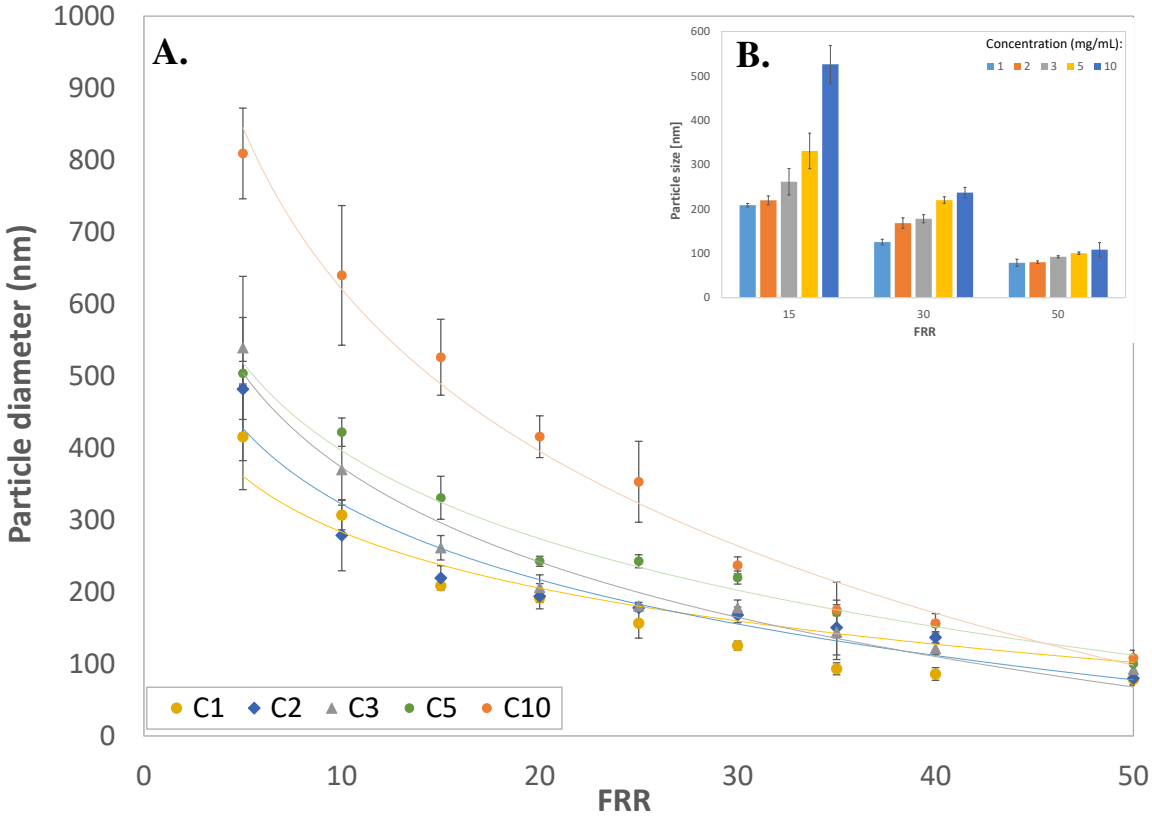

Figure 4: Particle size distribution profiles of 2D HFF synthesized liposomes as a function of DPPC lipid concentration at inlet (C=1-10 mg/mL) for various FRRs (5-50) (A), with (B) showing a stacked histogram representation of the NPs size distribution at given concentrations (C=1-10 mg/mL) and FRRs (15, 30 and 50) ($n \geqslant 15$).

crease of particle size with both a decrease in FRR and an increase in DPPC concentration is recorded. In addition, as the flow rate ratio (FRR) increases from 15-50, the differences in particle sizes at various concentrations are significantly smaller. For example, the size was almost doubled (550 nm in average) at FRR=15 and C_{DPPC}= 10 mg/mL than at FRR=15 and C_{DPPC}= 5 mg/mL where they average $\approx$ 350 nm. In addition, all liposomal DPPC formulations exhibited homogeneity with a polydispersity index (PDI) of less than 0.35. Overall, the average PDI index (an estimate of the width of the distribution) was higher at a lower FRRs and for lower DPPC concentrations. Average values of the polydispersity index for the liposomes prepared at two different FRRs (15 and 50) as various DPPC concentrations (in mg/mL) are reported in the Supplemental Information.

After confirming the core-shell structure of the lipid NPs, and knowing their range of size distribution based on the change in FRR, we investigated the possibility of controlling the NP's physicochemical properties, mainly size and surface charge while keeping other conditions such as lipidic and aqueous flow rates and flow ratios. Both the zeta potential (ZP) of colloidal systems and their size exert a major effect on the various properties of nano-drug delivery systems. Not only the stability of dosage forms and their release rate are affected but also their circulation in the blood stream and absorption into body membranes are dramatically altered by the ZP[59]. The coating material studied is often limited to neutral or anionic lipid mixtures such as DMPC or DPPC. Limited data is provided on the comparison between different lipid mixtures or on the use of cationic lipids, which may be more suitable for medical or biotechnological applications (e.g. as delivery systems for anticancer drugs or as transfection reagents), and which are routinely used in the industry[45]. Using DPPC as the main bilayer constituent, the effect of adding negatively charged DOPG or positively charged DDAB lipid molecules at different weight ratios to the lipid stream on the resulting liposome diameters and charge is investigated. The composition of the batch samples can be found in the Supplemental Information under the Liposome

Synthesis Section.
As we can see from Fig. 5 B., whereas the control (C_{DPPC}= 5 mg/mL) has a low -10 mV zeta potential, adding DDAB and DOPG increase either positively or negatively the charge. In fact, adding DDAB at a 1:5 ratio to the control C_{DPPC}= 5 mg/mL solution yields a high zeta potential of approximately 50 mV and results in highly stable lipid particles. On the other hand, adding DOPG gives a highly negative charge to the DPPC: EtOH particles with the maximum being at -30 for a 1:10 ratio which corresponds to a good particle stability. Further studies at higher DOPG: DPPC ratio need to be tested and a compromise between charge and size need to be found as this ratio (1:10 DOPG: DDPC gives the biggest size particles approx. 191 nm).
For DOPG, high weight ratio give solutions that are less homogeneous. For both conditions, a weight ratio of 1:5 constitutes the best compromise between size/stability.

Overall, results showed that the surface charge and size of the microfluidic synthesized liposomes can be finely tuned by changing the lipid stream composition and incorporating molecules with positively of negatively charged functional groups. Charge modification of nano-systems offer an opportunity for prolonging the blood circulation time of drugs, enhancing the possibility of its interaction with target cells of interest, and changing the pharmaceutical properties of nanosystems[36].

3.4 Effect of DPPC Concentration on Yield and Size Distribution of Liposomes

Nanoparticle tracking analysis (NTA) was used for the analysis of diluted samples of nanosized lipid particles and liposomes aggregates. A direct comparison with DLS was made in order to gain a more complete estimation of the size distribution of liposomes at various conditions. Figure 6 shows the HFF synthesized liposomal particles (C= 5 mg/mL, FRR=30) visualized by NTA:

Using the NTA technique, particles are seen as point scatterers moving under Brownian motion, with larger particles scattering significantly more light and appearing bigger[60]. The high resolution of the NTA make it possible to get an estimation of the sample polydispersity at any given condition (concentration, FRR) before quantitative capture and measurement. In Figure 6a, the sample captured is fairly monodispersed, with a polydispersity similar to what was observed by negative TEM microscopy.

Figure 6 displays the NTA particle concentration measurements at two different concentrations (C_{DPPC}= 5 mg/mL and C_{DPPC}= 10 mg/mL) and for three different flow rate ratios (FRR=15, FRR=30 and FRR=50). An inverse correlation between concentrations of lipid DPPC in ethanol and liposome particle concentration can be observed with DPPC solutions at C= 5 mg/mL being 37.9 % more concentrated in liposomes than solutions at C= 5 mg/mL at a FRR=15 and more than 22.3 % concentrated in liposomes at FRR=30. At FRR=50 however, no significant difference of concentration is noted between the two different DPPC concentrations (C =5-10 mg/mL). Alternatively, for a constant concentration of C_{DPPC}= 10 mg /mL, the difference in liposomal concentration is not significant at the various FRRs. On the other hand, for C_{DPPC} = 5 mg /mL, a tendency of a decrease in sample concentration with an increase in FRR can be observed. This difference amounts to more than 15.5 % between FRR15-30 and to $\approx$ 29.0% between FRR 30-50. Hydrodynamic flow-focusing technique using planar microfluidic devices for liposome formation is characterized as a low-throughput process due to the limited volumetric flow rates imposed by the small channel dimensions generally used although so far, no quantitative estimate of the concentration of the produced particles has been cited. The maximum flow rate and phospholipids concentration are generally restricted by limitations associated to fluid rheological behavior, which can increase internal pressure leading to clogging issues[46]. Overall, it is concluded that both DPPC concentration and FRR have a significant impact on the concentration of liposomes obtained by HFF synthesis, with the FRR playing a bigger influence on the resulting particle concentration to that played by the inlet concentration of DPPC[47]. Sample visualization and individual particle tracking are features that enabled a thorough size distribution analysis and made possible the characterization of the synthesized liposomal nanoparticles, complementing DLS. Live monitoring of the NPs provided information about potential aggregation and size distribution of liposomes.

4 Encapsulation of FITC-LC TAT

Subsequently, liposomes containing FITC-LC TAT were observed via microscopy, The representative sets of figures (Figure 7) are visualized under fluorescence with the FITC filter, DAPI and light microscopy, of on-chip, passively loaded FITC-LC TAT nanoliposomes.
After setting the DPPC concentration and FRR for liposomal synthesis to 3 mg/mL and 30, respectively,

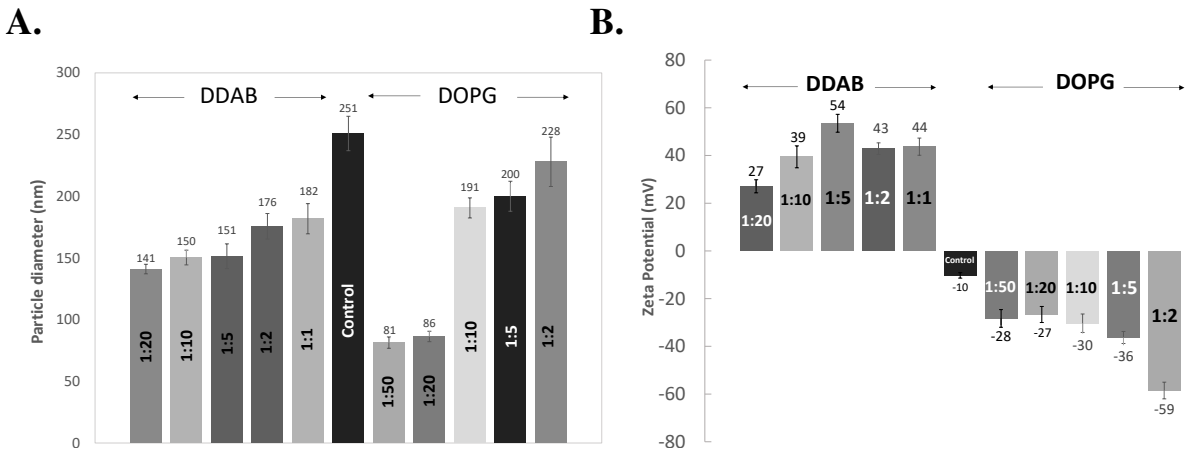

Figure 5: (A) Particle Size Distribution and (B) Zeta Potential Measurements of synthesized DPPC liposomes with different DOPG/DDAB weight ratios (n⩾10).

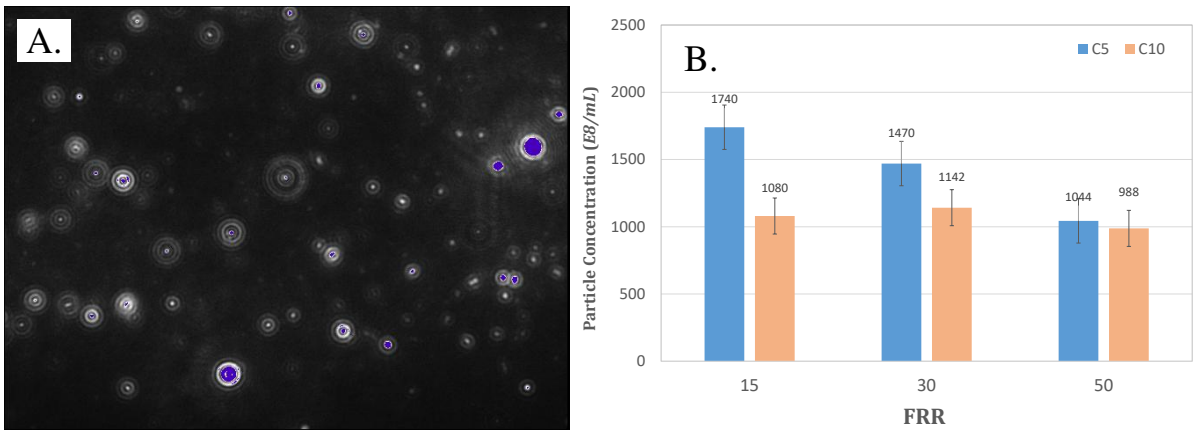

Figure 6: A) NTA video frame showing diluted liposomes particles at C= 5 mg/mL, FRR=30 (dilution = 100). Measured size by NTA = 250 nm ±50 nm (*Video can be found in the Supplemental Information*). B) Particle Concentration (E8 $particle/mL$) of the synthesized liposomes as a function of DPPC concentration (mg/mL) and FRR. The error bars displayed on the NTA graphs were obtained by the standard deviation of the different measurements of each sample (n⩾10).

FITC-LC-TAT encapsulation was attempted. Approximately 1 ml of product was obtained in less than three and a half minutes, with larger volumetric outputs, and in turn faster production times, achievable simply by increasing the fluid flow rates. As an example, by increasing the FRR to 50, 1 mL of liposomes encapsulating molecules can be made in approximately 2 minutes. Detailed preparation times for every FRR can be found in the Supplemental Information. From Fig.7, it can be observed that the fluorescence and vesicles overlap. Liposomes should not be affected by the loading time due to the minute volume of solvent present in the mixture[47]. The fluorescence images in Fig. 7 imply that the FITC labeled LC-TAT peptide was successfully encapsulated within the liposomes. Optical microscopy (not shown here) comparing batches of encapsulated liposomes with the fluorescent peptide prior and following filtration by dialysis confirmed the absence of any free FITC-LC-TAT peptides. A quantitative estimate of the number of encapsulated FITC-LC-TAT peptide in liposomes is provided in the Supplemental Information which shows the automated particle count averaged over the the microscopy areas ($B_{1\text{-}3}$, $C_{1\text{-}3}$) in Fig. 7.

From the encapsulation results, the microfluidic platform is therefore demonstrated to control liposome formation and compound encapsulation in a way that compete with existing conventional methods in liposome size homogeneity and adjustable encapsulation. Confining a water-soluble compound to be encapsulated to the immediate vicinity where liposome formation occurs has the added advantage of reducing

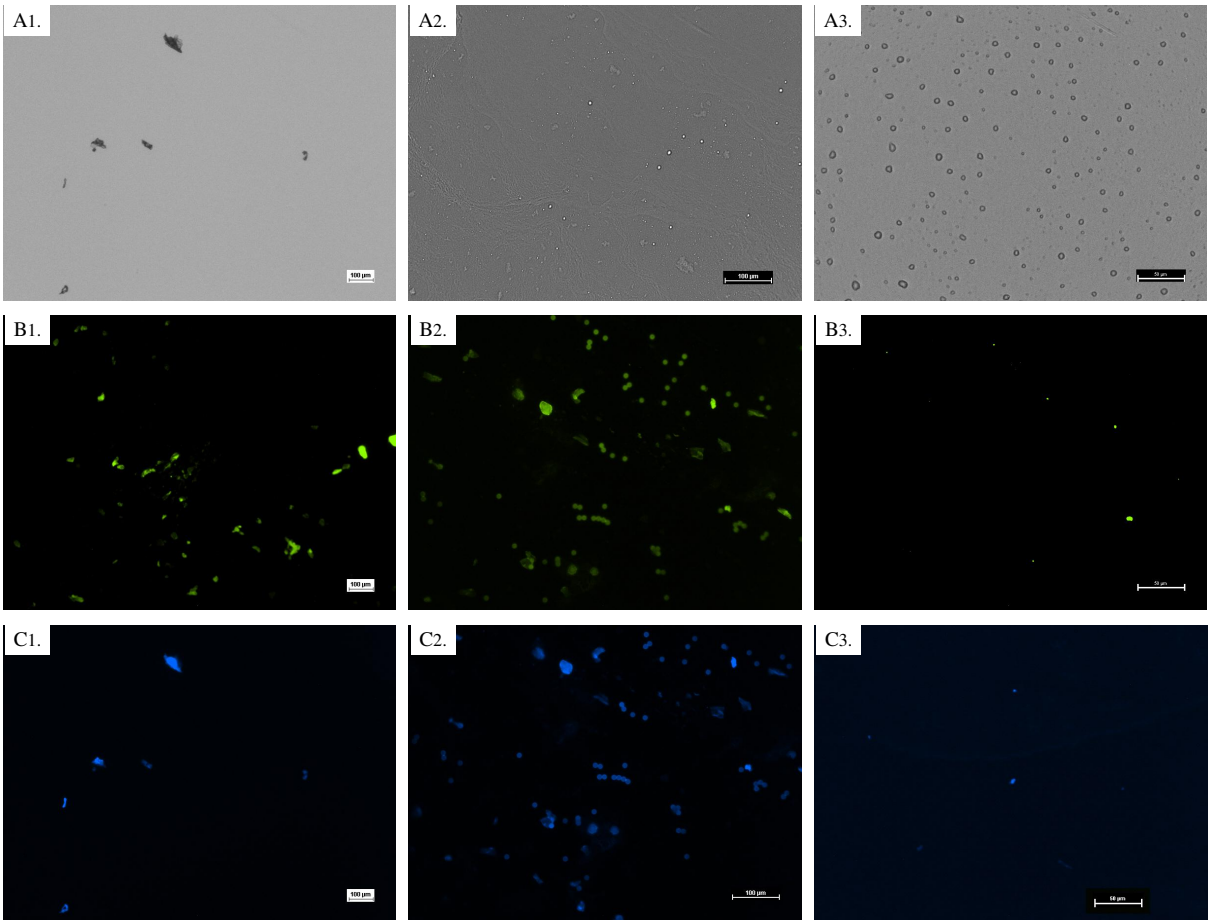

Figure 7: Optical imaging of a liposomes encapsulating FITC labeled LC-TAT peptide using different filters: FITC green (B1, 2 and 3) and DAPI blue (C1, 2 and 3) at 10 x (A1, B1 and C1), 20x (A2, B2 and C2) and 40x (A3, B3 and C3).

sample consumption without affecting liposome loading[30]. Moreover, having a precise control over the concentration and amount of encapsulated compounds within liposomes in a continuous-flow mode is another interesting feature of this platform.

5 Conclusion

In this study, we have developed and demonstrated the use of a microfluidic flow-focusing device for the continuous synthesis and loading of DPPC liposomes. This simple, low-cost, and easily scalable in parallel double flow-focusing device, enabled reproducible control of the size and size distribution of nanosized liposomal particles. With this platform, we reduced both the number of different apparatus required for liposomal fabrication as well as the amount of steps needed for the synthesis of monodisperse liposomes. Results revealed an interesting trend regarding increasing the dissolved phospholipid concentration whereby the particle diameter increases with an increase in DPPC concentration. Additionally, we established a correlation between increasing the FRR and the resulting decrease in particle diameter with a plateau reached around 60 nm.

The ability to alter the concentration and control the amount of encapsulated compounds within liposomes in a continuous-flow mode is another interesting feature towards tailored liposomal drug delivery for cancer therapy[31]. These findings suggest that this platform would provide the possibility of the development and optimization of not only liposomes but also various nano-/microparticulate systems in the emerging field of nanomedicine, along with offering the possibility of loading multiple encapsulated agents during their synthesis in a very time-effective manner. Such a microfluidic platform can control their self-assembly and potentially lead to applications as part of point-of-

care personalized therapeutics. However, the problem of scaling up the nano-/microparticulate systems production needs to be addressed during the implementation of microfuidics technology for practical applications[40].

SUPPLEMENTARY INFORMATION

For access to the Supporting Information Material *click here.*

ACKNOWLEDGMENTS

The authors extend their gratitude to the National Science and Engineering Research Council of Canada (NSERC) for their financial support towards this research. The authors also acknowledge the CGS-Masters Scholarship awarded to S.A. as well as the NSERC-CREATE grant in Continuous Flow and the Discovery grant awarded to M.T.

REFERENCES

[1] Pedro M. Valencia, Omid C. Farokhzad, Rohit Karnik, and Robert Langer. Microfluidic technologies for accelerating the clinical translation of nanoparticles. *Nature Nanotechnology*, 7(10):623–629, 2012.

[2] Chun-Min Lin, Peter Husen, Jonathan Brewer, Luis A. Bagatolli, Per L. Hansen, John H. Ipsen, and Ole G. Mouritsen. Size-dependent properties of small unilamellar vesicles formed by model lipids. *Langmuir*, 28(1):689–700, 2012.

[3] Peter Walde. Preparetion of vesicles (liposomes). *Encyclopedia of Nanoscience and Nanotechnology*, 9(9):43–79, 2004.

[4] P Chattopadhyay, B Shekunov, D Yim, D Cipolla, B Boyd, and S Farr. Production of solid lipid nanoparticle suspensions using supercritical fluid extraction of emulsions (sfee) for pulmonary delivery using the aerx system? *Advanced Drug Delivery Reviews*, 59(6):444–453, 2007.

[5] Udaya Sankar Kadimi, Deepan Raja Balasubramanian, Usha Rani Ganni, Manohar Balaraman, and Venkateswaran Govindarajulu. In vitro studies on liposomal amphotericin b obtained by supercritical carbon dioxide mediated process. *Nanomedicine: Nanotechnology, Biology and Medicine*, 3(4):273–280, 2007.

[6] D. Conchouso, D. Castro, S. A. Khan, and I. G. Foulds. Three-dimensional parallelization of microfluidic droplet generators for a litre per hour volume production of single emulsions. *Lab on a Chip*, 14(16):3011, 2014.

[7] Sarinnate Kunastitchai, Lars Pichert, Narong Sarisuta, and Bernd W. Muller. Application of aerosol solvent extraction system (ases) process for preparation of liposomes in a dry and reconstitutable form. *International Journal of Pharmaceutics*, 316(1-2):93–101, 2006.

[8] Mary Cano-Sarabia, Nora Ventosa, Santiago Sala, Cristina Patino, Roco Arranz, and Jaume Veciana. Preparation of uniform rich cholesterol unilamellar nanovesicles using co2-expanded solvents. *Langmuir*, 24(6):2433–2437, 2008.

[9] Sandy Ong, Long Ming, Kah Lee, and Kah Yuen. Influence of the encapsulation efficiency and size of liposome on the oral bioavailability of griseofulvin-loaded liposomes. *Pharmaceutics*, 8(3):25, 2016.

[10] Sheida Shariat, Ali Badiee, Seyed Amir Jalali, Mercedeh Mansourian, Mona Yazdani, Seyed Alireza Mortazavi, and Mahmoud Reza Jaafari. P5 her2/neu-derived peptide conjugated to liposomes containing mpl adjuvant as an effective prophylactic vaccine formulation for breast cancer. *Cancer Letters*, 355(1):54–60, 2014.

[11] Antonio P. Costa, Xiaoming Xu, and Diane J. Burgess. Freeze-anneal-thaw cycling of unilamellar liposomes: Effect on encapsulation efficiency. *Pharmaceutical Research*, 31(1):97–103, 2013.

[12] Bhushan S. Pattni, Vladimir V. Chupin, and Vladimir P. Torchilin. New developments in liposomal drug delivery. *Chemical Reviews*, 115(19):10938–10966, 2015.

[13] Shmuel Batzri and Edward D. Korn. Single bilayer liposomes prepared without sonication. *Biochimica et Biophysica Acta (BBA) - Biomembranes*, 298(4):1015–1019, 1973.

[14] Brian Lohse, Pierre-Yves Bolinger, and Dimitrios Stamou. Encapsulation efficiency measured on single small unilamellar vesicles. *Journal of the American Chemical Society*, 130(44):14372–14373, 2008.

[15] David Olea and Chrystel Faure. Quantitative study of the encapsulation of glucose oxidase into multilamellar vesicles and its effect on enzyme activity. *The Journal of Chemical Physics*, 119(6111-6118), 2003.

[16] Audrey Kerdudo, Alexandre Dingas, Xavier Fernandez, and Chrystel Faure. Encapsulation of rutin and naringenin in multilamellar vesicles for optimum antioxidant activity. *Food Chemistry*, 159:12–19, 2014.

[17] Louise A. Meure and Fariba Foster, Neil R.and Dehghani. Conventional and dense gas techniques for the production of liposomes: A review. *AAPS PharmSciTech*, 9(3):798, 2008.

[18] Theresa M. Allen and Pieter R. Cullis. Liposomal drug delivery systems: From concept to clinical applications. *Advanced Drug Delivery Reviews*, 65(1):36 – 48, 2013. Advanced Drug Delivery: Perspectives and Prospects.

[19] Wafa' T. Al-Jamal and Kostas Kostarelos. Liposomes: From a clinically established drug delivery system to a nanoparticle platform for theranostic nanomedicine. *Accounts of Chemical Research*, 44(10):1094–1104, 2011.

[20] Hongwei Zhang. *Thin-Film Hydration Followed by Extrusion Method for Liposome Preparation*, pages 17–22. Springer New York, New York, NY, 2017.

[21] M. J. Valle and A. Navarro. Liposomes prepared in absence of organic solvents: Sonication versus lipid film hydration method. *Current Pharmaceutical Analysis*, 11(2):86–91, 2015.

[22] Salima Varona, Angel Martin, and Maria Jose Cocero. Liposomal incorporation of lavandin essential oil by a thin-film hydration method and by particles from gas-saturated solutions. *Industrial & Engineering Chemistry Research*, 50(4):2088–2097, 2011.

[23] Catherine Charcosset, Audrey Juban, Jean-Pierre Valour, Sébastien Urbaniak, and Hatem Fessi. Preparation of liposomes at large scale using the ethanol injection method: Effect of scale-up and injection devices. *Chemical Engineering Research and Design*, 94:508 – 515, 2015.

[24] Chiraz Jaafar-Maalej, Roudayna Diab, Veronique Andrieu, Abdelhamid Elaissari, and Hatem Fessi. Ethanol injection method for hydrophilic and lipophilic drug-loaded liposome preparation. *Journal of Liposome Research*, 20(3):228–243, 2009.

[25] Yoshie Maitani. *Lipoplex Formation Using Liposomes Prepared by Ethanol Injection*, pages 393–403. Humana Press, Totowa, NJ, 2010.

[26] Yoshie Maitani, Saki Igarashi, Mamiko Sato, and Yoshiyuki Hattori. Cationic liposome (dc-chol/dope=1:2) and a modified ethanol injection method to prepare liposomes, increased gene expression. *International Journal of Pharmaceutics*, 342(1):33 – 39, 2007.

[27] F. Szoka and D. Papahadjopoulos. Procedure for preparation of liposomes with large internal aqueous space and high capture by reverse-phase evaporation. *Proceedings of the National Academy of Sciences*, 75(9):4194–4198, 1978.

[28] Wim Jiskoot, Tom Teerlink, E. Coen Beuvery, and Daan J. A. Crommelin. Preparation of liposomes via detergent removal from mixed micelles by dilution. *Pharmaceutisch Weekblad*, 8(5):259–265, Oct 1986.

[29] M. Reza Mozafari, Chad Johnson, Sophia Hatziantoniou, and Costas Demetzos. Nanoliposomes and their applications in food nanotechnology. *Journal of Liposome Research*, 18(4):309–327, 2008.

[30] Andreas Jahn, Wyatt N. Vreeland, Michael Gaitan, and Laurie E. Locascio. Controlled vesicle self-assembly in microfluidic channels with hydrodynamic focusing. *Journal of the American Chemical Society*, 126(9):2674–2675, 2004.

[31] Andreas Jahn, Wyatt N. Vreeland, Don L. DeVoe, Laurie E. Locascio, and Michael Gaitan. Microfluidic directed formation of liposomes of controlled size. *Langmuir*, 23(11):6289–6293, 2007.

[32] Mounir Traikia, Dror E. Warschawski, Michel Recouvreur, Jean Cartaud, and Philippe F. Devaux. Formation of unilamellar vesicles by repetitive freeze-thaw cycles: characterization by electron microscopy and 31 p-nuclear magnetic resonance. *European Biophysics Journal*, 29(3):184–195, 2000.

[33] Ruthairat Benjakul, Busaba Panyarachun, and Narong Sarisuta. Preparation of dry reconstituted liposomal powder by freeze-drying at room temperature. *Journal of Liposome Research*, 21(1):28–37, 2010.

[34] Bo Yu, Robert J. Lee, and L. James Lee. Microfluidic methods for production of liposomes. In *Methods in Enzymology*, volume 465 of *Methods in Enzymology*, pages 129 – 141. Academic Press, 2009.

[35] Zhenjun Huang, Xuan Li, Ting Zhang, Yanzhi Song, Zhennan She, Jing Li, and Yihui Deng. Progress involving new techniques for liposome preparation. *Asian Journal of Pharmaceutical Sciences*, 9(4):176 – 182, 2014.

[36] Elvin Blanco, Haifa Shen, and Mauro Ferrari. Principles of nanoparticle design for overcoming biological barriers to drug delivery. *Nature Biotechnology*, 33(9):941–951, 2015.

[37] Kristen Bowey, Jean-François Tanguay, and Maryam Tabrizian. Liposome technology for cardiovascular disease treatment and diagnosis. *Expert Opinion on Drug Delivery*, 9(2):249–265, 2012.

[38] Abolfazl Akbarzadeh, Rogaie Rezaei-Sadabady, Soodabeh Davaran, Sang Woo Joo, Nosratollah Zarghami, Younes Hanifehpour, Mohammad Samiei, Mohammad Kouhi, and Kazem Nejati-Koshki. Liposome: classification, preparation, and applications. *Nanoscale Research Letters*, 8(1):102, 2013.

[39] M Brandl. Liposomes as drug carriers: a technological approach. *Biotechnology Annual Review*, 7:59 – 85, 2001.

[40] Lorenzo Capretto, Dario Carugo, Stefania Mazzitelli, Claudio Nastruzzi, and Xunli Zhang. Microfluidic and lab-on-a-chip preparation routes for organic nanoparticles and vesicular systems for nanomedicine applications. *Advanced Drug Delivery Reviews*, 65(11-12):1496–1532, 2013.

[41] Renee R. Hood and Don L. DeVoe. High-throughput continuous flow production of nanoscale liposomes by microfluidic vertical flow focusing. *Small*, 11(43):5790–5799, 2015.

[42] Ryan T Davies, Donghwan Kim, and Jaesung Park. Formation of liposomes using a 3d flow focusing microfluidic device with spatially patterned wettability by corona discharge. *Journal of Micromechanics and Microengineering*, 22(5):055003, 2012.

[43] Rinbok Wi, Yeonsu Oh, Chanhee Chae, and Do Hyun Kim. Formation of liposome by microfluidic flow focusing and its application in gene delivery. *Korea-Australia Rheology Journal*, 24(2):129–135, Jun 2012.

[44] Prashant Pradhan, Jingjiao Guan, and Dongning Lu. A facile microfluidic method for production of liposomes. *Anticancer Research*, 28:943–948, 2008.

[45] Dario Carugo, Elisabetta Bottaro, Joshua Owen, Eleanor Stride, and Claudio Nastruzzi. Liposome production by microfluidics: potential and limiting factors. *Scientific Reports*, 6(1), 2016.

[46] Mariano Michelon, Davi Rocha Bernardes Oliveira, Guilherme de Figueiredo Furtado, Lucimara Gaziola de la Torre, and Rosiane Lopes Cunha. High-throughput continuous production of liposomes using hydrodynamic flow-focusing microfluidic devices. *Colloids and Surfaces B: Biointerfaces*, 156:349 – 357, 2017.

[47] Ryan V. Tien Sing Young and Maryam Tabrizian. Rapid, one-step fabrication and loading of nanoscale 1,2-distearoyl-sn-glycero-3-phosphocholine liposomes in a simple, double flow-focusing microfluidic device. *Biomicrofluidics*, 9(4):046501, 2015.

[48] Liang Hui, Xuesong Chen, Norman J Haughey, and Jonathan D Geiger. Role of endolysosomes in hiv-1 tat-induced neurotoxicity. *ASN Neuro*, 4(4):AN20120017, 2012.

[49] H. Xiao, C. Neuveut, H. L. Tiffany, M. Benkirane, E. A. Rich, P. M. Murphy, and K.-T. Jeang. Selective cxcr4 antagonism by tat: Implications for in vivo expansion of coreceptor use by hiv-1. *Proceedings of the National Academy of Sciences*, 97(21):11466–11471, 2000.

[50] Andrew Evan Kamholz and Paul Yager. Theoretical analysis of molecular diffusion in pressure-driven laminar flow in microfluidic channels. *Biophysical Journal*, 80(1):155–160, 2001.

[51] Melanie Ohi, Ying Li, Yifan Cheng, and Thomas Walz. Negative staining and image classification: powerful tools in modern electron microscopy. *Biological Procedures Online*, 6(1):23–34, 2004.

[52] P. J. Crosland-Tayor. A device for counting small particles suspended in a fluid through a tube. *Nature*, 171(4340):37–38, 1953.

[53] James B. Knight, Ashvin Vishwanath, James P. Brody, and Robert H. Austin. Hydrodynamic focusing on a silicon chip: Mixing nanoliters in microseconds. *Physical Review Letters*, 80(17):3863–3866, 1998.

[54] Bingcheng Lin. *Microfluidics: Technologies and Applications.* Springer Berlin, 1 edition, 2013.

[55] Marek Dziubinski. *Hydrodynamic Focusing in Microfluidic Devices*. INTECH Open Access Publisher, 1 edition, 2012.

[56] C. G. Hebert, S. J. R. Staton, T. Q. Hudson, S. J. Hart, C. Lopez-Mariscal, and A. Terray. Dynamic radial positioning of a hydrodynamically focused particle stream enabled by a three-dimensional microfluidic nozzle. *Biomicrofluidics*, 9(2):024106, 2015.

[57] Sacha De Carlo and J. Robin Harris. Negative staining and cryo-negative staining of macromolecules and viruses for tem. *Micron*, 42(2):117–131, 2011.

[58] Barbara Ruozi, Daniela Belletti, Andrea Tombesi, Giovanni Tosi, Lucia Bondioli, Flavio Forni, and Maria Angela Vandelli. Afm, esem, tem, and clsm in liposomal characterization: a comparative study. *International Journal of Nanomedicine*, page 557, 2011.

[59] S Honary and F Zahir. Effect of zeta potential on the properties of nano-drug delivery systems - a review (part 2). *Tropical Journal of Pharmaceutical Research*, 12(2), 2013.

[60] Vasco Filipe, Andrea Hawe, and Wim Jiskoot. Critical evaluation of nanoparticle tracking analysis (nta) by nanosight for the measurement of nanoparticles and protein aggregates. *Pharmaceutical Research*, 27(5):796–810, 2010.